ON TOPOGRAPHICALLY IDENTIFIABLE SOURCES OF CATHODOLUMINESCENCE IN NATURAL DIAMONDS

By P. L. HANLEY,† I. KIFLAWI‡ and A. R. LANG, F.R.S.
H. H. Wills Physics Laboratory, University of Bristol, Bristol BS8 1TL

(*Received* 30 *July* 1975 – *Revised* 11 *March* 1976)

[Plates 1–8]

CONTENTS

† Present address: Bablake School, Coventry CV1 4AU.
‡ Present address: Racah Institute of Physics, Hebrew University, Jerusalem, Israel.

An extensive examination of the cathodoluminescent emissions from natural diamonds has been performed with due regard to their inhomogeneity, correlating cathodoluminescence properties point-by-point with the local crystal lattice texture and imperfection content as revealed by other topographic techniques (in particular X-ray topography). Some dozens of crystals have been examined, mainly prepared in the form of cut and polished sections but in some cases as whole stones in their natural state. The cathodoluminescence observations have been made by visual microscopy, by photomicrography, and by 'spectrum topography' with spatial resolution down to 5 μm. Particular attention was devoted to those crystals, not uncommon, whose growth stratigraphy included zones of type II (ultraviolet-transmitting) diamond intercalated within regions of the more usual type Ia (ultraviolet-absorbing) diamond. These type II zones prove to be particularly rich in fine structure within their patterns of cathodoluminescent emission, and in the spectral variety of their emissions. Joint cathodoluminescence topographic and X-ray topographic examinations were made on all specimens. Where feasible, the specimens were also characterized by ultraviolet transmission topographs, and by topographic recording of the anomalous 'spike' diffuse X-ray reflexions.

Many cathodoluminescence emissions (including both well-known and little-known spectral systems) were discovered to have clearly defined topographically localized sources, e.g. dislocation lines or regions which had sustained natural α-particle irradiation. Some findings among many of this nature which are set out in detail concern the emission system (known as H3) which has zero phonon line at 2.46 eV and strong coupling to phonons of *ca.* 40 meV energy. Its sources include curvilinear growth bands in regions where crystal growth has been of non-faceted, 'cuboid' habit rather than of the usual {111} faceted habit, slip traces and individual dislocation lines in matrices of type II character, and occasionally, in similar matrices, {100}-orientation platelets ranging from *ca.* 1 μm to several tens of micrometres in diameter. The H3 system emission from the platelets is more than 90 % linearly polarized with ***E*** vector in the platelet plane. (These platelets also emit in the near infrared, at energies of *ca.* 1.25 eV.) Another emission system with zero phonon line at 2.46 eV, but with only weak phonon coupling (dominant phonon energy *ca.* 66 meV), was found solely in emissions from the natural radiation-damaged rinds of diamonds, or from patches of natural radiation damage on their external surfaces.

Noteworthy is the occurrence of dislocations blue-emitting and of dislocations emitting the H3 system in close juxtaposition within type II matrices. The deep blue broad-band spectral emission from dislocations is strongly polarized with ***E*** vector parallel to the dislocation line. The H3 system emission from dislocations is unpolarized. In dislocation-rich type II crystals possessing a mosaic texture the blue emission from dislocations is the dominant source of visible cathodoluminescence at room temperature.

Evidence bearing upon the relation of the visible {100} platelets to the submicrometre size {100} platelets which give rise to the anomalous 'spike' diffuse X-ray reflexions is examined: as far as their X-ray diffracting properties show, they are indistinguishable.

1. Introduction

The experiments here described came about in the course of efforts to decipher the growth history of diamonds, especially those which contain both type I and type II regions. (Type classification is reviewed by Berman (1965). Type I diamonds contain up to 0.25 at. % nitrogen, show X-ray 'spike' reflexions and are strongly ultraviolet absorbing below about 300 nm. Type II are transparent to about 225 nm.) For studying the spatial relations between type I and type II regions, the following experimental techniques were used to give topographical resolution: (*a*) phase contrast micrography of differential abrasion resistance of lightly polished surfaces; (*b*) ultraviolet absorption topography of specimens in the form of well polished,

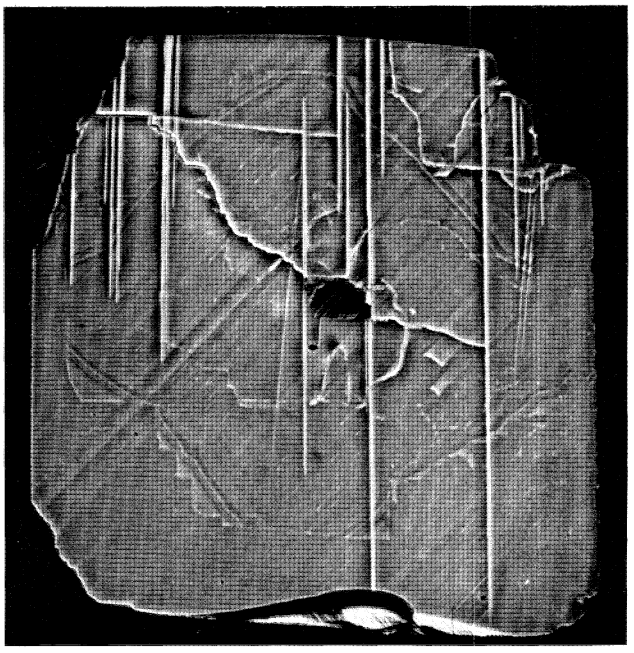

(*a*)

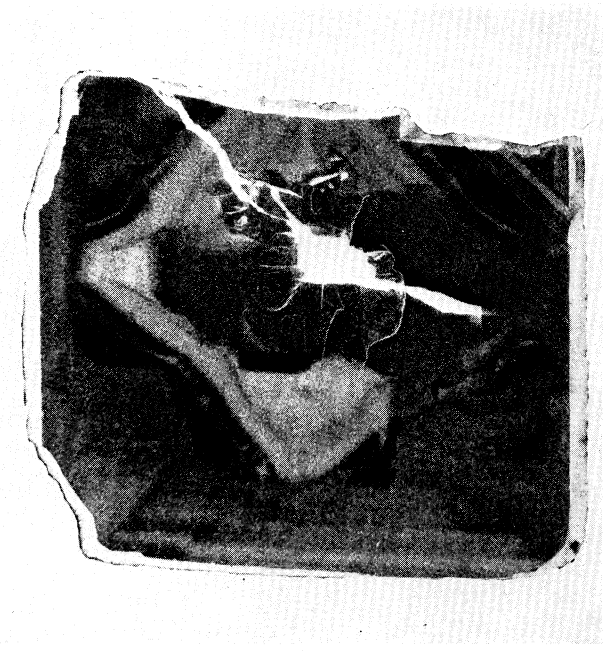

(*b*)

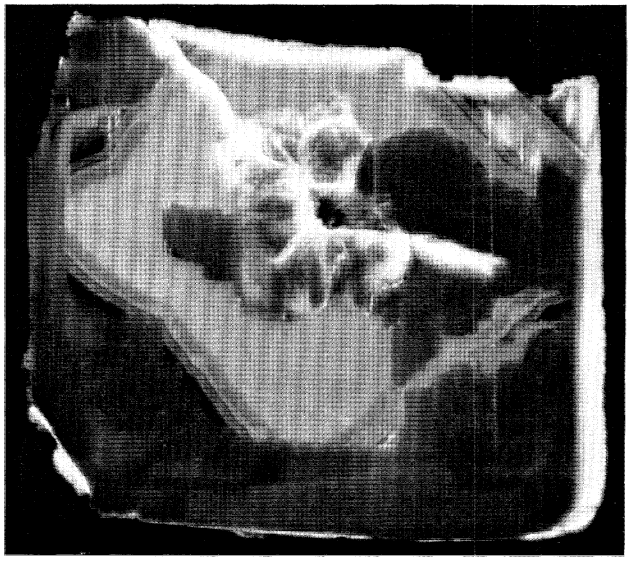

(*c*)

(*d*)

FIGURE 1. (*a*) Phase contrast micrograph of polished surface of diamond S5, orientation near (001). Specimen width is 2.60 mm, and thickness 0.16 mm. The direction [110] points horizontally to the right; the surface normal is tilted about 7° off [001] towards [$\bar{1}$00]. Polishing marks (grooves and scratches) run from lower left to upper right, along the direction of polishing, [010]. Small upstanding triangular areas and curving bands of type II material show lighter than their surroundings and are seen best in the lower left quadrant.

(*b*) Ultraviolet transmission topograph of specimen S5, wavelength 257.5 nm. Image density roughly proportional to ultraviolet transmission. Cracks appear opaque because of reflexions and scattering. The specimen height is smaller in this figure (and in figures 1*c* and *d*) compared with figure 1*a* because of loss of a strip about $\frac{1}{2}$ mm wide from the top of the specimen, the break completing the partial fracture seen running across the top part of the specimen in figure 1*a*.

(*c*) Cathodoluminescence topograph of specimen S5 taken through Kodak–Wratten filter no. 15 which transmits less than 1% at wavelengths below 510 nm. Electron beam energy 20 kV, current density 1 μA mm^{-2}. The small, very dark areas correspond to regions easily transmitting in the ultraviolet: the slip traces give strongest luminescence where they cut through these regions. (Bright images of cracks and bevelled edges of the specimen, due to reflexion of light, have no structural significance and should be disregarded.)

(*d*) X-ray projection topograph of specimen S5. Cu$K\alpha_1$ radiation, reflexion 1$\bar{1}$1 (projection of diffraction vector points downwards). Distorted regions appear black, except for those tilted more than about 2′ off the mean orientation and which in consequence are non-Bragg-reflecting and appear white. Individual dislocations are recognizable in areas not heavily distorted, e.g. the lower left quadrant. Some polishing lines show in the lower right corner. Horizontal traces of boundaries between type Ia and type II regions show stronger diffraction contrast than vertical traces because displacements due to the latter boundaries are principally orthogonal to the diffraction vector.

(*Facing p.* 330)

parallel-sided plates; (*c*) cathodoluminescence topography; (*d*) X-ray topography, including 'spike' topography (Takagi & Lang 1964). Figure 1*a–d*, plate 1, shows topographs of the same crystal obtained by each of these methods. Slightly upstanding in figure 1*a* (Chen 1973) are small areas which were suspected (by virtue of their shape) as being little 'windows' of type II diamond embedded in type I matrix, and confirmed as such by ultraviolet absorption topography (figure 1*b*) (Hanley 1972). Considerably more upstanding are narrow ridges which X-ray topographic examination confirmed to be coincident with traces of slip on {111}. Most striking in the pattern of figure 1*c* is the cathodoluminescence at the outcrops of the slip bands whose outcrops also showed up, as ridges, in figure 1*a*. This green-yellow cathodoluminescence is especially bright where the slip traces pass through type II regions. The slip bands can be seen in projection in the X-ray topograph (figure 1*d*).

Combined X-ray and cathodoluminescence topographic studies have now been performed on some dozens of natural diamonds. It is believed that the features described below constitute a fair sample of the varieties of topographically localizable sources from which known cathodoluminescent emission spectra are produced. Section 3 summarizes all the luminescence phenomena encountered, with the particular aim of making clear the crystallographic setting of each. Later sections deal in turn with some leading cathodoluminescent spectral systems, enumerating their topographic associations so far discovered.

2. Ultraviolet and cathodoluminescence techniques

The ultraviolet transmission topographs were taken with radiation monochromatized by a quartz double-prism constant deviation monochromator. When the variation of specimen transmission with wavelength was studied, lines at 302.4, 292.5, 280.4, 269.9 and 257.5 nm from a high-pressure mercury lamp were chosen as standard illuminations. Two recording methods were used. For high resolution, the diamond plate was laid directly on the emulsion of an Ilford G5 nuclear plate, just as in earlier work (Takagi & Lang 1964), and a contact print of ultraviolet transmission was obtained by reflecting downwards on to the specimen a nearly parallel beam issuing from the monochromator. For quick inspection of crystals, ultraviolet television was found helpful. The ultraviolet-sensitive vidicon camera tube employed (E.M.I. type 9677UV/1) has a target with a low leakage rate. This allowed weak images to be integrated for periods up to 10 s or longer and then transferred to an electronic image storage tube so that they could be viewed continuously on the television monitor. In another mode of operation, the variation of signal strength along any chosen line of the television raster scan could be displayed on an oscilloscope. This provided point-by-point values of the ultraviolet transmission of the specimen since the ultraviolet-sensitive vidicon produces a signal current directly proportional to illumination over most of its useful range of outputs. The simplest television optical arrangement was analogous to the photographic technique: the diamond plate, ringed by an opaque mount, was placed almost in contact with the window of the vidicon and was illuminated by a parallel beam from the monochromator. Alternatively, an image of the specimen formed by a quartz lens or concave mirror could be projected on to the vidicon target.

Photographs of the cathodoluminescence from areas large enough to encompass the whole specimen were taken using a Cambridge Instruments Ltd, mark II Stereoscan scanning electron microscope in the manner previously described (Lang 1974). Smaller specimen areas, up to $\frac{1}{2}$ mm

in diameter, were photographed in a JEOL model JXA-3A electron probe microanalyser (Hanley 1972; Kiflawi & Lang 1974; Woods & Lang 1975). Specimen temperatures could be measured and controlled in the former apparatus but not in the latter. With the microprobe, photographs could be taken at kilovoltages from 10 to 50; and whereas photography was usually performed with an electron current per unit area of specimen in the range 1–10 μA mm^{-2}, informative visual observations were possible at specimen specific currents up to three orders of magnitude both higher and lower than the values customary in taking photographs. Much use was made of Kodak–Wratten filters to give colour discrimination when recording with non-colour film (Ilford FP4 panchromatic film). Chief among these were the filters nos 47B and 12. The former is a blue-band-passing filter having a transmittance of 50 % at 430 nm which falls to less than 1 % for wavelengths below 380 nm or above 490 nm. Filter no. 12 was used for passing longer wavelengths: below 500 nm it transmits less than 1 %.

As a guide to estimating the depth at which cathodoluminescence production is strongest the experiments of Ehrenberg & King (1963) are directly relevant. They took microphotographs of the 'glow lobes' below the point of impact of a fine electron beam upon a homogeneous phosphor. Scaling their data on polystyrene to the case of diamond by allowing just for the differences in electron density of these substances indicates that at 50 kV (the highest voltage used in the present experiments) the maximum generation of cathodoluminescence occurs between 4 and 5 μm below the specimen surface, but about 10 % of the energy of the incident electron beam is expended below 10 μm.

The topographic recording of cathodoluminescence spectra was performed in two ways. When the Stereoscan was used as an electron source, the image of the specimen (magnified by factors ranging from 2.7 to 5 depending upon the size of the specimen or area of interest) was focused on the entrance slit of a Hilger Medium Quartz Spectrograph. Kinematically designed translation tables supported the spectrograph so that its entrance slit could be precisely positioned to admit a selected ribbon on the image. When the microprobe was used, the image produced by its reflecting objective was projected on to the entrance slit of a Beck direct-vision spectroscope. The location of the specimen region imaged on the slit was monitored with the aid of a beam splitter and an eyepiece containing a pointer. These 'microprobe' spectra were photographed with a lens of 50 mm focal length. This gave a dispersion at 500 nm of only 40 μm nm^{-1} compared with 140 μm nm^{-1} using the Hilger spectrograph, but exposure times were roughly a hundred-fold shorter than with the latter instrument. Spectra taken by both methods are here reproduced to give the same linear separation between 503 nm and 575 nm. Entrance slit widths were usually such as to limit resolution to about 0.7 nm at 500 nm in the case of the Hilger spectrograph, and about 1 nm with the Beck instrument. Recording was made either on Ilford FP4 developed to give a gamma of 0.8, or on Ilford Astra III plates developed to a gamma of 1.8. As regards the topographic resolution on the spectra, it was possible to register spectra from specimen regions delimited within an area of about 20 μm square with the Stereoscan arrangement and about 5 μm square with the microprobe arrangement. Whether or not spectra characteristic of defects covering such small areas could be satisfactorily recorded depended of course upon their intensity relative to the luminescence from the matrix in which they were embedded.

3. Review of phenomena observed

(*a*) *Crystals containing intercalated type II and type Ia zones*

Specimen S5, shown in figures 1 and 4, plates 1 and 4, and specimen S1, of which a part is shown in figure 5, were prepared by polishing roughly sawn slices which had been excised from diamonds in order to remove regions near the crystal centres where there were inclusions and internal cracks. Features of interest in S5 briefly mentioned in § 1 will now be considered further. The most strongly visible ridges running nearly vertically on figure 1*a* are traces of slip on $(\overline{1}11)$. Those rather less visible, which run downwards to the left of vertical, are traces of slip on (111). After the phase-contrast photograph figure 1*a* had been taken the specimen was more finely polished with the consequence that the surface relief was reduced. Multiple-beam interferometry then showed the slip-trace ridges to be upstanding by between 100 and 150 nm, whereas the elevation of the small type II regions with respect to their surroundings was not more than 10 nm. The ridge profile was cusp-like, being steeper on the side that had faced oncoming diamond grit on the polishing scaife. All the topographs showed that at the stage of growth when the crystal had reached about half its present diameter hummocky surfaces of mean orientation {100} ('cuboid' surfaces, Lang (1974)) had dominated over normal {111} facets. In the outermost parts of the crystal no obvious exception to growth exclusively on {111} facets could be discerned. The principal localities of good ultraviolet transmittance are in thin bands within the outer layers of cuboid growth, and also, slightly further out, in roughly triangular-shaped sections bounded on the inside by cuboid surfaces and on the outside by surfaces parallel to {111} or nearly so. The latter transmitting 'windows' resemble the triangular-shaped transmitting area shown in figure 4 of Takagi & Lang (1964). Correlations between the four types of image shown in figure 1 become clearer when figures 1*b* and *d*, which represent projections of the crystal volume, are compared with the phase contrast and cathodoluminescence patterns of both surfaces of the specimen. The monochrome illustration of cathodoluminescence in figure 1*c* cannot depict the range of tints that appear in the strongly luminescing areas. For example, on colour photographs it can be seen that whereas the cathodoluminescence from all parts of this specimen (with the exception of the bright green-yellow slip traces) falls within the general description of the broad-band blue emission known as 'band A' (Dean 1965; Collins 1974), there are certain regions of cuboid growth, relatively strongly ultraviolet absorbing, which emit a greater proportion of longer wavelength radiation than do regions of {111} growth comparable in the strengths of their ultraviolet absorption and overall brightness.

From observations such as the above it was evident that specimens with a somewhat less complicated growth history, and less distorted, should be studied. Luckily, the specimen illustrated in figures 7–13 of Takagi & Lang (1964) was regained for renewed investigation. Cathodoluminescence topographs of both faces of this specimen (number GH2) are presented in figures 2*a*, *b*, plate 2, and the corresponding surface-reflexion X-ray topographs in figures 3*a*, *b*, plate 3. Since the Bragg reflexion, spike reflexion and ultraviolet absorption topographs of this specimen have been previously described (Takagi & Lang (1964) only certain essentials concerning the crystallography of its imperfections need be recalled here. The inner zone of the slice, which produces a bright blue cathodoluminescence, is quite strongly ultraviolet absorbing. It is enclosed by highly ultraviolet transmitting bands constituting a zone of dominantly type II material. From figures 2*a* and *b* it is now evident that this type II zone is rich in

strong sources of green-yellow cathodoluminescence which in certain regions are clearly identifiable with slip traces (as in specimen S5), with individual dislocation lines, and with isolated bodies up to a few micrometres in diameter embedded in the very feebly blue-luminescing type II matrix. The conclusion drawn from the earlier X-ray topographic examinations that the type II zone contained decorated dislocations and precipitates is thus supported. Higher-magnification cathodoluminescence topographs of some regions of this specimen appear in figures 6, 7 and 8, plates 5 and 6. The zone of type II material can be resolved into a sequence of bands whose traces for the most part follow {111} planes closely. Bands of green-yellow luminescence parallel to $(\bar{1}11)$, $(\bar{1}\bar{1}1)$ and $(1\bar{1}1)$ outcrop on the left side of figures 2 and 3 (the figures 2*b* and 3*b* have been printed left-to-right to facilitate comparison of patterns on the two surfaces). Since the plane $(\bar{1}\bar{1}1)$ is inclined steeply to the specimen surface, little shift in position of outcrop of bands parallel to $(\bar{1}\bar{1}1)$ can be seen when the pattern on the 'a' face (figures 2*a* and 3*a*) is compared with that on the 'b' face (figures 2*b* and 3*b*). However, surface 'a' also cuts through the type II zone where the layers within the latter run parallel to (111). Thence follows the identification of surface 'a' as being more remote from the crystal centre than surface 'b'; together with an explanation for the major differences between the geometry of the patterns exposed on the right half of the illustrations of the 'a' and 'b' surfaces, both with respect to cathodoluminescence and to the arrays of dislocations seen on the surface reflexion X-ray topographs. Some traces of curved surfaces can be seen in figure 2*a* and *b*. Usually they coincide with one boundary of a type II band, often as boundaries of areas of strong green-yellow cathodoluminescence (which are in type II regions).

In the paper by Takagi & Lang an anomaly was noted: whereas the outermost crystal zone that the specimen includes produced a weaker spike intensity than did the innermost zone, it is the most strongly ultraviolet absorbing region in the whole specimen. (The outermost zone is represented in the strip, about $\frac{1}{2}$ mm wide on the crystal, which is adjacent to the left-hand edge of figures 7–10 in Takagi & Lang (1964) and of figures 2 and 3 in the present work.) In figures 2*a* and *b* a further unexpected property of this strip presents itself. It produces only comparatively weak cathodoluminescence (under the conditions of stimulation operative), and is the only exception so far discovered to the general rule that weak band A cathodoluminescence is associated with weak ultraviolet absorption. However, care must be exercised in discussing correlations of band A strength with other properties because of the sensitive dependence of the former on both specimen temperature and, so present experiments indicate, on specimen current density as well. Indeed, in order to obtain satisfactory colour photographs of the whole face of specimen GH2 with a single exposure its temperature was raised to 385 K. Photographic tests had established that an increase in specimen temperature from 335 to 385 K (with a few degrees uncertainty in temperature measurement) effected roughly a threefold reduction of the bright band A cathodoluminescence from the innermost zone in specimen GH2 relative to the green-yellow luminescence from its type II zone. This finding is in line with the measurements of Dean, Kennedy & Ralph (1960) who investigated the effect of specimen temperature on natural diamond cathodoluminescence, using nontopographic recordings of spectra. Since specimen GH2 displayed extensive arrays of green-yellow luminescing dislocations, the spectral characteristics of these defects could be positively identified on spectrum topographs taken of this crystal. Their outstanding feature was the band with zero phonon line at *ca.* 503 nm, an emission system first studied in detail in ultraviolet-excited fluorescence spectra of natural diamonds (Mani 1944*a*), and later detected in cathodolumi-

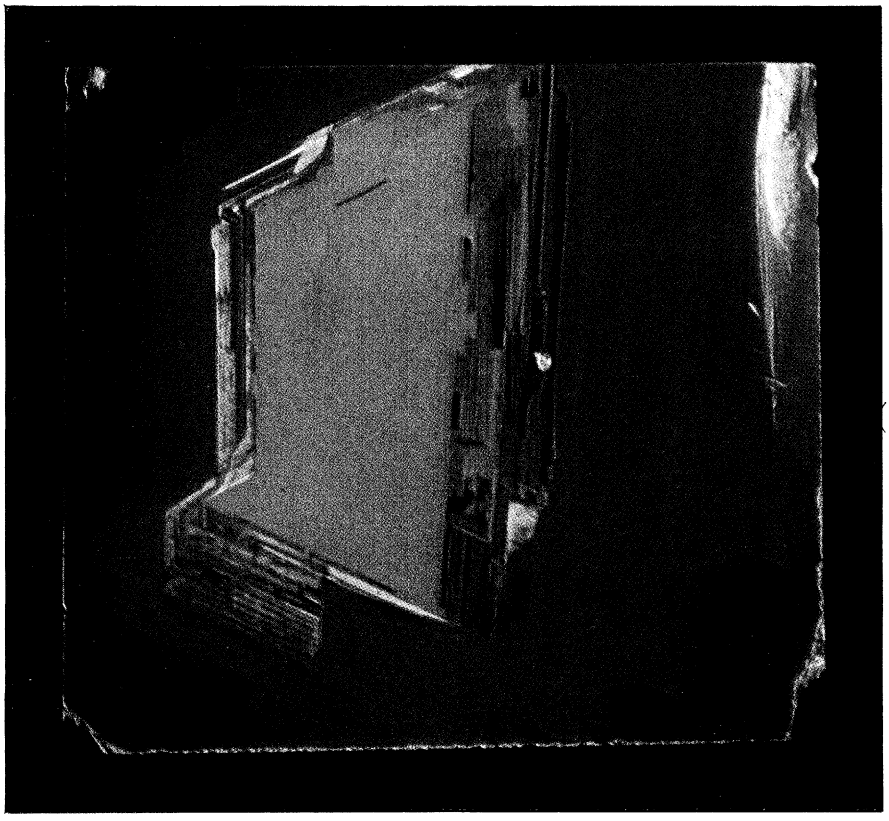

(2*a*)

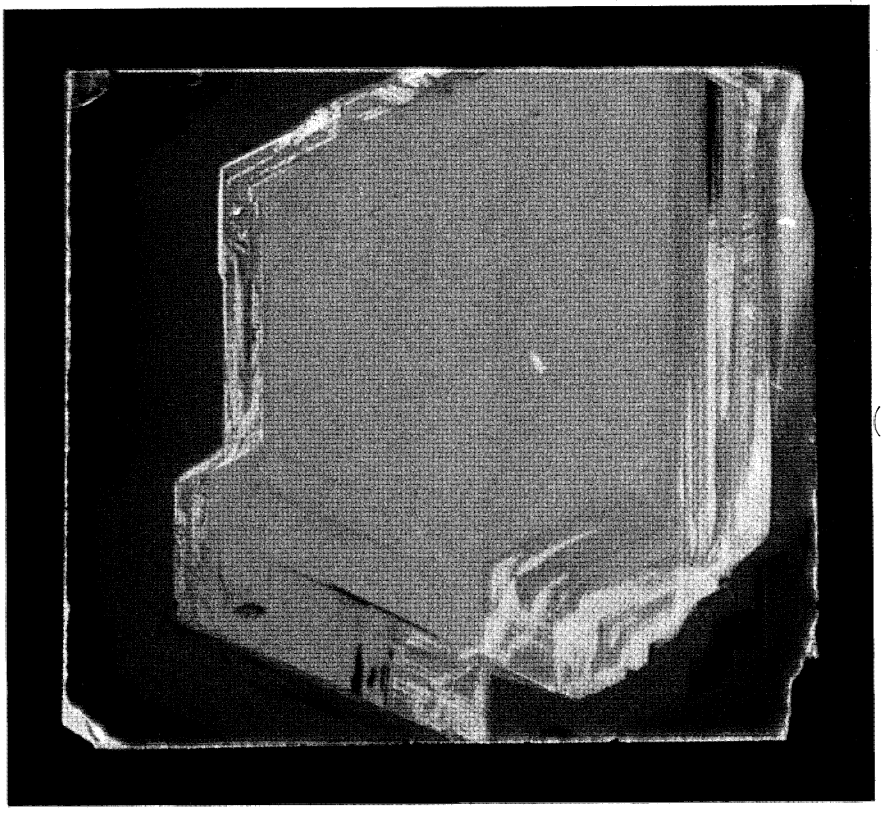

(2*b*)

FIGURE 2. For description see opposite.

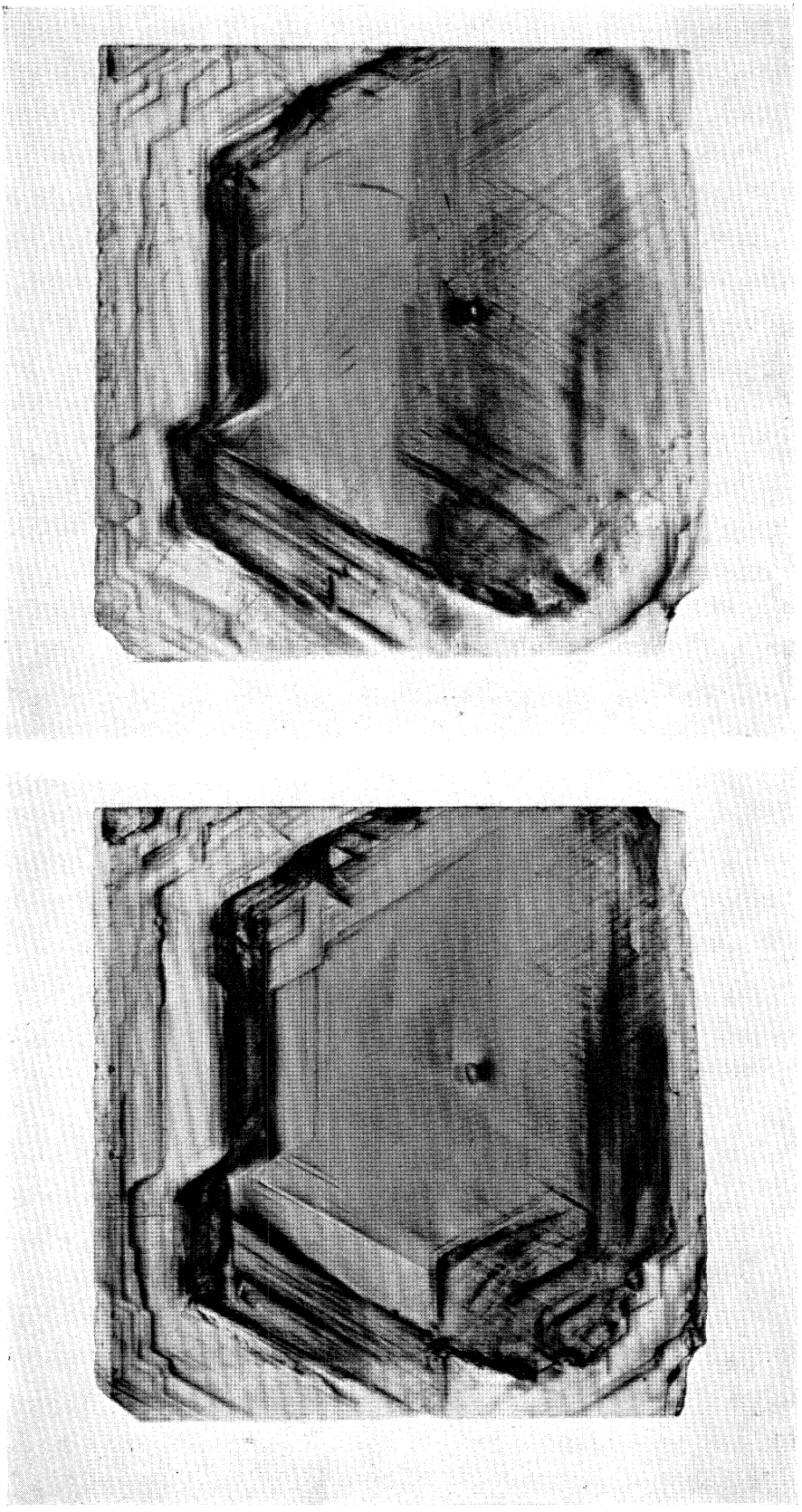

(*a*)

(*b*)

FIGURE 3. Surface reflexion X-ray topographs of specimen GH2, radiation CuKα_1. (*a*) Surface designated 'a', 113 reflexion. (This specimen surface is close to (112) orientation; the direction [1$\bar{1}$0] is nearly parallel to the vertical direction in the plane of the figure but is rotated about 2° out of the specimen surface, towards the observer.) (*b*) Surface designated 'b', $\bar{1}\bar{1}\bar{3}$ reflexion, image printed left-to-right to aid comparison with image of surface 'a'.

FIGURE 2. Cathodoluminescence topographs of surface of specimen GH2 recorded on Ektachrome-X. Specimen width is 6 mm, thickness 0.42 mm. Electron beam 20 kV, current density 0.24 μA mm^{-2}. Specimen temperature about 385 K. (*a*) Surface designated 'a'; (*b*) surface designated 'b', with image printed left-to-right to facilitate comparison with pattern of surface 'a'.

(*Facing p.* 334)

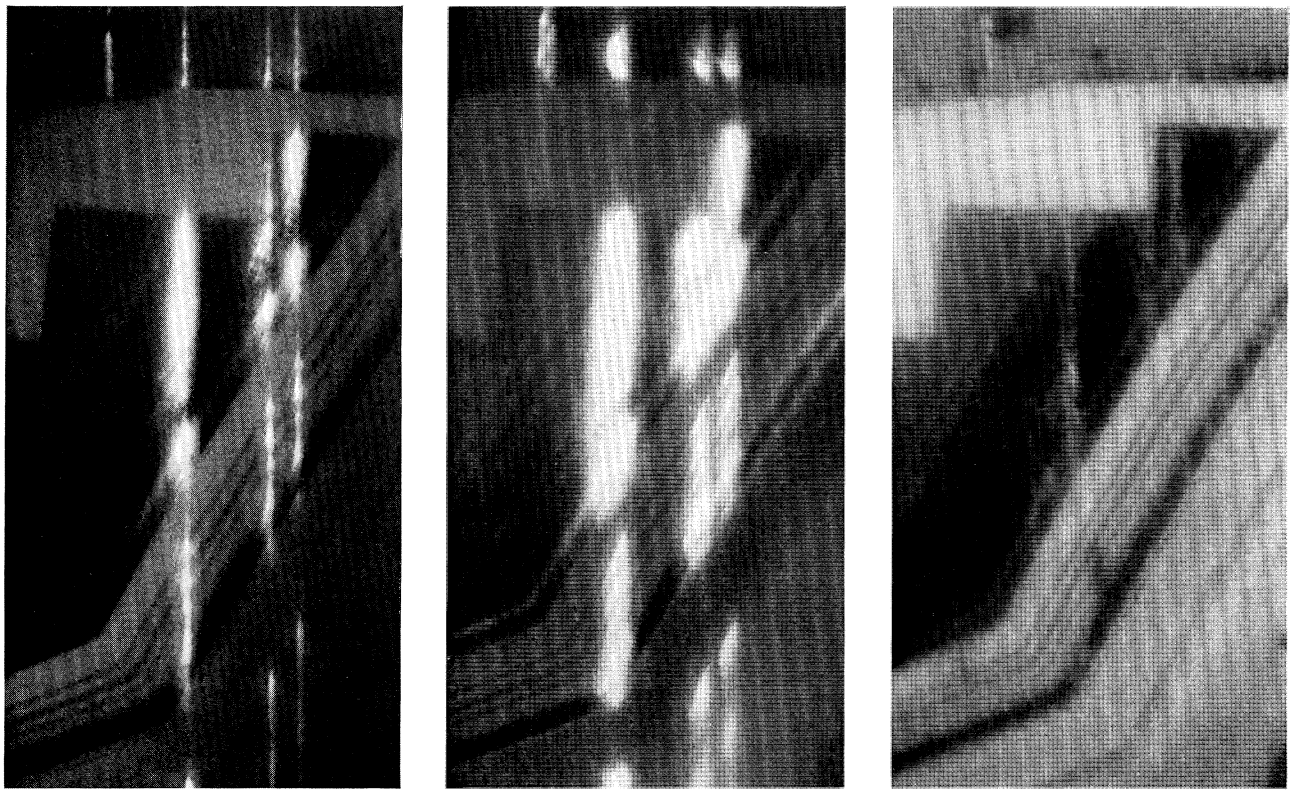

(*a*) (*b*) (*c*)

FIGURE 4. Cathodoluminescence micrographs of a region in the upper left quadrant of specimen S5 (figure 1) where it is cut by slip bands parallel to $(\bar{1}\bar{1}1)$. The micrographs are oriented similarly to figure 1. Field width is 150 μm. (*a*) Electron beam 10 kV, 40 μA mm^{-2}, Kodak–Wratten filter no. 12 transmitting under 1 % of wavelengths below 500 nm. The 503 nm-system emission from slip bands appears bright. (*b*) Electron beam 50 kV, 40 μA mm^{-2}, Kodak–Wratten no. 12. Luminescence from slip bands spreads leftwards from their surface outcrops as a consequence of the dip leftwards of $(\bar{1}\bar{1}1)$ below the specimen surface. (*c*) Electron beam 20 kV, 40 μA mm^{-2}, Kodak–Wratten narrow-band, blue-passing filter no. 47B. Image brightness roughly indicates strength of band A cathodoluminescence.

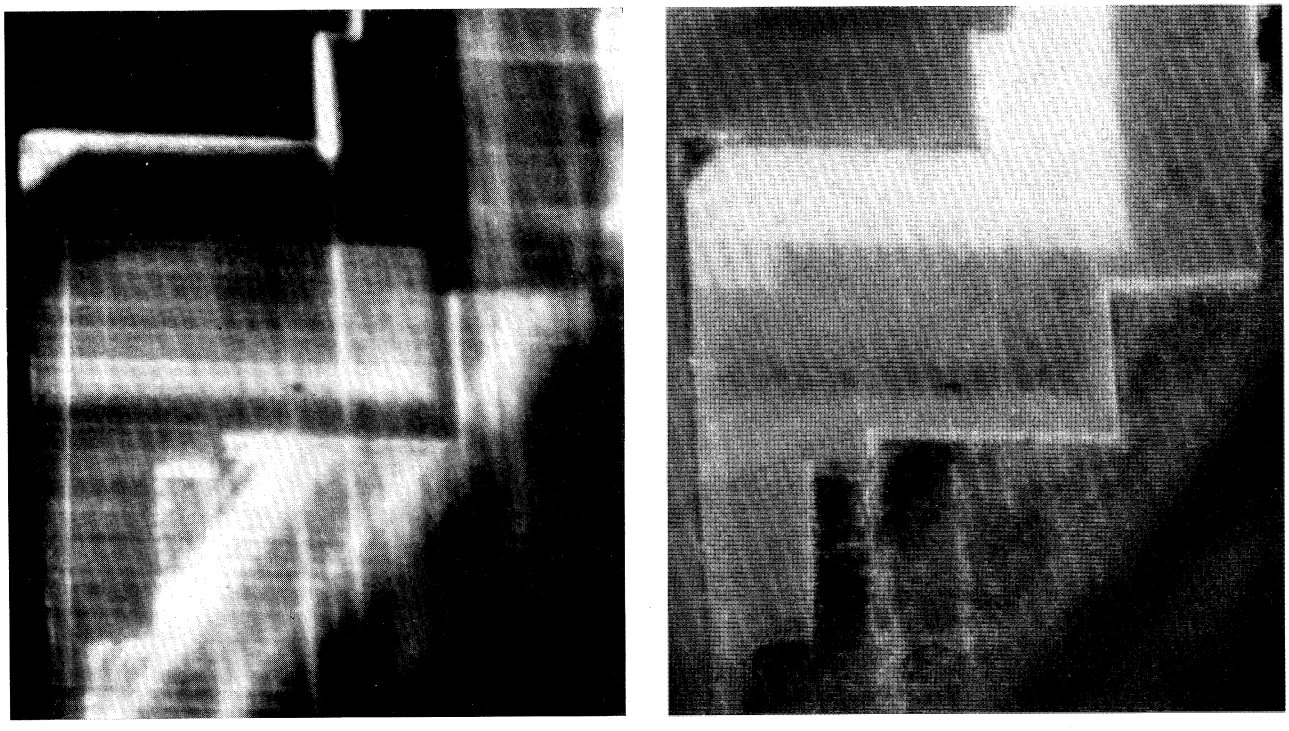

(*a*) (*b*)

FIGURE 5. A region of specimen S1 containing both cuboid and faceted growth layers. The centre of the crystal lies about 2 mm away, below and to the right of the field. Specimen surface roughly parallel to (001). Orientation of figure corresponds to that of figures 1 and 4. Field width is 325 μm. Electron beam 15 kV, 11 μA mm^{-2}. (*a*) Kodak–Wratten filter no. 12. (*b*) Kodak–Wratten filter no. 47B.

nescence spectra by Dean *et al.* (1960). All but one type of green or green-yellow luminescing feature found in the natural diamonds examined in the present work produced a band with an intensity envelope similar to that recorded from GH2, though it has not been feasible to record spectrographically the presence of the 503 nm line in each instance so far. The 503 nm-system spectra will be discussed more fully in §4.

Thin layers of alternating stronger and weaker band A-cathodoluminescent crystal, parallel to (111), dip gently into surface 'a' of specimen GH2 and intersect slip bands on other octahedral planes. Geometric details in the resultant cathodoluminescence pattern could be significantly modified by changing the energy of the primary electron beam, demonstrating thereby the need to take into account the range of electron penetration when analysing patterns involving measurements in the micrometre range. Such allowance must also be made when investigating the contributions (if any) of photoluminescence and electroluminescence to the observed emission from a given feature. Defects lying on planes of known inclination to the specimen surface can provide data on how luminescence production varies with depth below the surface. Slip bands on {111} satisfy the condition of known geometry; and they show clearly that the maximum depth from which their 503 nm-system luminescence can be seen depends not only upon the energy of the primary electrons but also upon the type of diamond matrix in which they lie. (This property will be discussed further in §§4(*a*) and 7(*c*).) The lateral resolution of the microscope incorporated in the microprobe apparatus was not better than 1–2 μm, and its depth of focus in air was between 2 and 3 μm. Under such viewing conditions no significant changes in topographic resolution were recognized with a kilovoltage variation from 5 to 20; but, as figures 4*a* and *b* illustrate, 'electron penetration effects' are quite appreciable in 50 kV images. Figure 4 encompasses the transition zone from cuboid growth to mainly faceted growth which appears in the upper left area of the surface of specimen S5 shown in figure 1. The curvilinear bands of cuboid growth producing alternating strong and weak band A cathodoluminescence in the lower right part of the field are nearly perpendicular to the surface. Consequently the resolution of their images is little affected by a kilovoltage increase from 10 to 50. The wider dark band of ultraviolet transparent, type II material which occupies the left-central area is terminated abruptly by traces of {111} facets. Images of these traces become noticeably diffuse at the higher voltage. A few other features of the topography in figure 4 will be pointed out. Appearing above the {111} facets just mentioned is a zone of very strong band A cathodoluminescence in which the 503 nm-system emission from the slip traces is greatly reduced. The slip traces reappear with good visibility in the topmost part of the field where they cut through a zone of weaker band A cathodoluminescence. Within the type II regions the slip-trace luminescence can be locally resolved into bright specks. In figure 4*c* faint webs of blue lines lie parallel to, but not quite coincident with, the slip traces.

Figure 5 shows a small portion of a polished surface of specimen S1 which cuts through the crystal close to its centre. The figure includes zones of cuboid growth (lower right) and of superseding faceted growth. Hence it exhibits some geometrical features in common with the pattern in figure 4. Specimen S1 contrasts with S5 in that it contains much fine-scale slip, locally intensely developed, whereas neither cathodoluminescence nor X-ray topographs disclose any slip planes cutting right across (or a large way across) the crystal slice such as are seen in figure 1. In figure 5*a* many 503 nm-system-emitting slip traces, both bold and faint, run approximately vertically. (Opposite tilts from the vertical indicate oppositely dipping octahedral slip planes.) Multitudinous slip traces run horizontally: these are parallel to the octahedron facets whose

traces are horizontal in the figure. Note the frequent appearance of especially bright slip traces as prolongations of facet traces, either outwards from corners or inwards from re-entrants. Such corners and re-entrants will have been loci of stress maxima if, as is considered most probable in slip patterns of the type shown in figure 5, the slip took place to relieve stresses between adjacent zones. Figure 5*a* shows two crystallographically definable associations of 503 nm-system luminescence in addition to the slip traces: these will be discussed in §4(*c*).

The wispy blue lines which appear light in figure 5*b* are believed to be individual dislocations, but their density and propinquity to other strain centres precludes X-ray topographic verification of this relationship. They can be detected dispersed in much of the field of figure 5, appearing most strongly in the ultraviolet transparent region below and left of centre, but invisible in the block of strongly band A cathodoluminescent material in the upper part of the figure. As in figure 4, they appear concentrated at, but not necessarily confined within slip bands.

When it was reported that sharply defined, blue-emitting lines seen in cathodoluminescence topographs of natural and synthetic diamond produced luminescence strongly polarized with electric vector parallel to the line direction (Kiflawi & Lang 1974) it was not possible to offer proof that the lines truly were dislocations by demonstrating a one-to-one correspondence between their optical and X-ray topographic images. Despite the subsequent finding of blue-emitting lines in many more natural diamonds, there has to date† been discovered only one specimen in which such one-to-one correspondence can straightforwardly be demonstrated. However, when configurations of blue-emitting lines appear in cathodoluminescence like those reproduced in figures 6*b–e* it would be unreasonable to dispute their interpretation as patterns of dislocations, so close are the resemblances to dislocation configurations in silicon and germanium recorded by X-ray topographic and other techniques. Figure 6 (and figures 7 and 8 following) show areas on one or other surface of specimen GH2. Their locations in figures 2*a* and *b* will be given by fractional coordinates (x, y) in a right-handed Cartesian system having its x-axis running to the right along the bottom edge of the image of the specimen surface, and its y-axis upwards along the left-hand edge of the image as printed on the photographs. (Thus, for example, a point on the right-hand edge of the image has coordinates $(1, y)$, and one on the top edge $(x, 1)$, neglecting minor edge irregularities.) The centre of figure 6 has coordinates

† *Note added January* 1976: reported in Kiflawi & Lang (1976) *Phil. Mag.* **33**, 697–701.

Description of plate 5

Figure 6. Example of juxtaposition of 503 nm-system emission from slip traces and linearly polarized blue emission from dislocation lines. Specimen GH2, surface 'a'. Coordinates of centre of this field on the image of surface 'a', figure 2*a* are (0.57, 0.27). Orientation of image is rotated relative to figure 2*a* so as to bring traces of $(1\bar{1}1)$ parallel to horizontal axis: traces of $(11\bar{1})$ slope from upper left to lower right, and those of $(\bar{1}11)$ from upper right to lower left. Field width is 200 μm. Electron beam 35 kV, 2.2 μA mm^{-2}. Kodak–Wratten filter no. 12 used in (*a*); filter no. 47B in (*b*) to (*e*). (*a*) Pattern of 503 nm-system emission. (*b*) Full pattern of blue-emitting dislocations: Polaroid analyser removed. (*c*) Analyser turned to attenuate horizontal ***E*** vector and horizontal dislocation images. (*d*) Analyser attenuates ***E*** vector and dislocation images parallel to $[\bar{1}10]$ (upper left to lower right). (*e*) Analyser attenuates ***E*** vector and dislocation images parallel to $[01\bar{1}]$ (upper right to lower left). (Arrows in (*c*)–(*e*) indicate plane of E vector transmitted.)

Figure 7. Population of green-yellow-emitting precipitates seen in a matrix of feebly band A-emitting diamond. Zones producing stronger band A cathodoluminescence run parallel to left- and right-hand edges of field. Location on face 'a' of specimen GH2, figure 2*a*, is about six-tenths of distance from lower left corner to upper right corner of surface. Orientation same as in figure 2*a*; width of field in 160 μm. Electron beam 35 kV, 6 μA mm^{-2}. Kodak–Wratten filter no. 12.

(*a*) (*b*) (*c*)

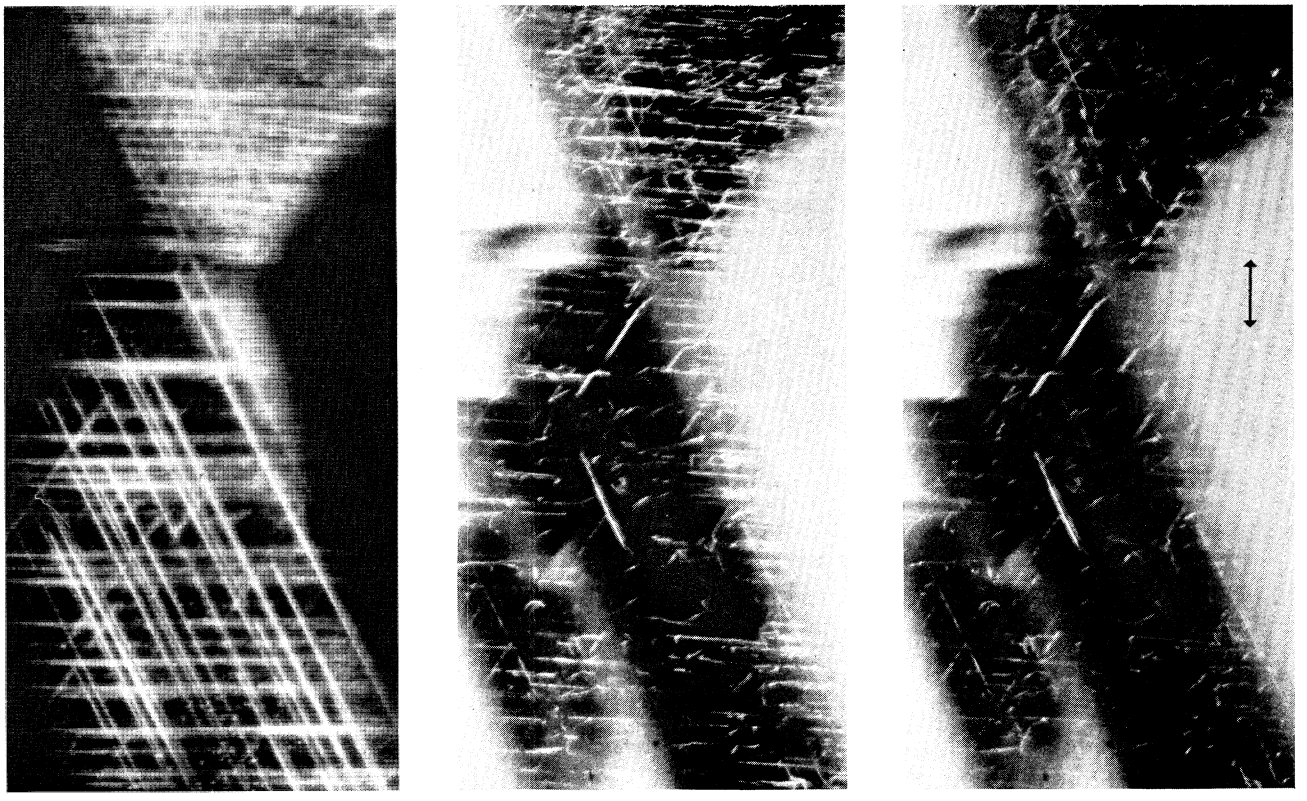

FIGURE 6

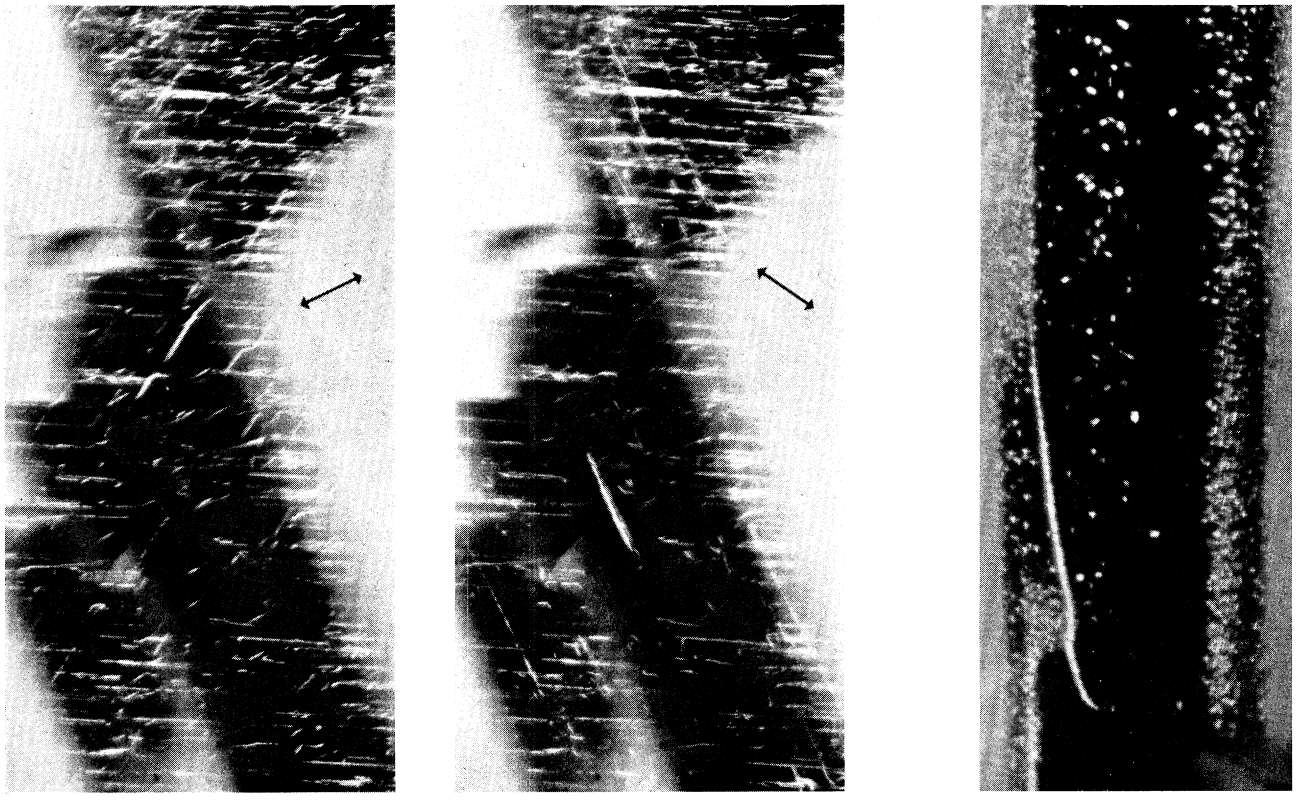

(*d*) FIGURE 6 (*e*)

FIGURE 7

(*Facing p.* 336)

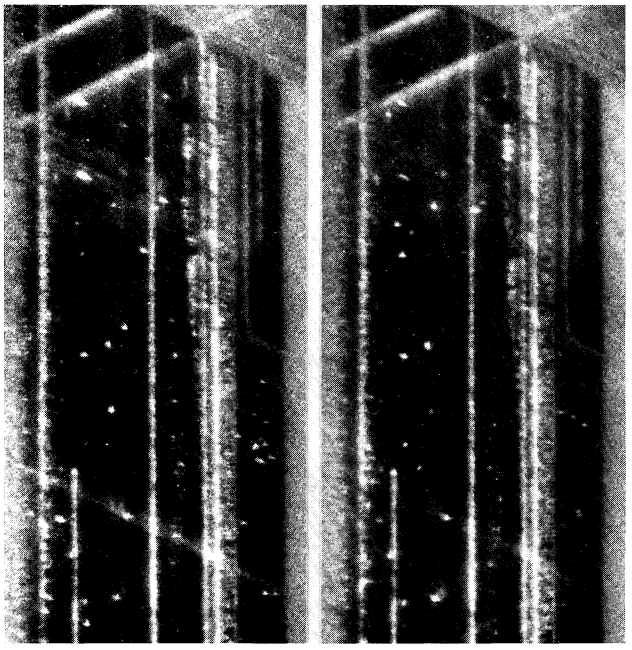

(*a*) (*b*)

FIGURE 8

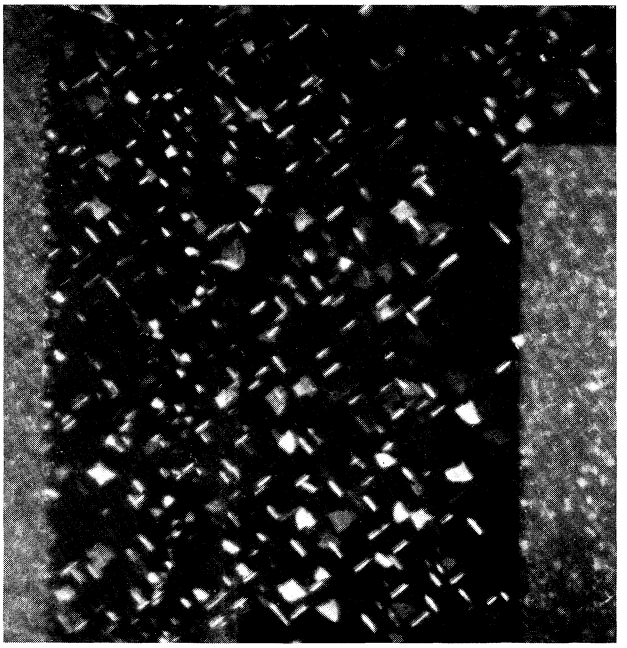

(*a*)

FIGURE 9

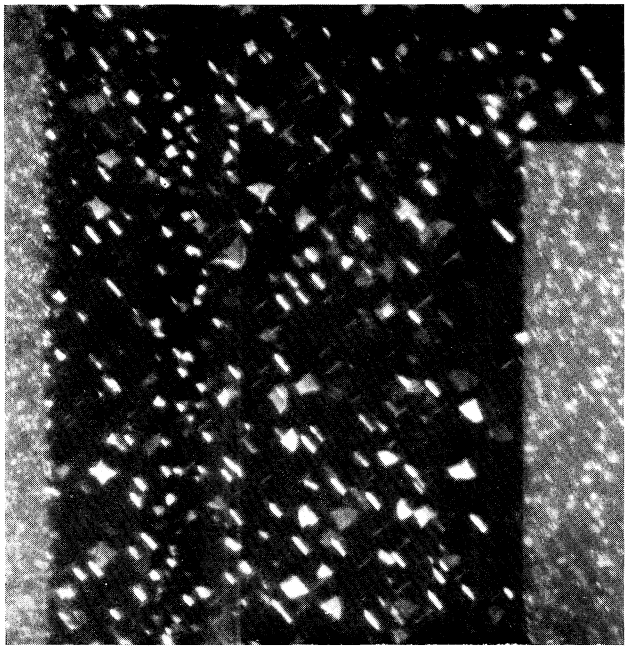

(*b*)

FIGURE 9

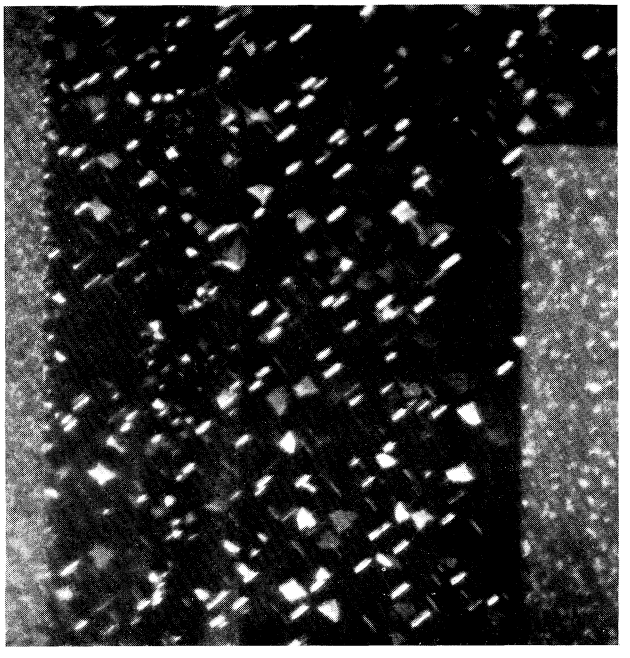

(*c*)

FIGURE 8. Polarization of emission from isolated precipitates in a layer of feeble band A cathodoluminescence which is located near the top right corner of face 'b' of specimen GH2, figure 2*b*. Orientation of figure 8 is same as that of figure 2*b*. Traces of $(11\bar{1})$ are vertical, slip traces parallel to $(\bar{1}11)$ slope down to left at about 30° with the horizontal axis, slip traces parallel to $(1\bar{1}1)$ slope down rightwards at about 30° to the horizontal and this is also approximately the direction $[10\bar{1}]$. Electron beam 35 kV, 10.5 μA mm^{-2}. Kodak–Wratten filter no. 12. (*a*) Analyser set to transmit ***E*** vector parallel to $[10\bar{1}]$. (*b*) Analyser perpendicular to setting in (*a*).

FIGURE 9. Polarization of emission from platelets parallel to {100}. Specimen CI9, surface orientation near (001), the direction [110] points horizontally to the right. Field width is 300 μm. Zones of stronger band A cathodoluminescence appear near both left- and right-hand margins. Electron beam 35 kV, 2 μA mm^{-2}. Kodak–Wratten filter no. 12. (*a*) Without Polaroid analyser. (*b*) Analyser rotated to transmit electric vector parallel to [100], i.e. along field diagonal from upper left to lower right. (*c*) Analyser set to transmit electric vector parallel to [010], i.e. along diagonal from upper right to lower left.

(0.57, 0.27) on face 'a', figure 2*a*. Figure 6 is rotated anticlockwise by about 30° relative to figure 2*a* so as to align images of 503 nm-system-emitting traces of $(1\bar{1}1)$ with the horizontal direction. (The reason for this rotation, and further description of the patterns, will be given in §7(*c*).) The upper section of figure 6, above the constriction in the layer of feebly band A-emitting crystal which forms the dark background against which the blue-emitting dislocations are seen in figures 6*b–e*, lies in one of the strongest 503 nm-system-emitting areas of specimen GH2. This area is bounded on its side more remote from the crystal centre by a curved surface, but whether the curvature is a growth feature or dissolution feature is not in this instance at all clear.

In the lower part of figure 6*a* there appear some green-yellow-emitting specks. These objects are found in several locations within type II layers in specimen GH2. An example is shown in figure 7 which shows part of the very dark strip which runs vertically on figure 2*a* upwards from the point (0.58, 0.59), some distance above the field of figure 6. This dark region abuts on its left against the rising $(11\bar{1})$ surface of a step on the local growth face (111). The material of the step produces fairly strong band A cathodoluminescence: it is seen along the left-hand edge of figure 7. The centre and right-hand areas of the figure contain growth which has filled up the re-entrant under the step. Here the green-yellow emitting objects are plentiful. The diameters of the largest are about 5 μm. Their image shapes do not conflict with identification of the objects as being platelet precipitates on {100}, but inadequate microscopic resolution frustrates closer geometric definition. Remarkable in the lower left half of the field is the bright curving line composed of a dense chain of smaller precipitates. It is believed not to be a heavily decorated dislocation (or array of dislocations), for on X-ray topographic evidence (albeit hampered by interference from polishing scratches and other accidental surface damage) this region appears dislocation-free. More likely the line represents a trace of a very thin layer parallel to a growth surface, which in this case curves off octahedral orientation. Somewhat similar traces have been encountered in other specimens.

When observing the green-yellow specks in figure 7 through a Polaroid filter it was found that rotation of the Polaroid caused relative variations in brightness between one speck and another. This phenomenon can be demonstrated better through comparison of figures 8*a* and *b* which show an area where there is a sparser population of isolated precipitates. See, for example, in figure 8*b* the lesser brightness, compared with figure 8*a*, of the two largest precipitates which appear in the upper left part of the field. Figure 8 shows the upper part of the very dark band near the top right-hand corner of face 'b' of specimen GH2, running downwards from the point (0.86, 0.98). Here the crystallography is a little simpler than in figure 7: the vertical lines, brightly decorated with green-yellow emitting specks, are traces of $(11\bar{1})$ and are parallel to the local growth layers in this zone of very weakly band A-cathodoluminescent material. Green-yellow emitting precipitates can also be seen along the edge of the stronger band A-emitting zone which runs down the left-hand side of the field: they give the impression of protruding out of this zone. It is not clear whether all of the bright vertical $(11\bar{1})$ traces contain arrays of dislocations or whether some at least are just very thin growth sheets in which the precipitate population is exceptionally dense, as in the curving line seen in figure 7. The X-ray topographs do not suggest that there are many dislocation arrays parallel to $(11\bar{1})$ in this region.

Among the cathodoluminescence observations made by S. Tolansky & M. J. Mendelssohn (1969, private communication) which helped to stimulate the work now reported were some

which showed a diamond containing green-yellow luminescing platelets up to 50 μm or greater in diameter distributed at random on {100} planes. Through the courtesy of Dr M. Mendelssohn and Dr J. Milledge this diamond (specimen CI9) was obtained on loan for optical and X-ray topographic examination. It was found to exhibit polarization phenomena very clearly, as figure 9 shows. Platelets seen edge-on give maximum intensity when the electric vector transmitted by the analyser is parallel to the platelet; whereas platelets seen face-on do not change in intensity with rotation of the analyser. Specimen CI9 was obtained in the shape of rather less than half of a slightly rounded octahedron. The internal structure was in detail quite complicated, consisting of a complex sequence of octahedral zones giving different strengths of band A cathodoluminescence and of integrated X-ray reflexion. However, the specimen as a whole could be pictured very roughly as comprising just two zones. First there was an octahedral core, about $1\frac{1}{2}$ mm in diameter (about one-third the diameter of the specimen) which was found to be a good transmitter of ultraviolet radiation. It produced weak band A cathodoluminescence and contained the large {100} platelets (the largest being in its innermost regions). Then, outside the core, growth was more normal, of type Ia, with a moderate density of grown-in dislocations. The strong integrated X-ray reflexion from the outer part of the crystal suggested a high density of sub-micrometre-sized {100} platelets therein, a supposition confirmed by the exceptionally intense and sharp 'spike' reflexion X-ray topographic images of this region. The giant {100} platelets in the core produced individually recognizable images in Bragg reflexion topographs; but the overall size of the specimen and large number of platelets, together with strong diffraction contrast generated by the zones immediately surrounding the innermost region, inhibited systematic exploration of their X-ray diffracting properties. To date, green-yellow emitting platelets have been found in eight specimens besides GH2 and CI9. In each case the radiation from individual platelets showed a high degree of polarization. In one of the eight specimens the platelets ranged up to 20 μm in maximum dimension and so were comparable in size with those shown in figure 9, plate 6.

(*b*) *Natural radiation damage*

Consider next another type of cathodoluminescence that appears in a distinctive topographic context. The association now is with the external surface of the crystal, and by this is meant the *present* surface which more often than not is a dissolution surface cutting across growth zones (as it does in diamonds with the commonly occurring rounded rhombic dodecahedral habit (Moore & Lang 1974)). In specimen S1 and other thin slices occasional reddish tints were noticed around the specimen edge, especially at points where green-yellow emitting bands reached the edge. An opportunity arose to look for cathodoluminescence definitely associated with external surfaces during the study of polished sections prepared from a whole diamond, of

---

DESCRIPTION OF PLATE 7

FIGURE 10. Emission of the 2.16 eV (575 nm) system occurring as a characteristic of proximity to the natural external surface of the crystal. Sections of specimen (number GDO6) polished parallel to (001). Traces of {111} run horizontally and vertically. Field width 265 μm. Electron beam 35 kV, 5.7 μA mm^{-2}. (*a*) Corner of section including some sloping external surface. (*b*) Field near a section corner showing weak 575 nm-system emission from some areas remote from the section edge in addition to strong emission from regions close to the edge. (*c*) Emission of 503 nm and 575 nm systems from regions containing slip traces. (*d*) Localized emission of 503 nm and 575 nm systems attributed to radiation damage surrounding an embedded radioactive inclusion near centre of field.

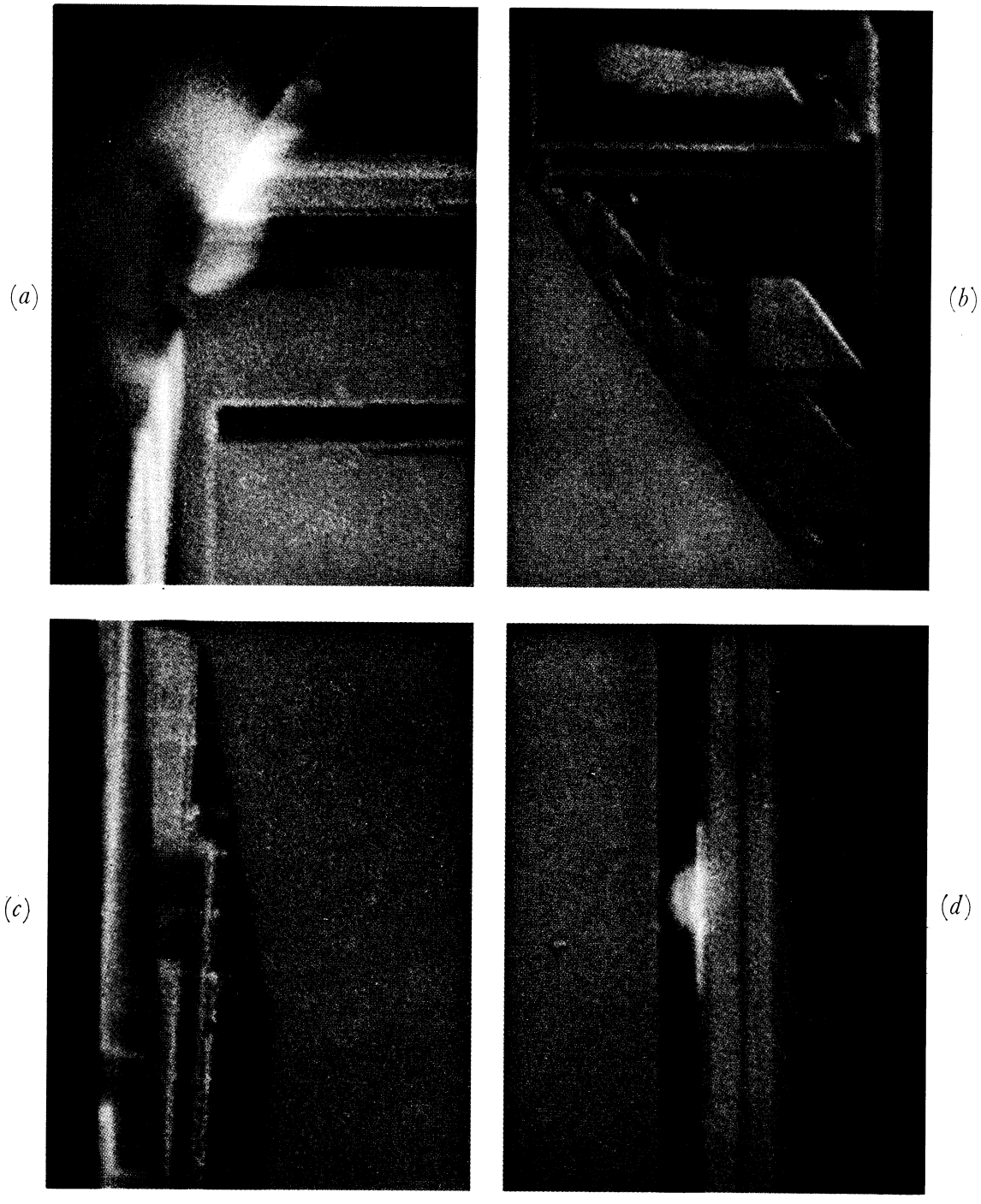

FIGURE 10. For description see opposite.

rounded habit, whose external surface had been examined before sectioning, and verified as being entirely natural. Consequently, except at a very few points where a little chipping had occurred during polishing, it was certain that the specimen edge coincided with the natural external surface. The crystal contained some thin bands of ultraviolet transparent and feebly band A-cathodoluminescent growth in its outermost regions. Figure 10*a–c*, plate 7, displays representative examples of the main types of cathodoluminescence pattern observed around the peripheries of the three polished sections examined. The phenomenon illustrated in figure 10*d*, on the other hand, is the sole representative of its class so far encountered. Figure 10*a* shows one of the rounded corners of a section. Where type II bands meet the surface they exhibit orange or red cathodoluminescence. The upper left of the field includes some of the external surface of the crystal, sloping away down below the plane of focus. The bright red type II bands could be followed downwards over the external surface by focusing the microscope downwards. Figure 10*b* is also near a corner, but here (as in figure 10*c*, *d*) no external surface comes into view beyond the edge of the polished section. In this field the stratigraphy is extremely complex and includes traces of surfaces other than {111} facets. Some blue-emitting dislocations can be seen. However, the chief feature to note is that some of the feebly band A-cathodoluminescent areas remote from the bright red 'rind' of the crystal do exhibit a reddish component in addition to their principally dark blue emission. The red emission seen in figure 10*a–d* was spectrographically identified as the 575 nm system: its spectrum, and its occurrences in other crystals, will be discussed in § 5. The field in figure 10*c* contains slip traces on octahedral planes which run out perpendicular to the crystal edge. Within the innermost dark blue zone the dislocations are mainly blue-luminescent. Closer to the crystal edge their luminescence is dominantly the 503 nm system. In the layer close to the surface the 575 nm system and the 503 nm system both appear. Observations on numerous external-surface outcrops of homogeneous type II bands free from slip traces show a monotonic decrease in strength of the 575 nm system emission with increasing depth below the external surface; and except in the few cases where the matrix shows a red component in its body tint, this system becomes imperceptible at depths below about 25 to 30 μm. The best estimate of maximum thickness of the red 'rind' is 29 μm. Figure 10*d* shows a circular orange patch of 503 nm and 575 nm system emission within a type II layer 100 μm below the crystal surface. The circular patch is surrounded by a halo about 30 μm in radius. There also appears a thin bright blue band along the right-hand border of the type II layer, extending from 40 μm above to 60 μm below the level of the centre of the orange disk. It may correspond to a grid of dislocations lying in the border, for there is some indication of dislocation images spreading from it inwards into the type II layer, below the lower limb of the halo. The most obvious explanation of the circular disk and halo is that they arise from radiation damage from α-particles emitted by a radioactive inclusion near the centre of the circular patch. No foreign particle can be seen, but it might have been embedded in material removed during polishing.

(*c*) *Mosaic type II diamonds*

Diamonds which are throughout their volumes wholly type II commonly exhibit one or other of two characteristic forms of birefringence, best recognized when the specimen is in the shape of a parallel-sided plate. In the one form the birefringence is very intense and exhibits the 'tatami' pattern (Takagi & Lang 1964; Lang 1967) interpreted as resulting from strong plastic deformation with little subsequent annealing. In the other form the birefringence is

milder: X-ray topographs show the crystal to be a close approach to the ideal mosaic, though still containing long-range elastic strains; and both X-ray and birefringence topographic patterns look rather similar. In the mosaic case the whole volume is divided into cells, usually about 10 μm in diameter but occasionally rather larger, mutually misoriented by angles of a few minutes of arc as measured by X-rays. It can be assumed therefore that the cell walls contain networks of dislocations: the X-ray topographic images are consistent with this model but the dislocations in the walls are too close together to be resolved individually. The mosaic structure is believed to result from polygonization of a plastically deformed diamond. Often the mosaic texture exhibits a well-defined 'grain', but whether this represents the remains of an original deformation pattern or is due to continued shear during or after polygonization is not known. The cathodoluminescence pattern of the crystal surface shown in figure 11, plate 8, exhibits a fairly distinct grain which can be picked out very well through rotation of the Polaroid analyser because the blue-emitting dislocations (which stand out brightly against the dark blue background of dislocation-free matrix) emit, as usual, radiation strongly polarized with $\boldsymbol{E}$ vector parallel to the dislocation line. It is not a photographic accident that many mosaic cell walls appear bolder in figure 11*a* than in *b*. The difference arises from the relatively high proportion of cell-wall dislocation segments running vertically parallel to [$\bar{1}$10]. Note in figure 11*a* the number of short bright vertical streaks produced by the individual dislocations within the cells, and the lesser number of horizontal (or near horizontal) streaks in figure 11*b*. Elsewhere on this surface there can be seen diffuse slip bands with vertical traces. Similar cathodoluminescence patterns were found in other type II diamonds characterized by X-ray topography as possessing the mosaic structure. The specimen shown here (number JT1) has a cell structure particularly well-defined and large (the cell diameters were mainly in the range 30 to 50 μm), and its cell interiors were unusually uncluttered by random dislocations. Specimen JT1 belonged to the rare semi-conducting class, type IIb; but neither in it nor in another type IIb specimen examined (number JT2) did X-rays or cathodoluminescence reveal dis-

---

Description of plate 8

Figure 11. Cathodoluminescence from dislocation networks and from individual dislocations in a type II diamond, specimen no. JT1. Surface 4° off (111) orientation, the direction [$\bar{1}$10] is vertical. Field width is 250 μm. Electron beam 25 kV, 12 μA mm^{-2}. (*a*) Polaroid analyser set to transmit electric vector in vertical plane, parallel to [$\bar{1}$10]. (*b*) Polaroid set to transmit electric vector in horizontal plane.

Figure 12. Spectrum topograph showing principally the H3, 2.46 eV, emission system from slip traces on face 'b' of specimen GH2. Spectrum height takes in a vertical strip 3.7 mm long on figure 2*b*, running from the point with fractional coordinates (0.22, 0.98) down to the point (0.22, 0.30). Hilger Medium Quartz spectrograph. Spectral range reproduced in figure runs from 401 nm to 593 nm. Electron beam 20 kV, 2.5 μA mm^{-2}. Specimen temperature 310 K: at this temperature the measured wavelengths of the lines indicated are 416 nm, 485 nm, 504 nm, and 540 nm. (Inset is a high-contrast print to show up the weak 485 nm line at the location on spectrum topograph where it is most visible.)

Figure 13. Spectrum topographs showing principally the 3H, 2.46 eV, system emitted from regions close to the natural surface of a type IIb diamond (specimen JT1). Spectral range reproduced is 468 to 600 nm, photographed via the direct-vision spectroscope on to Ilford FP4 emulsion. Electron beam 50 kV, 1 mA mm^{-2}. Strips on specimen surface in spectra (*a*) and (*b*) are each 38 μm long. Below (*b*) from left to right, the calibrating low pressure Hg arc lines are at 491.6 nm, 496 nm, 546.1 nm, 577 nm and 579.1 nm.

Figure 14. Spectrum topograph showing principally the 2.16 (575 nm) system emitted from regions close to the natural surface of specimen GDO6. Spectral range reproduced is 486 to 650 nm, photographed through the direct-vision spectroscope on to Ilford Astra III plate. Electron beam 50 kV, 1 mA mm^{-2}. A strip of length 100 μm on the specimen surface is imaged in the spectrum. Calibrating low pressure Hg arc lines visible on the print are, from left to right, at 491.6 nm, 546.1 nm, 577 nm and 579.1 nm.

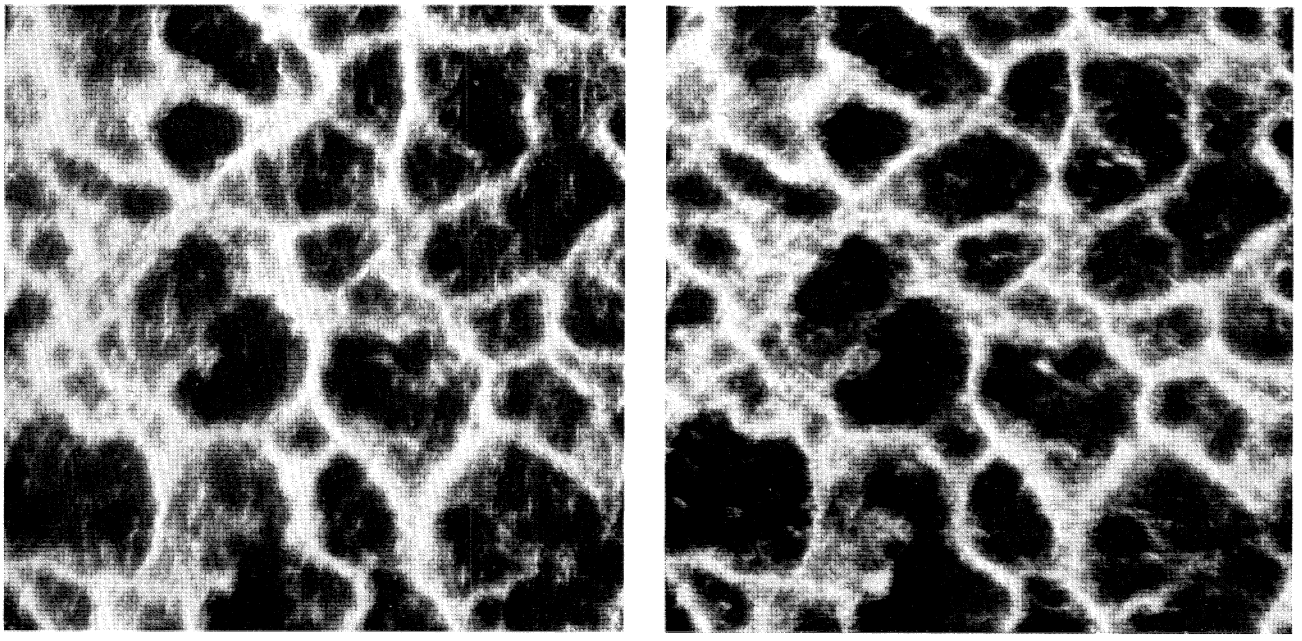

(*a*) FIGURE 11 (*b*)

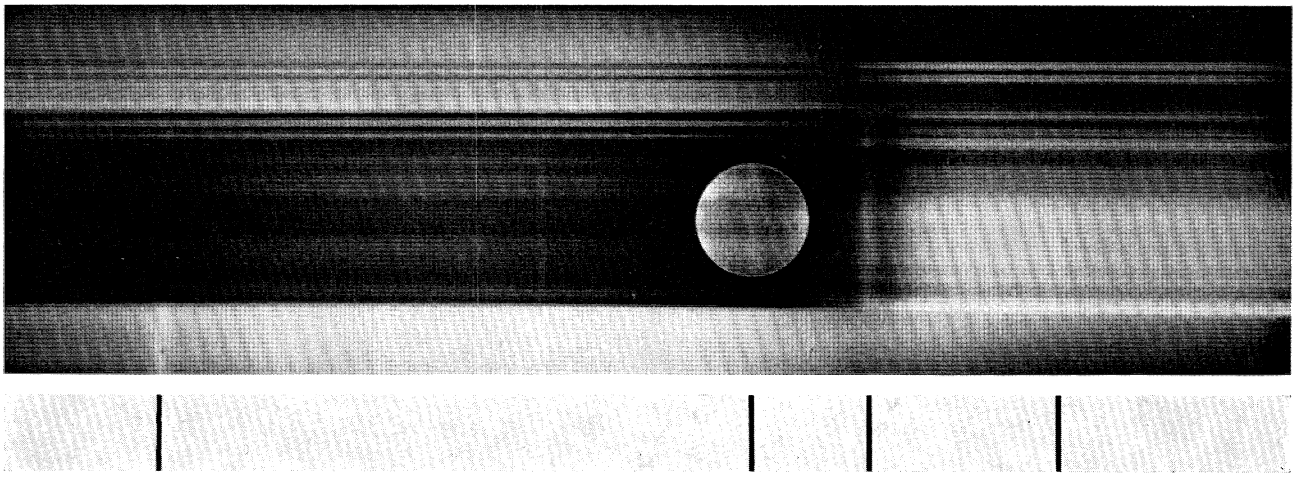

FIGURE 12

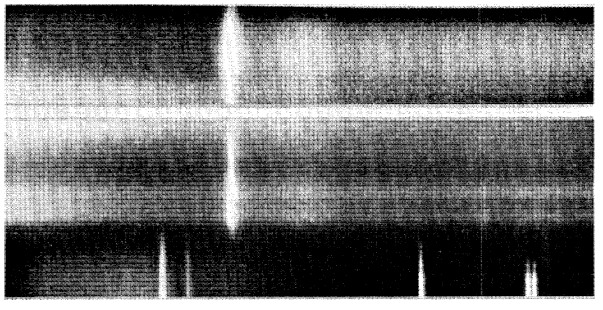

FIGURE 13

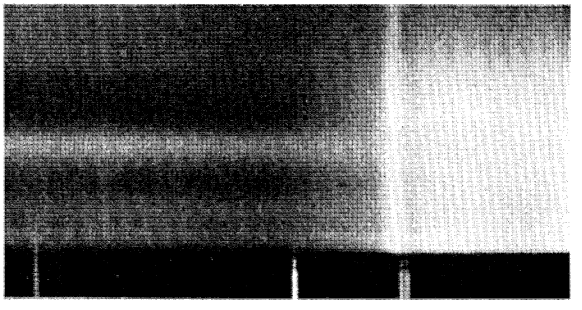

FIGURE 14

(*Facing p.* 340)

location configurations which would distinguish them from other mosaic diamonds belonging to the more common type IIa, insulating class. The dislocation configuration shown up by cathodoluminescence quite strongly resembles that found on a scale about ten times larger in magnesium oxide crystals (Lang & Miuscov 1964). In the latter substance the configuration could be made clearly visible by X-ray topography because of the larger mosaic cell size and the nearly complete removal of long-range elastic strains by annealing.

(*d*) *Framesite*

Finally, cathodoluminescence observed from the natural polycrystalline diamond, framesite, will be briefly mentioned. The recently published finding by De Vries (1973) that slip traces on {111} in individual grains in framesite show greater abrasion resistance than the crystal immediately surrounding them, standing up as narrow ridges about 1 μm wide and 40 to 60 nm high, bears a striking similarity to the observation of upstanding slip traces in specimen S5 (figure 1*a*) which was made at an early stage of the investigations reported in this paper. In a preliminary study of framesite cathodoluminescence a roughly spherical lump of framesite about 8 mm in diameter was polished on one side sufficiently to produce a few square millimetres of tolerably flat surface. Unfortunately, no upstanding slip traces could be positively identified on this area. On the other hand, the cathodoluminescence patterns were quite rich in evidence of slip. There was a fairly low level of band A cathodoluminescence in most grains, and this provided favourable conditions for observing both the polarized blue emission from dislocations (occurring individually or in slip bands) and the unpolarized 503 nm system emission which was also largely associated with slip bands. Sometimes both emissions occurred quite close together within the same grain.

4. Localized sources of 2.46 eV (503 nm) system emission

(*a*) *Slip traces*

Figure 12, plate 8, shows one of many spectrum topographs crossing regions of interest on the surfaces of specimen GH2 which were recorded with the Hilger spectrograph. It includes the typical spectrum produced by bright green-yellow emitting slip traces found in this and other diamonds. The calculated width of the strip on the crystal that contributes to this spectrum topograph is 20 μm, but making an allowance for optical aberrations puts its effective width nearer to 30 μm. The top of the strip corresponds to the point (0.22, 0.98), near the upper edge of figure 2*b*, where the boundary of the zone of feeble band A cathodoluminescence occupying the extreme left of figure 2*b* turns upwards to run straight towards the top edge of the specimen. From this starting point the strip runs vertically downwards through the band A-emitting zone of medium strength outside the ultraviolet transparent zone. Then it crosses two narrow layers containing arrays of dislocations parallel to $(\bar{1}11)$: the spectral images of these two layers stand out sharply in the top quarter of figure 12. In the middle levels of figure 12 the strip keeps within the vertical ultraviolet transparent zone parallel to $(\bar{1}\bar{1}1)$. In the lowest part of the spectrum topograph the strip has entered the strongly band A-emitting innermost zone on this specimen surface; and its termination is at the point (0.22, 0.30). Figure 12 illustrates the generally observed complementarity of the band A and the 503 nm system emissions (at least so far as crystal interiors rather than surfaces are concerned, cf. §4 (*d*)). Accuracy of wavelength measurement cannot be expected from these vertically extended spectra because of line curvature

in the spectral image plane. Moreover, the high specimen temperature (310 K) compared with that (*ca.* 80 K) at which diamond spectra are usually recorded introduces an upward shift of about 1 nm in the wavelengths of the recognizable sharp lines compared with their commonly quoted low-temperature values. Thus the zero phonon lines of the systems called N3 (Clark, Ditchburn & Dyer 1956*a*) and H3 (Clark, Ditchburn & Dyer 1956*b*), whose energies and wavelengths are given by Clark (1965) as 2.989 eV, 415.2 nm, and 2.463 eV, 503.2 nm, respectively, appear in figure 12 at 416 nm and 504 nm. In all that follows the 503 nm system which is exhibited in figure 12 will be called by its name H3, both for reasons of brevity and also to distinguish it from another system with zero phonon line at 2.46 eV which will be described in §4(*d*). (The weak lines appearing at 485 nm and 540 nm indicated in figure 12 will be discussed in §6(*a*).) An incidental advantage of this particular technique, whereby spectra from localized sources are recorded spatially separated, is the good spectral contrast that may be realized even at temperatures higher than 300 K. Thus, for example, on the original plates the first and second phonon-assisted peaks of the H3 system (maxima at about 513 nm and 520 nm respectively) can be seen distinctly. These peaks do not appear to be resolved in recordings by conventional methods of the H3 system in room-temperature cathodoluminescence (cf. figure 6*a* of Collins 1974), nor in ultraviolet excited fluorescence at room-temperature (Dyer & Matthews 1957). It does seem, on the other hand, that in the room-temperature fluorescence spectrum topographs taken of two purely yellow-luminescent diamonds by Mani (1944*b*) a spectral definition of the H3 system comparable with that obtained in the present experiments was achieved. (It was discovered at the conclusion of the work here reported that the topographic recording of diamond spectra had been initiated by Mani (1944*b*, *c*), and applied to ultraviolet excited luminescence spectra.)

No polarization has been detected in the intense cathodoluminescence from strong slip traces such as appear in figures 1*c*, 2, 4*a*, 5*a* and 6*a*; nor, at the other extreme of brightness, from a very feeble green-yellow luminescence (H3 system, it may be assumed) emitted by individual dislocations in the innermost zone of specimen CI9. However, in some intermediate cases, where fine-scale networks of blue-emitting and H3 system-emitting dislocations occurred together, and with their images in part superimposed, the H3 emission did have a semblance of partial polarization, with its plane of polarization the same as that of the strongly polarized blue emission from the dislocations. Unfortunately, there is a degree of spectral overlap between the H3 system and the polarized broad-band blue emission from the dislocations which is sufficient to render it most difficult to establish to what extent, if indeed any at all, there exists polarization of the H3 system emission in these instances.

The best contrast of the H3 system relative to the band A background was obtained at specimen currents less than 1 μA mm^{-2}. However, band A-emitting regions differed among themselves in their responses to current changes. Indeed the brightness of band A emission from some areas increased faster than linearly with current density. Nevertheless, it appeared definite that at specimen currents above a few μA mm^{-2} the H3 system, when associated with slip traces, began to saturate. For example one assessment of brightness changes occurring in the high current-density range may be cited, the subject being a region of strong H3 emission surrounding an inclusion near the centre of one specimen (number S2). A decrease in electron spot diameter from 500 μm to 100 μm and increase in current from 0.3 μA to 8 μA, giving a 670-fold increase in current density from 15 μA mm^{-2} to 1 mA mm^{-2}, was accompanied by only a 100-fold increase in brightness of the H3 system emission. However, the factor which

affected the images of H3-system emitting slip traces most remarkably was the nature of the matrix in which they lay. The lower the level of band A cathodoluminescence background (and, in those cases where it was measured, the higher the ultraviolet transparency) the greater the depth from which slip-trace luminescence was visible. This effect could be demonstrated very well in a narrow (*ca.* 50 μm wide) highly ultraviolet transparent zone in specimen S1. An intense astigmatic electron spot (30 kV and 1.5 μA impinging on a strip 100 μm long by 10 μm wide) was aligned parallel to the zone so that no flanking region giving appreciable band A emission was directly hit. Under these conditions those H3 system-emitting slip bands cutting across the type II zone which were also intersected by the electron beam flared out strikingly, both laterally and in depth. They displayed bright images extending across the full width of the type II zone, but not beyond it; and they could also be seen dipping into the specimen, down to true depths from 25 to 30 μm below the surface.

(*b*) *Platelets on* {100}

In spectrum topographs of fields containing large platelets the spectra of individual platelets stand out as fine streaks upon the band A background. In the yellow and orange regions of the spectrum the contrast is good; but at lower wavelengths the platelet emission becomes lost in the rising intensity of the band A spectrum, and in observations made so far, all of which were at or above room temperature, the line at 2.46 eV has not yet been photographically detected. However, no reason for doubting that the emission is the H3 system has been uncovered in any experiment. When fields containing both platelets and H3-system emitting slip bands are examined through a graded-spectrum interference filter no difference between their emissions can be detected in any part of the spectrum. Strong evidence that both platelets and slip bands exhibit the same emission system is derived from the indistinguishability of their behaviour under a wide range of excitation conditions, sufficient to vary their brightness by a factor of at least 10^4; for it appears that the law of intensity variation under varying conditions of stimulation stamps a cathodoluminescence centre as characteristically as does its spectrum.

No colour differences between platelets parallel to (100) and parallel to (010) can be detected when they are viewed simultaneously along [001] through a rotating Polaroid filter. This is a sensitive test showing that effectively all their visible spectral emission is polarized to the same degree. Measurements of the polarization ratio were performed on the largest platelets, maximum diameters *ca.* 80 μm, by visual brightness matching by means of combinations of Polaroid and neutral density filters. The ratio of intensity of light emitted with $\boldsymbol{E}$ vector in the plane of the platelet to that with $\boldsymbol{E}$ vector normal to the platelet was 10.5, with an error believed not to exceed 10 %. No evidence of circular polarization was found in the emission from platelets viewed perpendicularly to their planes.

When large platelets just below or cutting the specimen surface were viewed through the blue-band passing filter number 47B it was noticed that band A cathodoluminescence immediately surrounding each platelet was weaker than average: the platelets were surrounded by a dimmer zone between 5 and 10 μm thick overall, measured normal to the platelet. This phenomenon (which, so it later came to light, had been noticed by Dr M. Mendelssohn on her original cathodoluminescence photographs of this specimen (Mendelssohn 1971)) was visible to the eye over the current–density range 1.5–30 μA mm^{-2}. Photographic studies of the dim zones, recorded through the 47B filter, were performed within a current density range from 6.5 down to 5×10^{-2} μA mm^{-2}. At the upper end of the range the contrast was quite marked,

the brightness of the dim zone being about half that of the surrounding matrix. At the lower end of the range the contrast of the dim zone had almost disappeared. In these experiments the general behaviour of the band A cathodoluminescence, within this current density range, can be described as follows. Whereas the brightness of the dim zone increased linearly with current density, that of the matrix as a whole increased faster than linearly. From this difference arose the better visibility of the dim zone at the higher current densities. It was also noticed that in the regions of weakest band A cathodoluminescence the platelets themselves became faintly visible in photographs taken through the 47B filter when current densities of 1.25 μA mm^{-2} or lower were used. This platelet visibility implies either a redistribution of intensity in the platelet spectrum towards lower wavelengths when current densities are lower, or an increase in intensity of the H3 system as a whole relative to the band A cathodoluminescence. That the above-mentioned platelet visibility should be attributed to absence of saturation of the H3 emission at the lower current densities is regarded as the more probable explanation, and is not unexpected in view of the patent saturation of H3 emission from slip traces at very high current densities, as described above in §4(*a*). It may be that the platelet emission spectrum, like that of slip bands shown in figure 12, does contain weak components at wavelengths lower than 503 nm: but the presence of such would be hard to confirm spectrographically. (The transmittance of the 47B filter is 0.17 % at 500 nm, but rises to 1.3 % at 490 nm.)

(*c*) *Growth bands in 'cuboid' growth sectors*

As mentioned in §3(*a*), figure 5*a* shows features demonstrably emitting the H3 system which are other than obviously recognizable slip traces. First, there are thin bands of strong H3 system emission running parallel to traces of octahedral facets. These are seen in the top part of figure 5*a*. Secondly, some of the curvilinear bands parallel to cuboid surfaces in the lower half of the figure exhibit very intense H3 system emission. Now whether the thin bands parallel to {111} are always associated with dense networks of dislocations in an interface between zones of differing lattice parameter, or whether they represent a volume distribution of sources not associated with dislocations, cannot be determined with the available topographic resolution. However, associations with high dislocation density certainly occur in some instances, as in the flaring band in the top part of figure 5*a* which coincides with a strong vertical slip band. There occur elsewhere on the surfaces of specimens S1 and S5 larger areas of H3 system emission bounded on both inner and outer sides by traces of octahedral facets: but these also occur in association with the blue emission from dislocations. Returning to consider the bright curvilinear bands in regions of cuboid growth, it might be argued that their brightness (which is great enough to cause some flaring in the photograph figure 5*a*) arises from the enhancement of luminescence of closely spaced slip bands where they pass through particular cuboid layers. In dislocation-rich areas such as the field of figure 5 such may indeed occur; but on evidence from other fields in specimen S1, and from several other specimens, it is concluded that there definitely can exist volume distributions of unresolved sources of H3 system cathodoluminescence within the curving growth layers of cuboid growth sectors. They can occur in the absence of dislocations identifiable on X-ray topographs. (Thus, by this experimental criterion, the presence of a population of dislocation loops with diameters of 1 μm or less is not excluded.) They always occur where the band A cathodoluminescence is weak. The intensity can vary widely: in specimen S1 it is particularly intense, but in cuboid growth in other crystals it may be so weak as to be barely perceptible by eye or detectable with a graded-spectrum inter-

ference filter. One striking occurrence will be described. In the specimen concerned (number MS3) cuboid growth was dominant in the central parts of the crystal. Near the outer limit of cuboid growth there was a well-defined shell of very weak band A cathodoluminescence, about 15 μm thick. This could be easily recognized in each quadrant of the (001) surface of the near central slice through the crystal that this specimen comprised. A green-yellow band about 10 μm thick lay symmetrically in the centre of the shell, and was flanked on each side by dark bands about $2\frac{1}{2}$ μm thick occupying the space between it and the adjacent zones of higher band A cathodoluminescence. Also, in the regions of transition from cuboid to octahedral growth there existed areas of similar green-yellow emission which showed up as islands in the centres of the triangular-shaped areas of very weak band A emission which, similar to those illustrated in figure 4, were bounded on the inside by cuboid surfaces and on the outside by {111} facets. In this specimen the brightness of H3 system emission from bands in cuboid growth sectors was estimated by means of neutral density filters to be only about 1 % of that produced by a region of slip surrounding a central inclusion in the crystal. Though recognizable to the eye, such weak and localized H3 emission would be difficult to record spectrographically.

(*d*) *Regions contiguous with external surfaces*

While examining the surface of specimen JT1 visually through the microprobe microscope, using a low specimen current, we noticed that within a distance of about 20 to 30 μm from the periphery of the specimen the emission from dislocation networks (such as those illustrated in figure 11) was weaker than elsewhere. The weakening was evident at both high and low beam currents. Moreover, at high beam currents a green luminosity could be detected coming from the dislocation-free interiors of those cells whose bounding walls of dislocation networks exhibited the diminished blue emission. The green emission could be detected only in the narrow strip that lay between the specimen edge and points not further than 25 to 30 μm from the edge, however strong the electron beam was made. Figure 13*a* and *b*, plate 8, show two spectra of the green 'rind' of this crystal, obtained from points a few millimetres apart along the specimen edge. The photographs were taken with the Beck direct-vision spectroscope. Only the spectral range from 468 nm to 600 nm is reproduced in these prints. Below spectrum (*b*) can be seen the calibrating lines from a low-pressure mercury lamp. Dominating all other emissions in both diamond spectra, from near ultraviolet to the upper wavelength limit of sensitivity of the Ilford FP4 emulsion (*ca.* 650 nm), is the green line whose measured wavelength is 504 nm. The upper spectrum was deliberately over-exposed with respect to the 504 nm line so as to show better the longer-wavelength phonon assisted band associated with it. Other weak lines present in the spectra will be considered in §6(*b*). Patently this 504 nm emission system differs from the H3 system recorded in figure 12. Not only is the phonon-assisted band appearing in figure 13 very much weaker relative to the zero phonon line than is the case in the H3 system, but its energy spacing is quite different. The diffuse emission seen adjacent to the 504 nm line on its low-energy side in figure 13 spreads from roughly 2.41 eV (514 nm) to 2.37 eV (523 nm). The best estimate of the energy and wavelength at its maximum is 2.39_6 eV (518 nm), which is 65 meV lower in energy than the zero-phonon line. The diffuse phonon-assisted peaks resolved on the long wavelength side of the 504 nm line in figure 12, on the other hand, have the spacing of about 40 meV that is a well documented feature of the H3 system (Mani 1944*a*; Dyer & Matthews 1957; Dean *et al.* 1960). A further distinction between these two emission systems is that whereas the H3 system (at least when associated with platelets and

dislocations) saturates at high specimen current densities (as already described in §4(*a*) and §4(*b*)) the system shown in figure 13 presented no obvious signs of saturating, even at current densities as high as 1 mA mm^{-2}.

Now it is strange indeed that only very recently has it been realized that there are two (at least) absorption/emission systems with zero phonon lines of energy *ca.* 2.46 eV in diamond. Explicit cognisance of this fact is taken by Davies (1974) and Walker (1975) who both describe an absorption system exhibiting very weak phonon coupling compared with the H3 system, and in which the dominant phonon energy is *ca.* 66 meV. This system has been named '3H' by Walker, which designation will for convenience here be adopted. The spectra reproduced in figure 13 clearly provide good examples of the 3H system, as manifested in cathodoluminescent emission some degrees above room temperature.

The few spectrographic identifications of the 3H emission system performed so far in the course of experiments now reported have been confined to natural radiation-damaged material close to the external surfaces of diamonds. The 3H system was observed around the periphery of a polished section of another type IIb crystal (specimen number JT2) but in this case the cathodoluminescence not localized at dislocations was dominated by the 2.16 eV (575 nm) system which will be discussed in §5 below. On the natural surface of a type IIa specimen (number Ca/2) the 3H system could be locally excited strongly by an intense electron beam. The sites of this emission could be recognized by examining the external surface with a low electron beam current. The crystal was of the mosaic type, and dispersed among the tracery of blue emission from dislocation networks were irregular patches, roughly 50–100 μm in diameter, where the blue luminescence was dimmed. These were the areas from which 3H system emission could be well observed at higher beam currents.

A recent development in the study of diamond cathodoluminescence has been directed towards the correlation of the microtopographic relief on natural diamond surfaces (as seen with conventional optical techniques, e.g. phase contrast, Nomarski interference and multi-beam interference micrography) with the outcrop patterns of finely spaced growth strata differing in impurity content which can be mapped via microphotography of the colour and intensity of their cathodoluminescence (Moore & Lang, to be published). A fairly well-formed octahedron, of about 1½ mm edge length, was kindly lent to one of the authors (A. R. L.) by Dr A. D. Yoffé, Cavendish Laboratory, Cambridge, following the discovery of crystallographically oriented features in the pattern of cathodoluminescence on one of its faces when imaged by a scanning electron microscope operating in the cathodoluminescence mode (Howlett 1974). The features of immediate relevance to the present discussion were, however, non-crystallographic in their geometry, and consisted of areas of diminished cathodoluminescent intensity, as recorded by the photomultiplier output. These areas consisted either of haloes about 28 μm in diameter with a central dark patch, or of uniformly dark patches irregular in outline. Visual examination of the surface when it was illuminated by a broad electron beam in the authors' microprobe apparatus showed that whereas the diamond as a whole exhibited weak band A cathodoluminescence (roughly a few parts per cent the strength of that typically produced by diamonds which give strong 'spike' X-ray reflexions), in the dark patches the band A emission appeared so weak as to be barely visible to the eye at beam current densities of 1 μA mm^{-2}. Upon increasing the current density on the dark patches their behaviour was similar to those on the surface of the type IIa specimen, number Ca/2, described above. The dark areas brightened, appearing first grey, and then, at beam currents of 1 mA mm^{-2} or more,

distinctly green. However, irradiation for but a minute or two at 40 kV and 1 mA mm^{-2} sufficed to cause the green to fade and be replaced by a faint pink. Spectroscopic observation verified that the green emission was the 3H system, and that under electron irradiation the 575 nm system developed in its place (though generally not strongly). The rapid decay of the 3H system on this specimen rendered it difficult to record the wavelength of its zero phonon line; but it was possible to do so visually by means of a small constant-deviation spectroscope fitted with a low-power filar ocular, and the reading was $503\frac{1}{2}$ nm. It is necessary to consider whether the fading of the 3H system is due to heating by the electron beam or to irradiation *per se*. The diamond was embedded in a fusible alloy (Rose metal, m.p. *ca.* 100 °C). That the alloy did not melt was attested by absence of movement of the diamond. The heat flow situation is analogous to that in the target of a microfocus X-ray tube (Ehrenberg & Spear 1951). The comparison indicated that even at the highest current densities the temperature difference between the irradiated area and the surfaces in contact with the Rose metal would not exceed a few degrees. An upper limit of *ca.* 380 K is therefore assumed for the temperature of the irradiated area. Consequently, the observed fading of the 3H system at the surface of this crystal was attributed to the electron irradiation in the apparatus rather than to annealing.

However, it should not be thought that 504 nm emission from natural radiation damage at diamond surfaces necessarily implies the 3H rather than the H3 system, as was demonstrated by another experiment. Among a dozen or so small diamonds (mean mass about 0.07 g) sectioned and polished in the laboratory (for which work the authors are indebted to Dr G. S. Woods) several specimens showed signs of radiation damage locally or completely around their section peripheries: 575 nm system emission superimposed on H3 system emission, or green emission superimposed on band A cathodoluminescence being the relevant diagnostic features. One specimen (number A9), of diameter 2 mm, was a smooth-surfaced rounded rhombic dodecahedron, well exemplifying this common diamond dissolution form (Moore & Lang 1974). X-ray topography showed that it had crystallized by normal {111} faceted growth; and the diffraction contrast characteristics of its X-ray images suggested that it was a strong type Ia specimen. Its type Ia nature was confirmed by band A cathodoluminescence, which was in fact unusually deficient in growth stratigraphic detail. Very uniformly developed around the periphery of the section was the green rind, strongly visible up to a distance of 15 to 20 μm from the natural surface of the crystal, and then weakly from that depth down to a maximum depth below the surface of 28 to 29 μm. Not only was the H3 system displayed in the emission from the rind, but also the H4 system (Clark *et al.* 1956*b*; Collins 1974). In order to verify the apparent similarity of the spectrum with that reported as given by laboratory-irradiated and annealed specimens, a comparison was made with such a specimen which had been kindly lent by Professor W. A. Runciman (Australian National University, Canberra). This specimen, which was fashioned as a polished rectangular parallelipiped, is believed to be that whose infrared absorption spectrum was published by Runciman & Carter (1971) as their figure 1*b* (W. A. Runciman, private communication). The specimen was type Ia diamond, had been irradiated with a dose of 6×10^{18} electrons cm^{-2} of 1 MeV energy and subsequently annealed at 680 °C for 30 minutes. Cathodoluminescent topographic examination of this specimen revealed a well-developed fine-scale stratigraphic pattern following traces of {111} facets which was emphasized by the considerable variations between adjacent growth layers in the strength of the generally intense H3 and H4 system emissions which they were found to display. It was arranged experimentally that an edge of specimen A9 abutted against an edge

of Professor Runciman's specimen, with a minimum gap of about 50 μm between them, and with their polished surfaces raised to the same level so that they could be simultaneously brought into focus under the microprobe microscope. The intensity of H3 and H4 emissions from the laboratory-irradiated specimen was estimated to be at least an order of magnitude stronger than from the rind of the dodecahedral diamond. However, by controlling the distribution of the electron beam between the two specimen surfaces, their brightness could be roughly equalized. Then close comparison of their spectra could be effected by simultaneously focusing images of the two surfaces on the entrance slit of the direct vision spectroscope. The two spectra were remarkably alike, both with respect to the intensity ratio of the H4a line to the H3a line (the former having roughly one-quarter the intensity of the latter), but also with regard to the overall spectral distribution of emission. Indeed, the only noticeable difference was that the laboratory-irradiated specimen showed local strong emissions of the 2.16 eV (575 nm) system, whereas no 575 nm line could be detected visually in the emission from the periphery of the dodecahedron section.

5. Localized sources of 2.16 eV (575 nm) system emission

The two topographic associations of the 2.16 eV (575 nm) system discovered to date are, firstly, with regions contiguous to natural external surfaces of diamonds, and, secondly, with dislocation-free type II zones within the crystal interiors. A striking occurrence in the first case has been discussed in § 3 and exhibited in figure 10. In this topographic setting it would appear beyond reasonable doubt that radiation damage from natural α-particles has led to the development of the cathodoluminescent properties now displayed. In all the examples encountered where the 2.16 eV system is emitted from interior volumes of crystals, its intensity has been very much weaker than that from radiation-damaged rinds; so much weaker, in fact, that in only three cases was it possible to confirm its presence with the direct-vision spectroscope. (Professor Runciman's laboratory-irradiated specimen discussed in § 4(*d*) is of course excluded from this count.)

Figure 14, plate 8, shows part of the spectrum from one of the type II zones which was free from green-yellow emitting dislocations in specimen GDO6. (For the cutting and polishing of this stone the authors thank Dr S. Suzuki.) The cathodoluminescence micrographic fields shown in figures 10*a–c* were selected to show the presence of both the H3 and the 2.16 eV systems near the edges of polished sections. There were, however, many localities where type II zones outcropped at the natural surface of the specimen and at which no 2.46 eV line was detectable by visual spectroscopic inspection. One such locality is represented in figure 14. The slit of the Beck spectroscope was oriented so as to take in the bright 2.16 eV emission from a strip close to the specimen surface. The spectral region reproduced in figure 14 runs from 486 nm to 650 nm. The length of the strip on the crystal which is imaged in the spectrum topograph is 100 μm; and it can be seen to include some spatial fluctuations in the intensity of the low-level band A cathodoluminescence background. The zero phonon line of the 2.16 eV system is broad, about 2 nm in width. Its measured wavelength is 575 nm. The first and second phonon-assisted peaks which can just be resolved on its long-wavelength side are at 2.11 eV (587 nm) and 2.07 eV (599 nm), in good agreement with the measurements on this system performed at −180 °C by Ralph (1960). Just visible in figure 14 is a weak line at 504 nm. Since no phonon-assisted emissions associated with it can be detected, it would seem likely that this is the zero

phonon line of the 3H rather than of the H3 system. (Elsewhere on sections of this crystal, as previously remarked, it is the H3 system, often obviously associated with dislocations, that is observed.) Other weak lines recorded from the region emitting the 2.16 eV system will be discussed later in § 6 (*b*).

Among the observed interior-volume occurrences of the 2.16 eV system, one of the strongest is that already shown in figure 10*b*. Of comparable strength was an occurrence within another specimen (number MS5) where it was well displayed in curvilinear bands which appeared otherwise very dark, i.e. emitting minimal band A cathodoluminescence. These bands lay in sectors of cuboid growth. In specimen MS5 the 2.16 eV system was also found locally present within a region of strong H3 system emission surrounding a central inclusion.

Now it has been reported by Wight (1968) that the 2.16 eV system can be produced by the 50 kV electron beam used during cathodoluminescence spectroscopic studies of diamonds. Thus a cautious procedure is needed in experiments such as those under present review. In the cases described above it was checked that no change in strength of 2.16 eV emission could be detected between that from points inspected briefly and that from points nearby, in a similar matrix, upon which strong beams had impinged for several minutes. However, some cases in which changes did occur have been encountered. One was Dr Yoffé's crystal, described earlier in § 4 (*d*). Equally noteworthy behaviour was exhibited by a type IIb specimen, number JT2. The latter crystal possessed the mosaic structure, as did specimen JT1 illustrated in figure 11, but its low-dislocation-density cells were smaller than those of JT1. Specimen JT2 showed both 504 nm and 575 nm emissions from a thin rind (maximum thickness 15 μm, and less than 10 μm along some stretches), though in places the latter emission occurred without visually detectable presence of the former. A small area within the rind was deliberately irradiated for 2 min with the strongest beam that could be produced (50 kV and approximately 20 mA mm^{-2} on a 20 μm diameter spot). The strength of the 575 nm line was considerably enhanced thereby. However, when an irradiation of similar intensity was given for 5 min to a point 200 μm away from the edge of the crystal section, neither 504 nm nor 575 nm emission therefrom developed in consequence. It thus appears that, as far as this type of matrix is concerned, previous natural radiation damage is a prerequisite of the generation of 575 nm system emission, or for the intensification of such emission if it is already visible, during bombardment by 50 kV electrons in doses at least considerably stronger than those given during the usual experimental observation periods employed in the present investigations. The other two cases involved octahedral shells extremely low in band A emission within type Ia specimens. Recognizable 575 nm emission did develop following intense electron irradiation of points remote from the external surfaces, though such development was weak in comparison with that in the rinds.

6. Other spectral lines with topographically defined associations

(*a*) *Lines associated with slip traces*

Two line emissions registered on spectra from H3 system-emitting regions of specimen GH2 appear at 2.55 eV (485 nm) and 2.30 eV (540 nm). Since the work of Mani (1944*a*) the latter line has been several times reported as accompanying the H3 system, for example by Dean *et al.* (1960) in low-temperature cathodoluminescence studies. During the present observations

it was often noted by visual spectroscopy when it accompanied the H3 emission in various crystals; and it sometimes appeared with sufficient strength to stand out sharply above the strong background given at room temperature by the phonon-assisted peaks of the H3 system.

Unexpected, on the other hand, was the occurrence of the weak line at 2.55 eV (485 nm) in association with the H3 emission from slip traces. In only one of the 22 diamonds whose fluorescent spectral lines were listed by Mani (1944*a*) was a line recorded which could correspond to that observed at 485 nm in the present study. She measured its wavelength as 483.3 nm at liquid air temperature, and recorded it as present with one-fifth the strength of the H3a line in the emission from a diamond (specimen D13) having a spectrum exceptionally rich in lines and which exhibited a greenish tint by daylight. The few reports of cathodoluminescent emission at this energy describe it as occurring either in synthetic type Ib diamond (Wight 1968; Collins 1974) or, together with another weak line at 491 nm, in association with the 575 nm system in natural diamond both before and after laboratory irradiation (Dean *et al.* 1960; Ralph 1960). From specimen GH2 there was no line emission at 491 nm. Nor was the H4a line at 496 nm observed at all. There did appear on the spectrograms a weak diffuse band stretching from about 495 nm upwards towards the 504 nm line. It is speculated that this might be an anti-Stokes satellite of the 504 nm line. Many days were spent in attempts to obtain stronger records of the weak unsharp line at 485 nm, despite its appearance in association with the H3 emission from slip traces in specimen GH2 at all locations where their spectra were photographed. It was eventually concluded that the 485 nm luminescence centre must be to some degree labile under 20 kV electron irradiation. The line intensity apparently dropped to about one-third of its initial level after about 20 h irradiation with 20 kV electrons at a mean specimen current of 0.6 μA mm^{-2}. Thereafter it remained stable at the lower intensity.

(*b*) *Lines associated with natural radiation damage*

Table 1 records all the lines observed from the natural radiation-damaged rinds of specimen GDO6 and the type IIb specimen JT1. Listed therein are the emissions at lower wavelengths than those covered in the short spectral ranges reproduced in figures 13 and 14. The table entries relating to specimen JT1 at wavelengths at and below 504 nm are presented with confidence, but those at the longer wavelengths are less reliable. On the spectrum in figure 13*a* there is considerable structure above 504 nm: only the two sharpest among the many diffuse maxima have been listed, lines (g) and (h), these being regarded as possibly representing zero phonon lines. In the spectrum of figure 13*b*, on the other hand, there appear several quite sharp emissions, (i), (k), (l), (m), associated topographically with points very close to the specimen edge. They have been listed here in the hope that in due course further work may establish their origin.

The earliest reported observation met with concerning a line corresponding to (a) of table 1 is the line 'J' described by Wight (1968) who found it in association with the ultraviolet '5RL' cathodoluminescence system he studied. (Wight reported that the 5RL system, with photon energies in the range from 4.676 to 3.637 eV, was developed by fast neutron irradiation at doses of *ca.* 5×10^{18} neutrons cm^{-2} in 'Intermediate' and type IIa natural diamonds, and in both natural and synthetic type IIb specimens.) Wight's measurement of the energy of line J was 3.185 eV at 100 K. The wavelength measurement given in table 1 was assisted by mercury arc calibration lines at wavelengths below 404.7 nm down to 366.3 nm. The proximity of line

(a) to the mercury line at 390.6 nm encourages belief that the value for its energy derived in the present work (3.189 eV) is correct to better than one part in 10^3. Effort was devoted to this measurement because it conflicted with Ralph (1960) and Dean (1965) who reported cathodoluminescence emission at 3.15 eV and not at 3.19 eV. (The latter author associated the cathodoluminescence emission with the optical absorption centre at 3.15 eV first called R10 by Clark *et al.* (1956*a*), later called ND1 by Dyer & du Preez (1965), and much studied.) The puzzle of the conflict between the present measurements and those of Ralph is removed by a footnote in Davies (1972*a*) stating that Ralph was in error, and that his energy value given as 3.15 eV should have been 3.188 eV.

TABLE 1. LINE EMISSIONS FROM NATURAL RADIATION-DAMAGED REGIONS

line	energy/eV	wavelength nm	specimen JT1(a)	JT1(b)	GDO6
a	3.19	389	m	—	m
b	3.04 – 3.03	409 – 410	w, d	—	w, d
c	2·64	471	m	—	—
d	2·52	492	w, d	—	w, d
e	2.46	504	vs	vs	vw
f	2.32	535	—	vw, d	—
g	2.30	540	vw	—	—
h	2.25	552	vw	—	—
i	2.20	564	—	w	—
j	2.16	575	—	w	vs
k	2.14	580	—	w	—
l	2.11	588	—	w	—
m	2.07	598	—	w	—

Abbreviations: vs, very strong; s, strong; m, medium; w, weak; vw, very weak; d, diffuse.

The diffuse band (b) in table 1 could possibly have as its principal component the fairly strong broad line at 410 nm recorded by Ralph (1960) in his low temperature cathodoluminescence spectra. This line was assigned by him to the 3.19 eV emission system.

Correspondence of the line (c) at 471 nm with another line among several others assigned to the 3.19 eV system by Ralph is more doubtful. Line (c) (which can be seen near the left-hand edge of the spectrum print in figure 13*a*) is quite strong relative to the weak diffuse emission (b), whereas the line Ralph recorded at 2.63 eV (471 nm) was very weak compared with the 410 nm line. A likely interpretation of line (c) is that it represents the emission counterpart of the absorption line TR12 observed by Clark *et al.* (1956*a*) and by Walker (1975) in irradiated type II diamonds: the former authors do state that they observed this line in the emission spectra of all electron-irradiated type IIa specimens.

Wight, Dean, Lightowlers & Mosby (1971) reported the observation of sharp lines of unknown origin at 2.725 eV (455 nm) and 2.52 eV (492 nm) in the cathodoluminescence of every type IIb diamond, both natural and synthetic, that they studied. Line (d) may be the latter line since specimen JT1 is a type IIb diamond; but in no spectra of specimen JT1 was there any evidence of a line at 455 nm. Dyer & Matthews (1957) found an ultraviolet-excited fluorescence line at 491 nm in a couple of type IIa specimens. Also, as earlier mentioned during discussion of the 485 nm line which accompanies the H3 system in specimen GH2, weak cathodoluminescent emission lines at 484 nm and 491 nm have been reported as occurring in association with the 2.16 eV (575 nm system).

Lines (e) and (j) in table 1 have already been discussed, so has the identity of the line (g) at 540 nm of which there is some indication of presence in the figure 13*a* spectrum. No identification has been found for the emissions (f) and (h), but these features are very ill defined. The sharpness of the unidentified emissions (i), (k), (l) and (m), which appear from points very close to the external surface of the specimen, arouses the suspicion that they may arise from impurities outgassing therefrom.

7. Discussion

(*a*) *Introductory remarks*

Only those topics on which it is evident that new views of the properties of diamonds have been obtained will be discussed. Attention will focus in turn on just three questions, namely, what knowledge has been gleaned concerning (i) natural radiation damage in diamond, (ii) the optical behaviour of dislocations in diamond, and (iii) the impurity platelets which lie on {100} planes in diamond. Note that a conventional division of the features studied into optical properties on the one hand and growth histories and structural imperfections on the other clearly fails in view of the demonstrated intimate relationship between these two aspects of investigations of diamond. The variety and frequency of inhomogeneity of diamond, and the need for the 'topographic approach' when examining this crystal, are repeated motifs in the ground below each differing figure of topographic detail. Admittedly, most attention in the present work has been concentrated upon diamonds whose inhomogeneity has been previously disclosed by X-ray topography, or was at least strongly suspected on the basis of particular birefringent manifestations. On the other hand, the striking inhomogeneity exhibited by some of the smaller diamonds came as a surprise, for they belonged to a batch whose individual members were expected to be reasonably homogeneous optically since they had been selected on the basis of their low birefringence in the uncut state. Now this experience does not imply that there exist no diamonds which are homogeneous in their optical properties throughout volumes of at least some cubic millimetres, but only that such are probably rare, and some searching may be needed to find them. In view of the finesse nowadays achievable in optical experiments, and the weight attached to the detailed results thereof in the development of theories concerning defects in diamonds, it can be argued that such experiments do deserve experimental material whose homogeneity and lattice imperfection content have been submitted to prior inspection. The examination can be done non-destructively by X-ray topography. Indeed, experience accumulated in the course of the present work suggests that quite fair predictions can be made on the basis of X-ray examination alone regarding the probability of finding some noteworthy optical features, e.g. local occurrences of dislocations and platelets from which H3 system emission may be expected, and of those optical characteristics that go along with strong 'spike' reflexions. It is perhaps not surprising that some associations of spectral line emissions that have been disclosed via the microtopographic study of spectra are unexpected: for example, the suites of lines listed in table 1 have an unfamiliar look when viewed against previously published work. Additionally let it be remembered that the present experiments (with the exception of a single observation made in the near infrared, to be discussed in §7(*d*)) have included only the visible spectrum and slightly shorter wavelengths, the energy range concerned running only from *ca.* 3.2 to 1.8 eV. Thus ample possibilities remain for discovering topographically defined associations of known emissions at both higher and lower energies.

(*b*) *Natural radiation damage*

Undoubted physical and geophysical significance attaches to the spectra from the radiation-damaged rinds of diamonds. Underpinning the attribution of these emissions to irradiation rather than to the inward diffusion of impurities from the surrounding matrix is the observed maximum rind thickness. This, after some allowance for uncertainties of measurement, does not exceed what would be expected if sources of the most energetic natural α-particles had been in contact with the diamond surface. That in certain instances the rind has a thickness only some fraction (and perhaps not a constant fraction) of the maximum α-particle range can plausibly be explained by attrition and/or dissolution of the surface subsequent to immersion in a radioactive matrix. On some external surfaces of diamonds the regions giving rise to spectra associated with radiation damage may occur only as localized patches: in such cases it may be that the crystal had never been uniformly surrounded by radioactive material. Indeed, one possible inference to be drawn from the observation that some diamonds have patches only whereas others have quite uniform rinds of radiation damage is that the latter specimens underwent an epoch of immersion in a streaming medium within which radioactive particles were disseminated.

The range in diamond of the most energetic natural α-particles, those from thorium C′ (Po^{212}), energy 8.78 MeV, has been estimated in two ways: firstly by scaling the known range of these particles in aluminium to the case of diamond using the rule that equivalent thickness is proportional to the square root of the atomic weight, and, secondly, by scaling the known range of machine-accelerated 8.78 MeV protons in graphite. Both routes give an extrapolated range of thorium C′ α-particles in diamond of between 25 and 27 μm. Adding a few parts per cent to this for straggling, and allowing for the manifest limitations of the viewing microscope, suggests that the observed maximum rind thickness of about 29 μm is not too high a value to be accounted for by natural α-particles.

Although radiation-damaged surfaces have been closely examined in only six specimens so far, it is clear that their spectra exhibit considerable variety. Drawing upon such references to them as have already been made in §§3(*b*), 4(*d*), 5 and 6(*b*), some leading observations typifying this diversity of behaviour are here gathered together, as follows.

(*a*) A diamond emitting band A cathodoluminescence rather strongly and fairly uniformly over the surface of its section exhibited the H3 and H4 systems strongly in its rind. This behaviour of the rind is as would be expected (judging by published work) in a laboratory-irradiated type Ia diamond which had been annealed at temperatures above about 800 K. On the other hand, in another specimen (number GDO6) it appeared possible for some strongly band A-emitting regions outcropping at the surface, through a radiation-damaged rind, to be apparently unaffected there in their visible emissions (see such an outcrop just below centre level in figure 10*a*). However, in the case of band A-emitting regions which additionally gave some indication of 2.46 eV emission when they lay within this crystal, then the latter emission was enhanced in the rind.

(*b*) On a type IIa and a type IIb diamond, and also on a weakly band A-emitting diamond, the dominant emission from radiation-damaged regions at the surface was the 3H system, but in the case of another type IIb specimen it was the 2.16 eV system that produced the most strongly visible emission. That the 3H system was labile under the electron beam was demonstrated most strikingly by the weakly band A-emitting diamond. Only two exceptions were

found to the generalization that noticeable development of the 2.16 eV emission under the electron beam occurred only where there was evidence of previous natural radiation damage.

(*c*) As a general observation, it appeared that it was in regions of weak or minimal band A emission that natural radiation damage effects were most evident, and of the latter an intense emission of the 2.16 eV system was the most visibly striking.

(*d*) The line at 3.19 eV erroneously reported as being at 3.15 eV by Ralph (1960), has manifested itself as a leading minor component in rind spectra. (The spectrum JT1 (b) in Table 1 was generally weak at short wavelengths and did not show the line at 3.19 eV; but this line did appear clearly in another spectrum recorded from a point close by that from which the (*b*) spectrum was photographed.)

(*e*) An observation carrying implications concerning the density and nature of the natural radiation damage, and the effectiveness of the natural radiation damage centres in competing with other defects as electron-hole recombination centres, is the suppression of band A cathodoluminescence, and of the cathodoluminescence of dislocations in mosaic type II specimens, in regions where natural radiation damage is present. (It is this suppression, it will be recalled, which is the diagnostic for finding an emission of the 3H zero phonon line when high beam current densities impinge on these darker regions.) It may bear remarking that an observation such as this, involving the local absence or reduction of an otherwise ubiquitous emission from the specimen, is one which can only be made by the microtopographic study of luminescence.

It is very likely that factors contributing to the observed spectral variety are differences between specimens with respect to their thermal histories both during and since irradiation. Consider the type IIb specimen JT1, for example. The 2.64 eV emission in its spectrum is believed to be the TR 12 line. Walker (1975) reports that the TR 12 absorption line in irradiated diamonds is enhanced by anneals in the range 700 to 900 K of 1 h duration, but is annealed out after longer periods or subjection to higher temperatures. With regard to the 3H zero phonon line at 2.46 eV which dominates the rind spectrum of specimen JT1, Davies (1974) asserts that the 3H absorption system is readily annealed out, for example in less than 2 min at 873 K in a type Ia diamond. The conclusion must follow that diamonds exhibiting the 3H system in their radiation-damaged rinds received their irradiation at no great depth below the Earth's surface (at least not below the boundary between mantle and continental crust) and have been denied any opportunity to sink subsequently to greater depths, towards their neutral buoyancy level (Lang 1970), where higher temperatures would prevail.

(*c*) *The optical behaviour of dislocations*

(*i*) *Blue-luminescent dislocations*

In dealing with the topic of cathodoluminescence of dislocations, consideration will be given first to the blue-luminescent dislocations, and, subsequently, to those which exhibit H3 system emission. This separation is more than just one of descriptive convenience. Rather does it express one of the more striking puzzles uncovered in the work so far: namely, how does it come about that dislocations blue-emitting and dislocations H3 system-emitting often appear in close juxtaposition? Experience suggests that blue-emitting dislocations can appear wherever there is a sufficient dearth of competition from other recombination centres. The commonest competition comes from the centres responsible for band A cathodoluminescence; and in the presence of but the weakest level of band A emission the blue cathodoluminescence of individual dislocations disappears. Dislocations visible by cathodoluminescence may either be of the

'grown-in' variety or may be due to plastic deformation post growth: their nature is generally revealed by the distinctive configurations appropriate to each origin. It is clear that the dislocations in the mosaic type II diamonds studied are responsible for nine-tenths or more of the whole visible cathodoluminescence from these crystals at room temperature when they are stimulated by electron beams carrying current densities of not more than a few tens of microamperes per square millimetre. Considering how much effort has been expended over the years investigating the cathodoluminescence and other luminescent properties of type II specimens, how valuable would it be to know the configurations and densities of dislocations existing within those specimens. The brilliance of cathodoluminescence from individual dislocations diminishes as their spatial separation decreases, e.g. when they are crowded in bundles, as grown-in dislocations, or when they are closely spaced on slip planes. Mutual competition between dislocations acting in their rôle as recombination sinks can explain this observation. With the limited microscopic resolution available in the present work, the maximum dislocation density at which individual luminescent lines could be resolved was about 5×10^6 lines cm^{-2}; this happens to be of similar order to the maximum density for resolution of individual dislocation diffraction contrast images by X-ray topographic techniques.

Interesting though calculations of the electron and hole-trapping efficiency of ideal, 'clean' dislocations in diamond would be, their relevance to the practical situation in natural diamonds is probably not close. It is unlikely that the dislocations in natural diamonds have not become fully 'decorated' by impurity in the course of their long history. To form a single continuous chain of substituted foreign atoms along the core of every dislocation, at a dislocation density of, say, 10^7 lines cm^{-2}, would require a fractional impurity content in the bulk crystal of less than 10^{-8}. This is two or three orders of magnitude lower than the probable minimum bulk concentration levels of light elements such as hydrogen, boron, nitrogen and oxygen which would diffuse relatively easily and be electronically significant. However, it is experimentally apparent that even in the case of the mosaic type II diamonds, which represent the specimens having the highest dislocation density of all those studied, the dislocations only account for a small fraction of the recombination sites effective. Consider the probable rates of electron-hole pair production in the experiments. Now, as a broad generalization, the levels of specimen stimulation employed can be classed either as 'low', when areas of *ca.* 500 μm diameter are irradiated at a current density of *ca.* 1 μA mm^{-2}, or as 'high', when areas of *ca.* 20 μm in diameter are irradiated at a current density of *ca.* 1 mA mm^{-2}. At the high level, blue cathodoluminescence is visible from dislocation-free areas in type II crystals, and, indeed, from the most perfect and band A-emission-free regions of any specimen. Electron-hole pair production rates under these two conditions of stimulation can be roughly estimated as follows. First, since the coefficient of back-scattering of electrons of about 30 kV energy by diamond is low, say 0.07 (Oatley 1972), the net current into the specimen can be used as a measure of the number of high energy electrons impinging upon it. Next, let it be assumed that the average energy expenditure for production of an electron-hole pair in diamond is about three times the band gap energy, adopting the factor that is applied in the case of ZnS (Shockley 1961; Garlick 1966), and that a 35 kV electron will therefore produce *ca.* 2×10^3 electron-hole pairs. For simplicity the crude assumption is made that this production is spread uniformly within a layer extending from the crystal surface to a depth 10 μm below it. Take this depth as an appropriate unit of length to define a cubic volume that lies below an area 10 μm square on the specimen surface. This volume contains 1.76×10^{14} carbon atoms, and within it the rate of electron-hole pair

production is of order 10^{12} s^{-1} at the 'low' level of stimulation and of order 10^{15} s^{-1} at the 'high' level. Now if dislocations were distributed uniformly spatially, and their density were as high at 10^7 lines cm^{-2}, then there would be, on average, within each cube of 10 μm edge length *ca.* 10^6 impurity atoms on the dislocations if the latter were fully decorated in the manner suggested above. These could provide sufficient recombination centres to dispose of all electron-hole pairs at the 'low' level if the lifetime of an electron or hole trapped on an impurity did not exceed *ca.* 1 μs (and correspondingly shorter times for stronger excitations). In point of fact, the dislocations are generally far from homogeneously distributed on a 10 μm (or even much larger) scale. Indeed, within the nearly dislocation-free cells of a well-developed mosaic texture such as that exhibited by the type IIb specimen shown in figure 11 it is easy to find 10 μm-edged cubic volumes quite free from dislocations. Therefore, either recombination occurs within these volumes predominantly without visible radiation, or the electron-hole pairs must diffuse away (as free excitons, probably) until they reach a dislocation, and there recombine. Since the dislocations do not perceptibly luminesce outside the area of impact of the primary electrons, or at depths significantly greater than the maximum penetration range of the primary electrons, the former situation applies in the case of the mosaic type II diamonds. However, in some of the narrow type II zones occurring in dominantly type Ia diamonds, when the band A cathodoluminescence is of minimal strength and the individual dislocations most brilliant, the dislocation lines can be tracked into the crystal (by lowering the microscope focus) down to true depths of *ca.* 60 μm below the specimen surface. Similarly, in the case of synthetic diamonds, blue-luminescing dislocations can occasionally be seen at true depths down to *ca.* 70 μm below the surface (Woods & Lang 1975). These observations are interpreted as indicating that diffusion lengths of excitons (or of carriers in whatever form they are) can in certain rather rare matrices be comparable with or greater than the primary electron penetration range, and thus be roughly measurable by microscopic inspection. These inferred diffusion lengths of not less than 10 μm contrast with the shorter lengths in the direct-gap semiconductor GaAs (n-type) which were derived from analysis of its cathodoluminescence behaviour by Wittry & Kyser (1967). (They found lengths of 0.65 μm at high carrier concentration, 3.0×10^{18} cm^{-3}, and 3 μm at low carrier concentration, 5.1×10^{16} cm^{-3}.) In connection with synthetic diamond, one observation should be recalled. After a specimen had been inadvertently left for an hour in boiling concentrated sulphuric acid (temperature *ca.* 600 K) about half of its blue lines disappeared or shortened. It is believed that this change probably resulted from rearrangement of impurities in the matrix and/or on the dislocations whereby the density of nonradiative recombination sites was increased.

To separate the spectrum of a blue-luminescing dislocation from that of the matrix surrounding it has proved beyond the capacity of the simple spectrographic techniques used so far. In the case of crystals which contain both type Ia and type II regions it can be seen that the dislocations visible in the type II regions emit a deeper and more saturated blue than do the type Ia regions; but, as already noted in §3(*a*) when describing the emissions from the specimen shown in figure 1, the band A spectrum is both complex and variable from region to region, and can contain appreciable components at wavelengths longer than 500 nm. (This last-mentioned property of some band A-emitting regions will be considered again in §7(*d*).)

As already reported (Kiflawi & Lang 1974), the degree of linear polarization of the blue emission from dislocations can be 90% or more, and is greatest for long, straight dislocation segments parallel to ⟨110⟩ directions. The highest ratio of intensity of emission with

E vector parallel to the line to that with ***E*** vector perpendicular to it has been found by rough measurement to be 40:1. (The same visual brightness-matching technique with Polaroid and neutral density filters was used as in the somewhat easier task of estimating the polarization ratio of the H3 system emission from the large platelets shown in figure 9 and described in § 3 and § 4 (*b*).) The lower polarization ratio exhibited by dislocations not macroscopically parallel to a ⟨110⟩-type direction can be accounted for by the assumption (reasonable in the case of the diamond structure) that the observed line trajectory is at least in part the resultant of a microscopic zigzag of segments individually parallel to appropriate directions in the set ⟨110⟩, and that each segment emits radiation polarized with ***E*** vector parallel to its own line direction.

The explanation here put forward to explain the linear polarization phenomenon is that the electrons and holes trapped on the dislocations are sufficiently localized in real space so that when recombining they radiate as dipoles with the dominant dipole axis coinciding with the dislocation line direction. Note that this explanation only requires real-space localization of the electron and hole with respect to the coordinate describing distance from the dislocation line. If strong localization along the line also existed then the dislocation cathodoluminescence spectrum might exhibit resolvable peaks arising from discrete Coulomb interaction energies corresponding to discrete values of separation distance between electron and hole prior to their recombination.

(*ii*) *Relation between blue-luminescent and H3 system-emitting dislocations*

Figure 6 is informative since it illustrates both a characteristic difference in geometry distinguishing linear sources of H3 system emission from linear sources of blue emission, and also some exceptions thereto. As a general rule, the H3 system is emitted from continuous sheets on {111} planes. The blue emission, on the other hand, usually comes from individually resolvable lines (excluding emission from the cell walls of mosaic crystals). One exception to the generalization that dislocation-associated emission of the H3 system arises only from {111} sheets has been previously mentioned in § 4 (*a*): namely, the appearance of a few weakly green-luminescing lines within the core region of specimen CI9. Other exceptions can be seen in the upper parts of figure 6*a*. The specimen surface orientation in this case is close to (112). Figure 6*a–e* have been oriented so as to make traces of $(1\bar{1}1)$ run horizontally across the prints. This facilitates distinguishing between images of traces of $(1\bar{1}1)$ and images of individual dislocation lines parallel to $[10\bar{1}]$ lying in $(1\bar{1}1)$, since the lines appear rotated a few degrees clockwise from the horizontal. In the top part of figure 6*b* blue lines parallel to $[10\bar{1}]$ but no traces of $(1\bar{1}1)$ appear. Figure 6*a* shows the H3 system emission: in its lower part dislocations on $(1\bar{1}1)$ are represented by traces of $(1\bar{1}1)$, but in the top part of the figure, above the constriction in the type II zone, and also in a region close to the right-hand margin of this zone below the constriction, both H3 system-emitting $(1\bar{1}1)$ traces and H3 system-emitting lines parallel to $[10\bar{1}]$ can be seen.

Unfortunately it is not possible to state in what proportions the generally observed lack of resolution of individual lines on H3 system-emitting slip planes is to be attributed to high dislocation density on the slip planes, or to the dimensions of the H3 system-emitting 'decorations', or to the flaring characteristic exhibited by H3 system-emitting slip traces remarked upon at the end of § 4 (*a*). The presence of populations of H3 system-emitting specks in regions where slip traces similarly emitting are observed has been described in the case of specimen GH2 (and illustrated in figures 6, 7 and 8). Similar occurrences have been observed in specimen GDO6 and other crystals. It is reasonable to assume that the structures of the isolated emitters

and of the decoration on the slip-planes are closely related. Of course, the possibility that the small specks are merely decorated dislocation loops cannot be excluded. However, whenever they are large enough to be distinctly seen individually the specks manifest linearly polarized emission; and they grade upwards in size continuously, from specimen to specimen, or within a given specimen, until they do become large enough to be unmistakenly recognized as platelets on {100}. It is therefore believed that the smallest specks are also platelets on {100}. Indeed, the evidence does not disallow the possibility that the dislocation decoration itself consists of an unresolved chain of platelets on {100}: the absence of polarization in the emission could be accounted for by the presence of all {100} orientations with equal frequency.

The central problem of why some dislocations in type II zones emit the H3 system whereas others do not is unsolved, but some possible explanations will be canvassed. First, dislocations seen emitting blue cathodoluminescence are assumed never to have acquired the property of emitting the H3 system. This idea is preferred to the more complicated concept that all dislocations in the configurations at present visible once emitted the H3 system but some fraction of the population subsequently lost this faculty. Secondly, where H3 system-emitting slip traces are seen with little or no accompanying blue emission (as is so, for example, in the lower parts of figure 6*a* and *b*), one may either assume that the great majority of the dislocation lines have passed out of the slip plane, leaving the H3 system-emitting 'decoration' behind them, or that the dislocations are still present but blue emission is quenched in the presence of the H3 centres. The latter alternative is believed to apply. It is relevant to note that the restriction of observable cathodoluminescence from dislocations to those lying in type II zones, which applies very strictly in the case of blue luminescence, is not so rigorously enforced in the case of H3 system-emitting slip traces. Those traces that emit the H3 system very intensely in type II zones can sometimes be recognized extending, weakly emitting, into adjacent band A emitting zones. Figure 4 has shown an example on a small scale, and figure 1*c* demonstrates this phenomenon on a larger scale. The slip patterns exhibited by specimens GH2 and S1 patently arise from the relief of hoop stresses between concentric growth zones. On the other hand, the limited number of very strong slip bands exhibited by specimen S5 (figure 1) may have arisen at least in part from stresses externally applied to the crystal.

Now if the H3 system-emitting dislocations and the blue-emitting dislocations represent populations emplaced at different epochs in the crystal's history, then the question arises, which is older. The appearance presented in the fields of figures 4 and 5, where diffuse, curly webs of blue-emitting dislocations lie in proximity to rather than confined to the strictly crystallographic H3 system-emitting slip traces does somewhat suggest that the blue dislocations are the more recently emplaced, and represent dislocations that have diffused away from the decorated slip planes after the major slip event. With this assumed sequence of events, one adds the assumption that the agent unknown responsible for producing H3 system-emitting decoration of dislocations involved in the earlier slip failed similarly to decorate the dislocations that subsequently moved, either because of a change in temperature and pressure or because it had been otherwise sequestered in the interval. The alternative sequence of events, that the H3 system-emitting slip traces represent an intense re-activation of slip in narrow slip bands within broader bands where a low density of glide dislocations were already present is considered less likely. However, it may well be that timing within the sequence of deformation events was of less consequence than the dynamical conditions under which a given deformation took place in determining whether or not the dislocations acquired H3 system luminescence. From inspection

of the pattern of H3 system-emitting slip traces it could be inferred that they indicate dislocation movement at a higher ratio of dislocation driving stress to local yield stress than that which moved the blue dislocations into their present configurations. On this basis, then, it could be supposed that it was only the more vigorously moving dislocations which effected the atomic rearrangement that either directly or eventually led to the formation of H3 centres. (Perhaps a link with the production of H3 centres by irradiation followed by annealing may here be perceived.)

A final comment on dislocation cathodoluminescence concerns the flaring exhibited by H3 system-emitting slip planes when they pass through zones of minimal band A cathodoluminescence, as discussed in §4(*a*) and illustrated in figure 4. Complete explanation of this effect is far from evident, but some factors contributing to it can be suggested. Certainly the longer diffusion lengths of electrons and holes in the type II zone must be one factor, but it does not seem to account adequately for the effect, in particular that the H3 emission flares out only when the slip trace is actually struck by the primary beam. Fluorescence by resonant absorption of the 2.46 eV zero phonon line can be rejected because the type II and type Ia regions differ so little in transparency at this wavelength. More likely is fluorescence under stimulation by recombination radiation having wavelengths close to the fundamental absorption edge of diamond. However, the observations suggest that it would have to be recombination radiation produced on the slip band itself rather than in the type II matrix that was effective. This presumed excitation of the H3 centre by recombination energy released at the decorated dislocations themselves is consistent with the previously deduced quenching of blue luminescence of such dislocations. Additionally, with such strongly localized interactions, conditions would favour radiationless excitation of the H3 centres by an Auger process. This last-mentioned possibility will be considered again below when the related problem of the production of H3 system emission from platelets on {100} is discussed.

(*d*) *Impurity platelets on* {100}

As mentioned in §3(*a*), platelets emitting the H3 system linearly polarized have been observed in ten specimens to date. In two specimens (numbers CI9 and FA) which possessed regions where platelet dimensions exceeded 5 μm by a sufficiently large margin to enable a clear picture of platelet shapes to be recognized the platelets were viewed through a surface polished parallel to a cube plane so that undistorted images of platelets parallel to that plane were obtained. The two crystals differed markedly as regards platelet shapes. As figure 9 shows, the shapes in specimen CI9 are complex. A fan-like shape, and an irregular diamond shape with sides re-entrant so as to make a four-pointed star, are the two most commonly occurring forms. Edge segments parallel to ⟨110⟩ are rare. The commonest directions of straight edge segments are near ⟨310⟩: a pair of such directions often together compose the re-entrant edges joining adjacent apices. These shapes could have arisen through the filling-in of areas between two or more fingers of unequal length lying in ⟨110⟩ directions in the platelet plane, but this is quite uncertain. In specimen FA, on the other hand, the shapes were much simpler. They were trapezoidal, and elongated in the direction of the pair of parallel sides which took up one or other of the two ⟨110⟩-type directions in the platelet plane, apparently at random from platelet to platelet. The average ratio of length to width of the platelets was about three.

Much further experimental work will be required in order to establish how prevalent are H3 system-luminescing platelets of a size optically well resolvable. However, it is already

possible to put forward tentatively a prescription for finding them through X-ray examination, as follows. Look for diamonds which contain one or more layers of type II character intercalated between type Ia material particularly rich in sub-micrometre-sized platelets. Slip bands, if present, should not be as dense as in specimen S1 (shown in figure 5). The crystal growth should be basically of normal {111}-faceted type, not cuboid, in the type II regions concerned, but some local stratigraphic manifestations of bounding surfaces not closely parallel to {111} may well be a favourable indication. A low density of grown-in dislocations in the crystal as a whole (or at least from the centre out as far as the zones in question) appears to be a favourable sign. Type Ia zones rich in relatively large sub-micrometre-sized platelets can be identified by an especially high integrated Bragg reflexion, indicating presence of a significant population of unresolved lattice defects dispersed on a scale small compared with the X-ray Bragg reflexion extinction distance (*ca.* 20 μm in lowest-order reflexions with CuKα radiation). They can also be identified by especially strong and sharp 'spike' reflexions. It was from X-ray topographic evidence that the presence of visible platelets in the specimen FA was predicted; confirmation by cutting, polishing and cathodoluminescence observation followed.

The environment of large platelets, just described, highlights the question of their relation to the platelets of sub-micrometre size, and of the rôles that both play in the hierarchy of states of aggregation of nitrogen impurity in type Ia diamonds. At this juncture a brief resumé of current thinking on the topic of nitrogen impurity in type Ia diamond is pertinent. In the impurity-produced infrared absorption spectrum of type Ia diamond in the spectral range 10^3 cm^{-1} to 1.4×10^3 cm^{-1} there are three important peaks, at 1282 cm^{-1} (159 meV, 7.8 μm), 1172 cm^{-1} (145 meV, 8.5 μm) and 1370 cm^{-1} (170 meV, 7.3 μm). The first two are the principal peaks in broad features belonging respectively to the A and B group of absorption bands (Sutherland, Blackwell & Simeral 1954). The third peak, originally placed in the B group, is now excluded therefrom and is referred to as the B′ peak in current English literature. It is relatively sharp, of higher energy than the Raman frequency (1332 cm^{-1}) and represents either a local mode or an electronic transition. Kaiser & Bond (1959) and Lightowlers & Dean (1964) found good correlation of the absorption coefficient at 1282 cm^{-1} with total nitrogen content. Also, absorption at 1282 cm^{-1} correlates well with absorption at 306.5 nm (Kaiser & Bond 1959) and at 260 nm (Davies & Summersgill 1973). The estimates of total platelet area per unit volume made in the original transmission electron microscope study of the sub-micrometre-size platelets (having diameters in the range 10 nm to 100 nm) by Evans & Phaal (1962) gave credibility to the reasonable notion that substantially all the nitrogen in type Ia diamonds was precipitated in these platelets. However, Sobolev, Lisoivan & Lenskaya (1967) discovered that the integrated intensity of spike X-ray reflexions (which provides a measure of total platelet area per unit volume) correlated not with the A peak at 1282 cm^{-1} but with the generally much less conspicuous B′ peak at 1370 cm^{-1}. This correlation has recently been confirmed by Evans & Rainey (1975*a*, *b*). Subsequent to Sobolev's finding, detailed analysis of the optical absorption data available has led Davies (1970, 1971, 1972*b*) to conclude that probably only 5 to 10 % of the total nitrogen content is precipitated in platelet form, the bulk being in 'small clusters', invisible electron microscopically. The A and B absorption peaks are believed to be produced respectively by two forms of small cluster, the A and B forms, of as yet unknown structure. Davies's conclusions are here accepted as a basis from which to view the present observations of luminescent platelets and of band A cathodoluminescence. A few cautionary words should be added, however. First, none of the experimental works just referred to was

performed on specimens whose homogeneity was checked X-ray topographically. Only Kaiser & Bond (as far as the authors are aware) verified by birefringence tests that their cut and polished plates were free from appreciable zoning of impurity content. Secondly, the difficulty of making accurate measurements of integrated 'spike' intensity (especially in the case of the smallest platelets) should not be underestimated. In a specimen inhomogeneous in distribution of platelet sizes, the sharp spikes produced by large platelets will strongly dominate in the diffraction pattern. It is still not out of the question to conjecture that the strength of the 1370 cm^{-1}, B', peak is an indicator not so much of total platelet area, but rather of the size of *individual* platelets.

Since the concentration of nitrogen impurity exceeds that of any other known impurity in diamond by at least an order of magnitude in typical type Ia diamonds it will be taken for granted here that the structure of the spike-producing platelets is essentially a carbon–nitrogen structure. That these platelets possess a well-defined structure is attested by the weakness of the spike reflexion at the third order, i.e. of the spike in the direction [001], say, through reciprocal lattice points hk3 (Hoerni & Wooster 1955). (Recent experiments (Suzuki & Lang, in preparation) have demonstrated that the sharp spikes produced by large platelets (apparent mean diameter *ca.* 50 nm) lying in the {111} growth sectors of a diamond of mixed {111} and cuboid growth definitely give vanishingly small intensities at the third order. On the other hand, small platelets (apparent mean diameter *ca.* 15 nm) present in cuboid growth sectors behave anomalously in various respects when there is also present a population of microscopic and submicroscopic bodies producing diffraction contrast, and they then exhibit comparatively strong third order spike reflexions.) The significance of near absence of a third order reflexion has been often stressed (Frank 1956, 1964; Caticha-Ellis & Cochran 1958; Takagi & Lang 1964; Lang 1964); but so too has the ambiguity associated with vanishing at this order, for displacements of the matrix of magnitude $(3n \pm 1)\, a_0/3$ produce vanishing just as does the unit displacement $a_0/3$ (a_0 is the diamond face-centred cubic lattice parameter, n is an integer). However, with the possible exceptions of platelets nucleated on inclusions large compared with atomic dimensions, or on dislocations, it will be assumed that the spike-producing platelets are of minimum thickness, and are of the structure previously proposed (Lang 1964). (In one cell of this structure, cell dimensions $a_0 \times a_0 \times \frac{4}{3}a_0$, there are 6 carbon and 4 nitrogen atoms.) Since this platelet model offers no incentive of a structural nature for growth to take place by nucleation of additional unit layers upon existing unit layers, there is no reason for the manner of platelet growth to be other than that expected when precipitate growth is diffusion-limited, and precipitate shape is such as to minimize matrix strain energy. Consequently, a platelet, once nucleated, would be expected to grow by expansion in area rather than by thickening. Thus it is reasonable to assume that at least a substantial majority of nitrogen platelets exist in the state of minimum thickness. Estimates can then be made of what concentrations of precipitated nitrogen are involved on the supposition that in regions where H3 system-luminescing platelets are individually resolved these platelets constitute the entire population of nitrogen platelets and contain the above-described structure in unit thickness. As mentioned in § 3 (*a*), during discussion of figure 9, it has not yet been possible to establish fully how the visibility of individual large platelets varies with order of X-ray reflexion, but the strength of diffraction contrast they exhibit does not disallow the unit-thickness supposition, and indeed evidence is accumulating that they produce the same displacements of the diamond matrix as do the familiar, X-ray 'spike'-producing platelets. It is estimated that in the part

of the field of figure 9 where the band A cathodoluminescence is extremely low and the platelets large and sparsely distributed they would account for a nitrogen concentration of less than $1/10^6$. Fields where the platelets are smaller and closer together may be found both in matrices of minimal band A cathodoluminescence (the platelet clusters in figure 7 present an example) or in matrices of appreciable band A emission. In the former case visual resolution of individual platelets (using the optics available for the present experiments) would become impossible at values of platelet area per unit volume corresponding to nitrogen concentrations of more than about $20/10^6$; and in the latter case perhaps $10/10^6$ would be the upper limit. These figures are not only low compared with the likely total values in the matrices concerned (certainly in the case where the platelets were immersed in a matrix giving appreciable band A emission), but are even low compared with possible concentrations of light elements other than nitrogen. For example, as regards oxygen, the concentrations found by Sellschop, Bibby, Erasmus & Mingay (1974), using the method of fast neutron activation analysis, ranged from 24 ± 10 to 90 ± 40 per 10^6 in thirteen analyses.

Clearly, the question of the composition of the luminescing platelets is a particularly open one. Nevertheless, an attempt will be made to assess the relative merits of three alternatives regarding the nature of the platelets, which may be formulated in categorical terms as follows:

(*a*) they do not contain nitrogen and are independent of the population of platelets which give rise to the spike X-ray reflexions; or,

(*b*) they contain nitrogen only and are structurally the same as the common spike-producing platelets from which they differ only by their greater individual areas; or,

(*c*) they consist of nitrogen plus one or more other impurity species, in proportions of comparable order.

Platelets falling under the description (*c*) could materialize by various routes. One is that they consist of a substrate of 'normal' nitrogen platelet structure upon which other impurity elements have condensed. Another is that they contained nitrogen plus other impurities *ab initio*. Such flexibility imposes little restriction on the optical centres they might contain.

The first two alternatives carry distinct implications regarding the optical behaviour of nitrogen impurity in platelet form. The first implies that the spike-producing platelets have not revealed themselves by any specific optical behaviour during the course of the present study. This could happen either if the nitrogen platelets were non-radiating in the visible spectrum, as suggested by Dean (1965), or if they produced a visible spectrum so feebly distinguishable from that produced by nitrogen 'small clusters' in either A or B form that neither spatial nor spectral resolution of the platelet contribution to the emission from nitrogen-rich regions has been achieved. By contrast, the second alternative carries the remarkable implication that the nitrogen platelet structure contains H3 centres but that these only become recognizably active in cathodoluminescence when the platelets reach a sufficiently large size individually and/or reside in the appropriate environment.

Alternative (*a*) cannot be rejected on the visible optical evidence obtained so far. This alternative is unattractive on the grounds that it is simpler to assume that there is one population of platelets on {100}, possibly admitting of some variations in complete platelet structure and composition, rather than to assume two unrelated populations, one nitrogen-containing, the other not; but unattractiveness does not constitute grounds for rejection. However, alternative (*a*) will be rejected here on the basis of concurring evidence from two quite different types of observation. First, there is the X-ray diffraction evidence which, though circumstantial, does

appear weighty. It will be recalled that large luminescing platelets have been observed in type II, ultraviolet-transmitting zones most often when nearby type Ia zones are rich in relatively large spike-producing platelets. Sometimes it is possible to observe spatially a gradation in platelet size from those large and few, in zones of minimal band A cathodoluminescence, through progressively smaller sizes and greater numbers as zones of increasing nitrogen concentration are traversed, until optical resolution is lost but X-ray topography reveals an abundance of platelets of sub-microscopic dimensions. Such demonstrated associations between the luminescing platelets and the nitrogen-containing platelets point towards alternatives (*b*) and (*c*) as being substantially more probable than alternative (*a*). Secondly, it has been discovered that the large platelets in specimen CI9 exhibit quite bright cathodoluminescence in the near infrared. The observations were made with an infrared image converter. The in-built filtration and resultant spectral response of this device were not determined. However, it was found that the brightness of the large platelets relative to background was as good, if not better, when a Kodak–Wratten infrared-passing filter no. 87C was interposed ahead of the image converter than when a filter passing lower-wavelength infrared radiation (no. 87) was so placed. From the difference between the spectral transmittance characteristics of the two filters it was concluded that the emission observed was almost entirely of longer wavelength than 850 nm. Since the image intensifier sensitivity did not extend much beyond 1200 nm it appeared beyond reasonable doubt that it was the near infrared peak at 1.25 eV (990 nm) described by Wight *et al.* (1971) that was being seen. These authors established a good correlation between the strength of this emission peak and the B′ absorption peak at 1370 cm^{-1}. Having accepted (albeit with some reservations) that the latter is the best optical measure confirmed so far for the total area per unit volume of the platelets which produce X-ray spike reflexions, and believing that the platelets are nitrogen-containing, a rejection of alternative (*a*) is strongly indicated. Evidence which might help to discriminate between alternatives (*b*) and (*c*) will now be examined.

First, consider the polarization of H3 system emission from the platelets, as previously reported in §3 and §4(*b*). All that is known so far is that the emission is strongly polarized with $\boldsymbol{E}$ vector in the plane of the platelet. It has been established that a platelet does not emit radiation which is as a whole right-handedly or left-handedly circularly polarized in the platelet plane but this finding does not preclude the possibility that the observed emission arises from the incoherent superposition of sources of both right-handed and left-handed circular polarizations in the platelet plane. The intricate work of cutting and polishing small facets to enable individual platelets to be viewed from various directions would be specimen-destructive to a degree that has up to now been shunned. Such oblique views would offer a fair chance of establishing whether the $\boldsymbol{E}$ vector directions in the platelet plane were parallel to equivalent cube directions, or to equivalent dodecahedral directions, or were random.

The partial polarization of fluorescence from H3 centres in irradiated and annealed type Ia diamonds excited by polarized radiation at wavelengths of 365 nm and 436 nm has been extensively studied (Elliott, Matthews & Mitchell 1958; Clark, Maycraft & Mitchell 1962; Clark & Norris 1970); but from the complex behaviour of the H3 centre exhibited in fluorescence, as reported in those works, no obvious lead towards an understanding of the polarization of platelet emission discovered in the present experiments can be derived. If the cathodoluminescence observations standing on their own are considered, two explanations for the polarization can be mooted. The first (not so much an explanation as a restatement of the question

in structural terms) holds that the polarization is an intrinsic property of the electronic structure of the platelet (whether describable under alternative (*b*) or (*c*)). The second explanation has features in common with the explanation offered in § 7 (*c*) to account for the polarization of blue cathodoluminescence from dislocations. It asserts that the platelets act as two-dimensionally extended traps for electrons and holes. Electron-hole pairs recombining on the platelet would radiate with ***E*** vector in the plane of the platelet. If, however, recombination excites the H3 centre by an Auger process, then it would appear plausible that out of all possible equivalent orientations of H3 centres the dominating excitations would be of those which could have been stimulated by an ***E*** vector in the platelet plane. The luminescence emitted when the H3 centre returned to its ground state would be correspondingly polarized.

Whichever of these 'explanations' is nearer the truth, from neither could a definite pointer to one of the alternatives (*b*) or (*c*) be inferred. However, it may be noted that the first explanation of polarization imposes stricter conditions than the second upon whatever model is conceived for the electronic structure in the platelet, and might be hard to satisfy in the case of alternative (*b*). The second explanation would not work if the platelet were many unit cells in thickness.

One idea prompted by the observation of polarized emission from the platelets is that their luminescence might be coherent stimulated emission. This idea is rejected both because of the short lifetime reported for the H3 centre, about 17 ns (Crossfield, Davies, Collins & Lightowlers 1974), and also because of the apparent tendency towards saturation of emission from the platelets at the higher levels of excitation, similar to that observed in the H3 system emission from slip traces, as discussed in § 4 (*a*).

Next consider the dim aureoles surrounding the largest platelets which are contained within the core region of specimen CI9 where band A cathodoluminescence is very low (described at the conclusion of § 4 (*b*)). Three views concerning the origin of this phenomenon may be entertained. The first holds that the dim aureole represents a volume from which certain impurity, one which is responsible for at least some fraction of the band A cathodoluminescence, has diffused towards the platelet. The second, opposite, view would have some impurity diffuse away from the platelet and partially quench the band A emission within the dim zone surrounding the platelet. The third view involves no compositional differences in the matrix and regards the dim zone as resulting from successful competition by the platelet against band A centres in its vicinity as a site for electron-hole recombination: the required electron-hole pair diffusion distances of *ca.* 5 μm are comparable with the diffusion lengths inferred from cathodoluminescence behaviour in other regions of very low band A emission, as discussed in § 7 (*c*). Of these three, the second is believed to be the least likely, the first most likely, and an observation generally unfavouring to the third will come up for consideration in the penultimate paragraph of this discussion; but none of the three comes into conflict with either alternative (*b*) or (*c*).

The third optical phenomenon to be discussed concerns the remarkably uniform brightness of the large platelets. This is not obviously apparent in figure 9 because of the varying depth below the surface at which platelets lie, and because of the departure of the polished specimen surface from true parallelism with the cube plane. The latter departure would be sufficient to cause one tip of a platelet of, say, 50 μm in extreme dimensions to differ in depth from an opposite tip by several micrometres, and over that depth difference a considerable change in rate of energy loss of the primary electrons could take place. For platelets near the surface,

the perturbing effects of the surface slope relative to the platelet plane can be averaged out by accumulating observations made over the widest range of kilovoltage available (5 to 50). These established that not only over the surface of a given platelet, but also from platelet to platelet, the luminosity is uniform under given conditions of local stimulation. In particular, no steps or other discontinuities in luminosity were perceived on any platelet. The essential proviso restricting such demonstration of uniformity is that the platelets concerned must reside in matrices indistinguishable in band A emission characteristics: what happens when this condition is not fulfilled will be discussed below. The property of uniform luminosity leads to the following conclusions. If the site of the H3 centre is within the platelet structure, then the platelets ought to be all of constant and equal thickness. If the centres are at the interface between diamond matrix and platelets (the latter now being possibly of multimolecular thickness), then the interface ought to have a uniform and similar structure over all platelets. Alternative (*b*) embraces identity of platelet thickness, bringing uniformity in luminosity as a natural concomitant. It could also be held that the simpler the platelet composition and structure, the more likely would uniformity in its properties be. Perhaps a slight bias towards alternative (*b*) follows from these observations.

Lastly, the circumstances that lead to departure from the above-described brightness uniformity will be considered. Some large platelets may extend across a boundary between zones which differ in strength of band A cathodoluminescence. There is then observed a diminution in luminosity of that section of the platelet which resides in the zone of higher band A emission. Some manifestations of this effect appear in the field of figure 9 (at least on the original film) where it is seen that those platelets that poke out of the zones of appreciable band A cathodoluminescence which run parallel to the right and left hand margins become more brilliant when they enter the region of minimal band A cathodoluminescence which occupies the major area of the field. It is a general observation that with increasing level of band A emission the platelets, when they can be resolved at all, diminish in brightness as well as in size. Their emission then appears spectroscopically as a broad hump between roughly 500 and 550 nm superimposed upon the band A spectrum. As far as visual assessments of band A cathodoluminescence are concerned, the spectral hump between 500 and 550 nm, coinciding with the peak in spectral sensitivity of the eye, makes an important contribution to the overall brightness of the band A-emitting regions, and increases the apparent lack of saturation in their colour. In room temperature observations the hump does not stand out recognizably as the H3 system spectrum, as does the emission from slip-bands in type II zones (exemplified by the spectrum in figure 12). Future experiments, with more refined techniques, should discover how closely matched are the spectra from slip bands, from large platelets in type II zones and from smaller platelets in zones not weak in band A cathodoluminescence. It can be said now that the cathodoluminescence patterns from regions of crystals which contain zones of different band A intensity within which lie individually resolvable platelets are quite consistent with the supposition that two populations of nitrogen impurity aggregates of very different dimensional order co-exist. Band A cathodoluminescence can be attributed to the 'small clusters', but the relative contributions of the A and B forms of small cluster under various conditions of stimulation are as yet unknown. The observations suggest that the fraction of nitrogen impurity present in platelet form is quite variable, but is not determinable from such observations on the basis of present understanding of the cathodoluminescence of the several types of defects concerned.

Two explanations may be put forward to account for the progressive weakening of individual

platelet brilliance in matrices of increasingly strong band A emission. One is that in such matrices the platelets have acquired less of the additional (unknown) impurity which is responsible for the H3 centres: this explanation implies alternative (*c*). The other is that band A centres compete successfully against platelets as recombination centres. This latter mechanism needs to be invoked in supporting alternative (*b*). (It is in apparent conflict with the third of the three explanations offered to account for the dim aureoles surrounding the very large platelets in regions of minimal band A cathodoluminescence; but it is not necessary to place much weight on that particular explanation of the aureoles. Moreover, the two observations relate to matrices greatly differing in concentrations of band A centres, and, quite possibly, in the average composition of the centres as well.)

Against alternative (*b*), which requires the presence of H3 centres in the 'normal' nitrogen platelet structure, there stands the objection that more widespread manifestation of H3 centre activity would be expected from nitrogen-platelet containing diamonds in their natural state (*before* irradiation and annealing in the laboratory) than is in practice observed. In the case of cathodoluminescence this difficulty can be obviated by the plausible assumption that the commonly occurring, sub-micrometre platelets, which are closely surrounded by the small clusters which form the band A luminescence centres, fail against the latter as electron-hole recombination sites. On the other hand, the objection stands with regard to the lack of ubiquitous H3 system absorption and fluorescence by platelet-containing diamonds. Nevertheless, rejection of alternative (*b*) in favour of (*c*) does not appear justifiable on the evidence solely of the cathodoluminescence phenomena reported in the present work. Clearly, there is a close parallel between the dimming or disappearance of H3 system emission from platelets in band A-emitting zones with the similar dimming or disappearance of the H3 system emission from the slip traces when they transect zones emitting band A cathodoluminescence. So an explanation of the cathodoluminescent properties of the platelets cannot be dissociated from any offered to account for H3 system emission from dislocations; and any structure proposed for the H3 centre itself must be compatible with these and other topographically defined associations of H3 system emission that have been disclosed.

For the loan of specimens the authors thank Dr R. Caveney, De Beers Consolidated Mines Ltd; Mr W. F. Cotty, Industrial Distributors Ltd; Dr M. J. Mendelssohn and Dr H. J. Milledge, University College London; Professor W. A. Runciman, Australian National University, Canberra; Dr M. Seal, D. Drukker & Zn.; Professor J. M. Thomas, Edward Davies Chemical Laboratory, University College of Wales, Aberystwyth; and Dr A. D. Yoffé, Cavendish Laboratory, Cambridge.

The authors also thank Mr D. P. Siddons for help in constructing electronic apparatus used in the ultraviolet television experiments.

Financial support from the Science Research Council is gratefully acknowledged.

Some electronic equipment used was constructed in the course of work supported by the Royal Society Paul Instrument Fund, which help is gratefully acknowledged. One of the authors (I. K.) expresses his indebtedness to Industrial Distributors Ltd for financial support.

Professor F. C. Frank, F.R.S., is thanked for his interest in the work.

The colour plates were reproduced by John Swain & Son Ltd, London, E.C.1.

References

Berman, R. (ed.) 1965 *Physical properties of diamond.* Oxford: Clarendon Press.

Caticha-Ellis, S. & Cochran, W. 1958 *Acta crystallogr.* **11**, 245–249.

Chen, L. W. 1973 Ph.D. thesis, University of Bristol.

Clark, C. D. 1965 In *Physical properties of diamond* (ed. R. Berman), ch. XI, pp. 295–324. Oxford: Clarendon Press.

Clark, C. D., Ditchburn, R. W. & Dyer, H. B. 1956*a* *Proc. R. Soc. Lond.* A **234**, 363–381.

Clark, C. D., Ditchburn, R. W. & Dyer, H. B. 1956*b* *Proc. R. Soc. Lond.* A **237**, 75–89.

Clark, C. D., Maycraft, G. W. & Mitchell, E. W. J. 1962 *J. Appl. Phys.* **33**, Suppl. no. 1, 378–382.

Clark, C. D. & Norris, C. A. 1970 *J. Phys.* C **3**, 651–658.

Collins, A. T. 1974 *Industr. Diamond Rev.* **34**, 131–137.

Crossfield, M. D., Davies, G., Collins, A. T. & Lightowlers, E. C. 1974 *J. Phys.* C **7**, 1909–1917.

Davies, G. 1970 *Nature, Lond.* **228**, 758.

Davies, G. 1971 *Proc. Int. Conf. on Phonons*, Rennes, France (ed. M. A. Nusimovici), pp. 382–386. Paris: Flammarion.

Davies, G. 1972*a* *J. Phys.* C **5**, 2534–2542.

Davies, G. 1972*b* In *Diamond research 1972*, pp. 21–30. London: Industrial Diamond Information Bureau.

Davies, G. 1974 *Proc. R. Soc. Lond.* A **336**, 507–523.

Davies, G. & Summersgill, I. 1973 In *Diamond research 1973*, pp. 6–15. London: Industrial Diamond Information Bureau.

Dean, P. J. 1965 *Phys. Rev.* **139**, A 588–602.

Dean, P. J., Kennedy, P. J. & Ralph, J. E. 1960 *Proc. Phys. Soc.* **76**, 670–687.

De Vries, R. C. 1973 *Mat. Res. Bull.* **8**, 733–742.

Dyer, H. B. & du Preez, L. 1965 *J. chem. Phys.* **42**, 1898–1906.

Dyer, H. B. & Matthews, I. G. 1957 *Proc. R. Soc. Lond.* A **243**, 320–335.

Ehrenberg, W. & King, D. E. N. 1963 *Proc. Phys. Soc.* **81**, 751–766.

Ehrenberg, W. & Spear, W. E. 1951 *Proc. Phys. Soc.* B **64**, 67–75.

Elliott, R. J., Matthews, I. G. & Mitchell, E. W. J. 1958 *Phil. Mag.* **3**, 360–369.

Evans, T. & Phaal, C. 1962 *Proc. R. Soc. Lond.* A **270**, 538–552.

Evans, T. & Rainey, P. 1975*a* In *Diamond research 1975*, pp. 29–34. London: Industrial Diamond Information Bureau.

Evans, T. & Rainey, P. 1975*b* *Proc. R. Soc. Lond.* A **344**, 111–130.

Frank, F. C. 1956 *Proc. R. Soc. Lond.* A **237**, 168–174.

Frank, F. C. 1964 *Proc. Phys. Soc.* **84**, 745–748.

Garlick, G. F. J. 1966 In *Luminescence of inorganic solids* (ed. P. Goldberg), pp. 685–731. New York: Academic Press.

Hanley, P. L. 1972 M.Sc. thesis, University of Bristol.

Hoerni, J. A. & Wooster, W. A. 1955 *Acta crystallogr.* **8**, 187–194.

Howlett, K. J. 1974 Ph.D. thesis, University of Cambridge.

Kaiser, W. & Bond, W. L. 1959 *Phys. Rev.* **115**, 857–863.

Kiflawi, I. & Lang, A. R. 1974 *Phil. Mag.* **30**, 219–223.

Lang, A. R. 1964 *Proc. Phys. Soc.* **84**, 871–876.

Lang, A. R. 1967 *Nature, Lond.* **213**, 248–251.

Lang, A. R. 1970 *Nature, Lond.* **226**, 345.

Lang, A. R. 1974 *Proc. R. Soc. Lond.* A **340**, 233–248.

Lang, A. R. & Miuscov, V. F. 1964 *Phil. Mag.* **10**, 263–268.

Lightowlers, E. C. & Dean, P. J. 1964 In *Diamond research 1964*, pp. 21–25. London: Industrial Diamond Information Bureau.

Mani, A. 1944*a* *Proc. Indian Acad. Sci.* A **19**, 231–252.

Mani, A. 1944*b* *Proc. Indian Acad. Sci.* A **20**, 155–161.

Mani, A. 1944*c* *Proc. Indian Acad. Sci.* A **20**, 323–328.

Mendelssohn, M. J. 1971 Ph.D. thesis, University of London.

Moore, M. & Lang, A. R. 1974 *J. Cryst. Growth* **26**, 133–139.

Oatley, C. W. 1972 *The scanning electron microscope. Part I. The instrument*, ch. IV. Cambridge University Press.

Ralph, J. E. 1960 *Proc. Phys. Soc.* **76**, 688–696.

Runciman, W. A. & Carter, T. 1971 *Solid State Commun.* **9**, 315–317.

Sellschop, J. P. F., Bibby, D. M., Erasmus, C. S. & Mingay, D. W. 1974 In *Diamond research 1974*, pp. 43–50. London: Industrial Diamond Information Bureau.

Shockley, W. 1961 *Czech. J. Phys.* B **11**, 81–121.

Sobolev, E. V., Lisoivan, V. I. & Lenskaya, S. V. 1967 *Dokl. Akad. Nauk SSSR* **175**, 582–585. English translation: Soviet Physics – Doklady (Crystallography) 1968 **12**, 665–668.

Sutherland, G. B. B. M., Blackwell, D. E. & Simeral, W. G. 1954 *Nature, Lond.* **174**, 901–904.
Takagi, M. & Lang, A. R. 1964 *Proc. R. Soc. Lond.* A **281**, 310–322.
Walker, J. 1975 In *Lattice defects in semiconductors 1974* (ed. F. A. Huntley), pp. 317–324. Bristol and London: The Institute of Physics.
Wight, D. R. 1968 Ph.D. thesis, University of London.
Wight, D. R., Dean, P. J., Lightowlers, E. C. & Mosby, C. D. 1971 *J. Luminescence* **4**, 169–193.
Wittry, D. B. & Kyser, D. F. 1967 *J. Appl. Phys.* **38**, 375–382.
Woods, G. S. & Lang, A. R. 1975 *J. Cryst. Growth* **28**, 215–226.

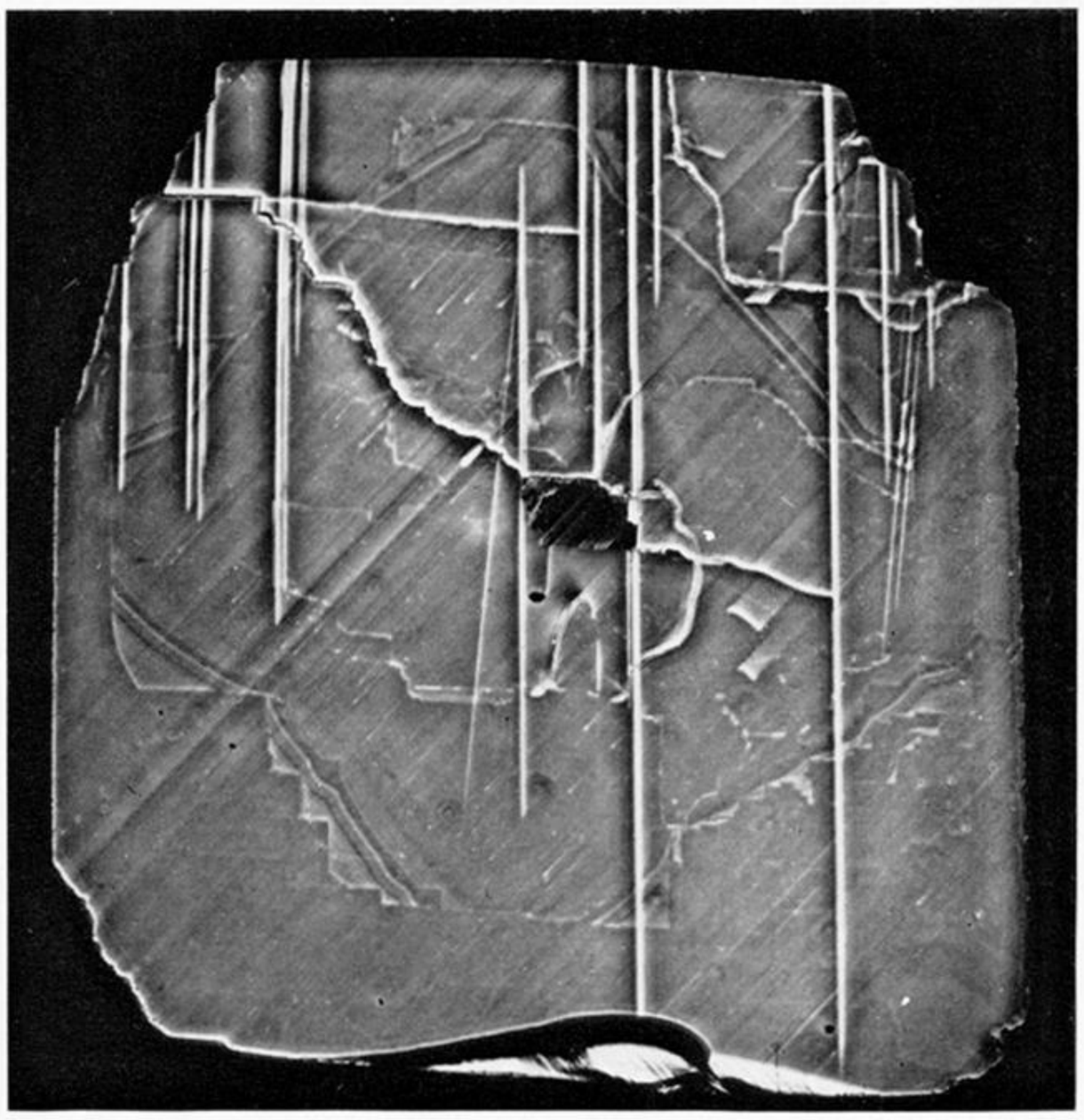

(*a*)

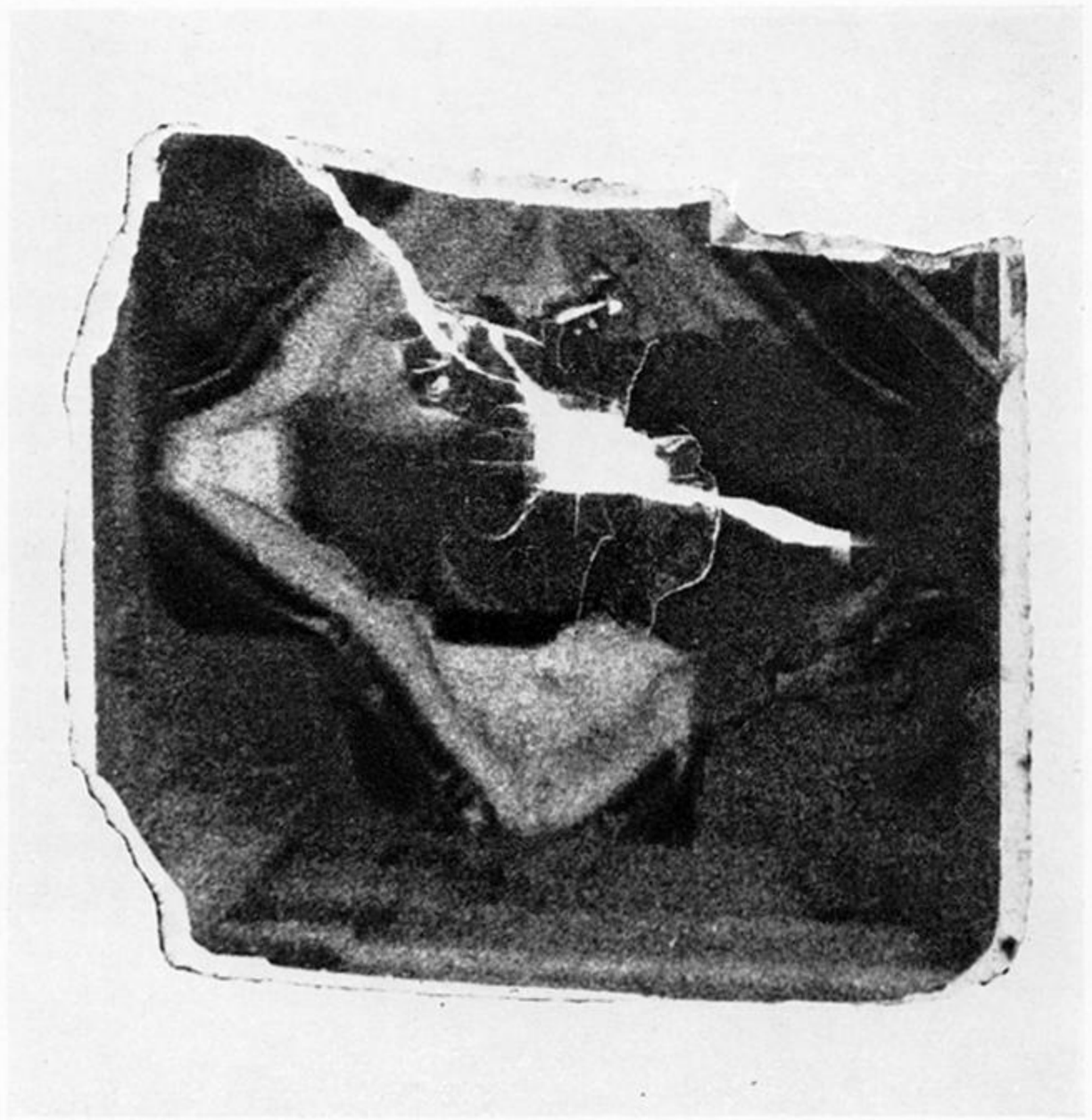

(*b*)

(*c*)

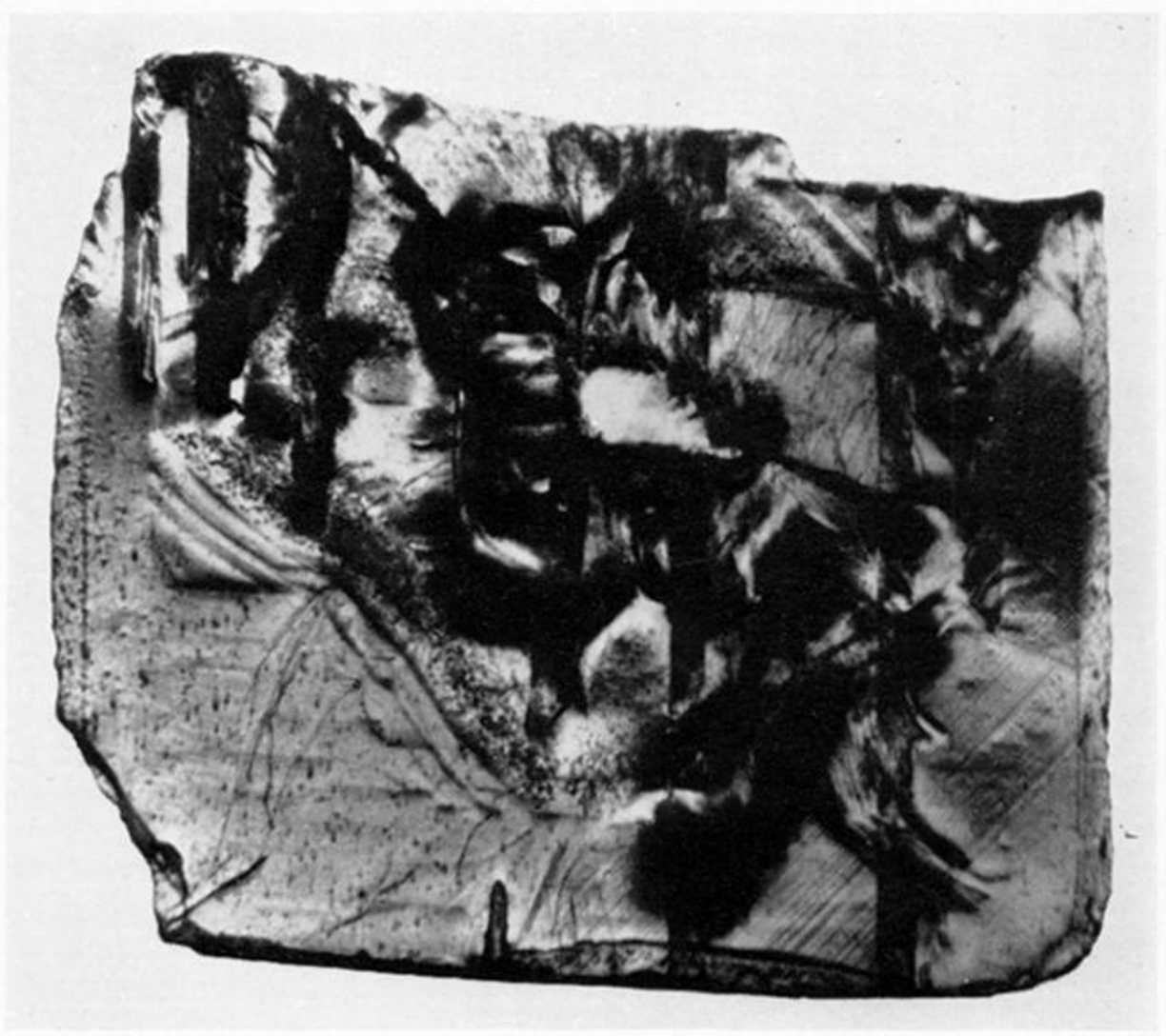

(*d*)

FIGURE 1. (*a*) Phase contrast micrograph of polished surface of diamond S5, orientation near (001). Specimen width is 2.60 mm, and thickness 0.16 mm. The direction [110] points horizontally to the right; the surface normal is tilted about 7° off [001] towards [$\bar{1}$00]. Polishing marks (grooves and scratches) run from lower left to upper right, along the direction of polishing, [010]. Small upstanding triangular areas and curving bands of type II material show lighter than their surroundings and are seen best in the lower left quadrant.

(*b*) Ultraviolet transmission topograph of specimen S5, wavelength 257.5 nm. Image density roughly proportional to ultraviolet transmission. Cracks appear opaque because of reflexions and scattering. The specimen height is smaller in this figure (and in figures 1*c* and *d*) compared with figure 1*a* because of loss of a strip about $\frac{1}{2}$ mm wide from the top of the specimen, the break completing the partial fracture seen running across the top part of the specimen in figure 1*a*.

(*c*) Cathodoluminescence topograph of specimen S5 taken through Kodak–Wratten filter no. 15 which transmits less than 1% at wavelengths below 510 nm. Electron beam energy 20 kV, current density 1 μA mm^{-2}. The small, very dark areas correspond to regions easily transmitting in the ultraviolet: the slip traces give strongest luminescence where they cut through these regions. (Bright images of cracks and bevelled edges of the specimen, due to reflexion of light, have no structural significance and should be disregarded.)

(*d*) X-ray projection topograph of specimen S5. Cu$K\alpha_1$ radiation, reflexion 1$\bar{1}$1 (projection of diffraction vector points downwards). Distorted regions appear black, except for those tilted more than about 2′ off the mean orientation and which in consequence are non-Bragg-reflecting and appear white. Individual dislocations are recognizable in areas not heavily distorted, e.g. the lower left quadrant. Some polishing lines show in the lower right corner. Horizontal traces of boundaries between type Ia and type II regions show stronger diffraction contrast than vertical traces because displacements due to the latter boundaries are principally orthogonal to the diffraction vector.

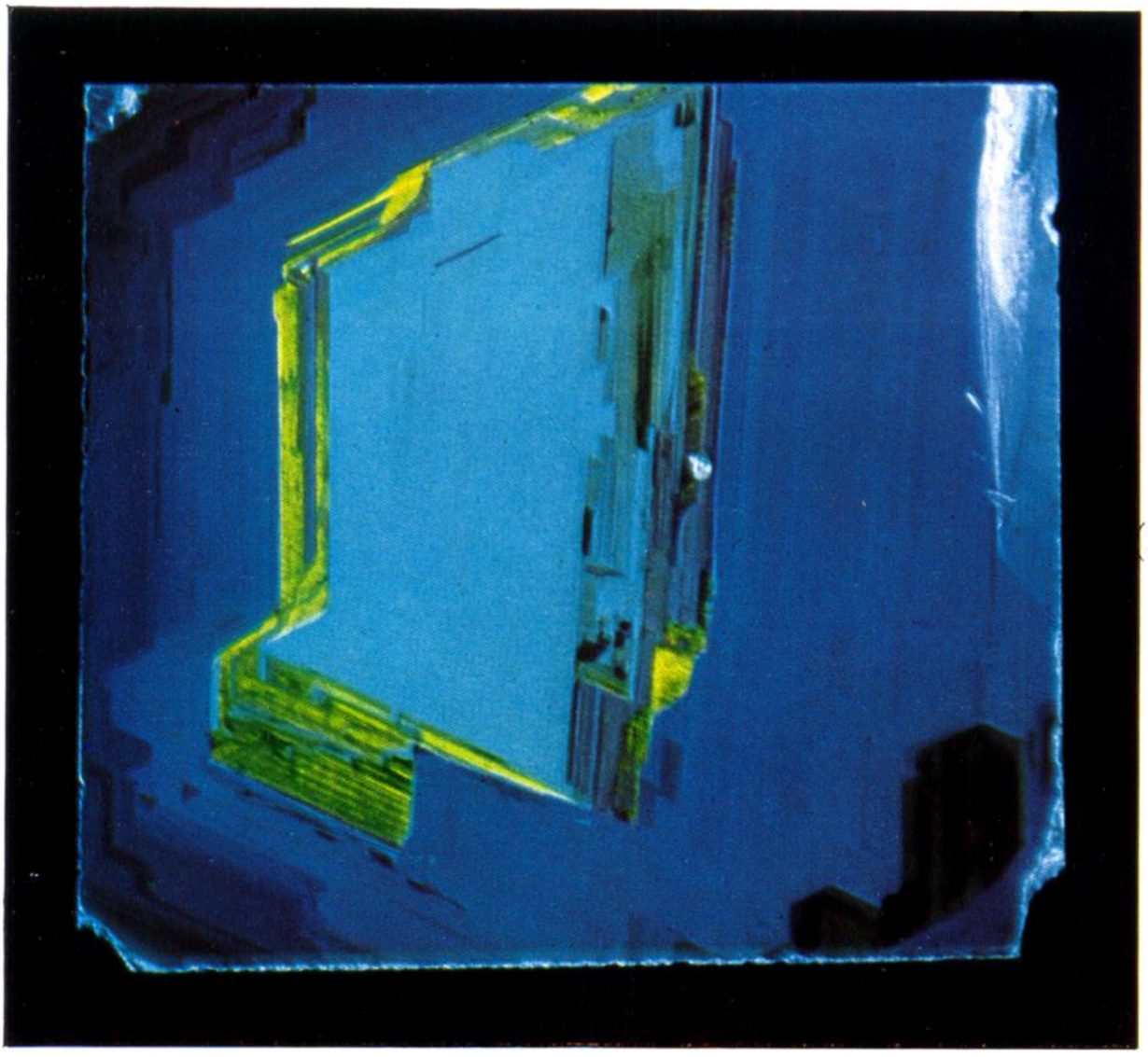

(2a)

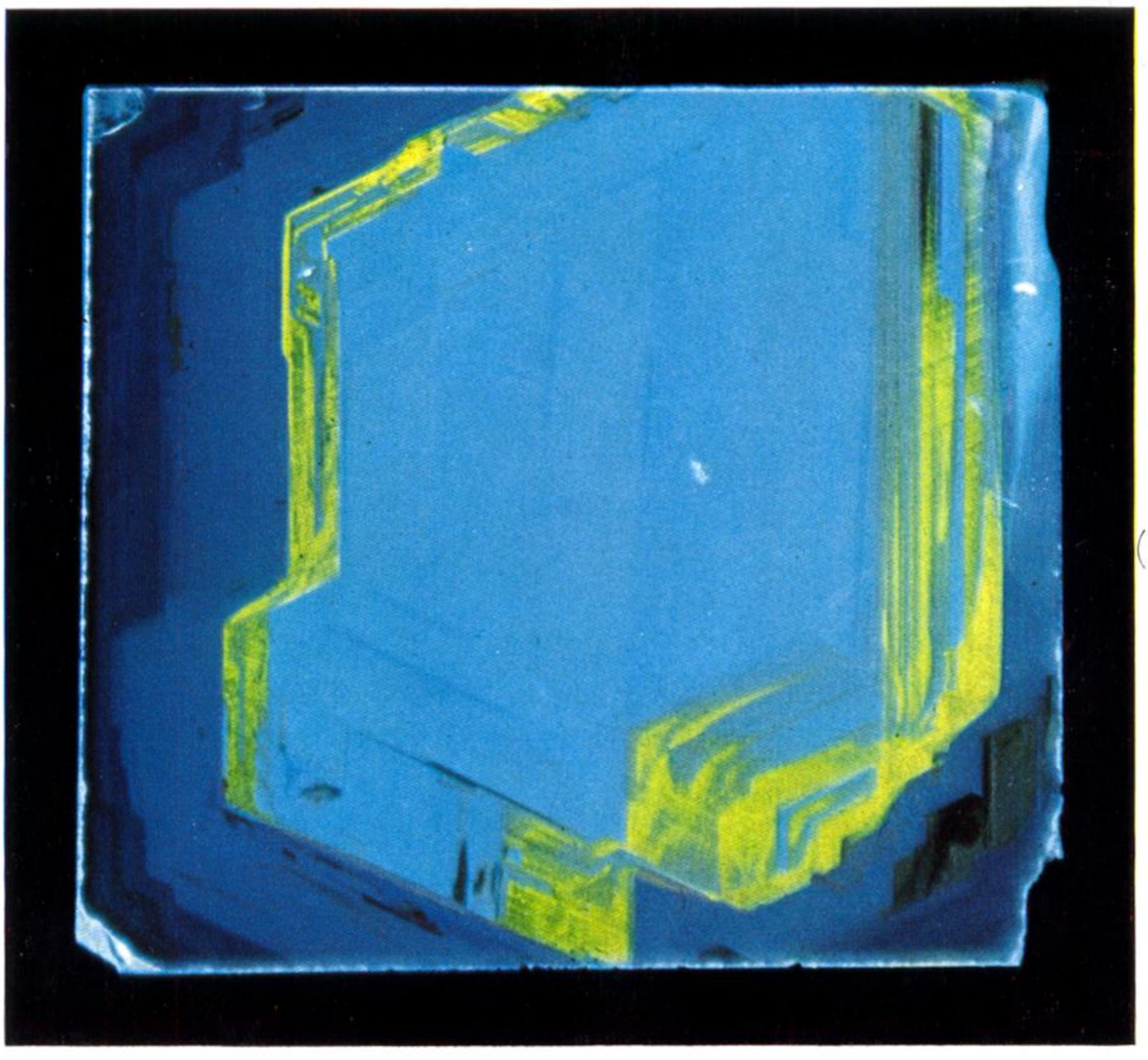

(2b)

FIGURE 2. For description see opposite.

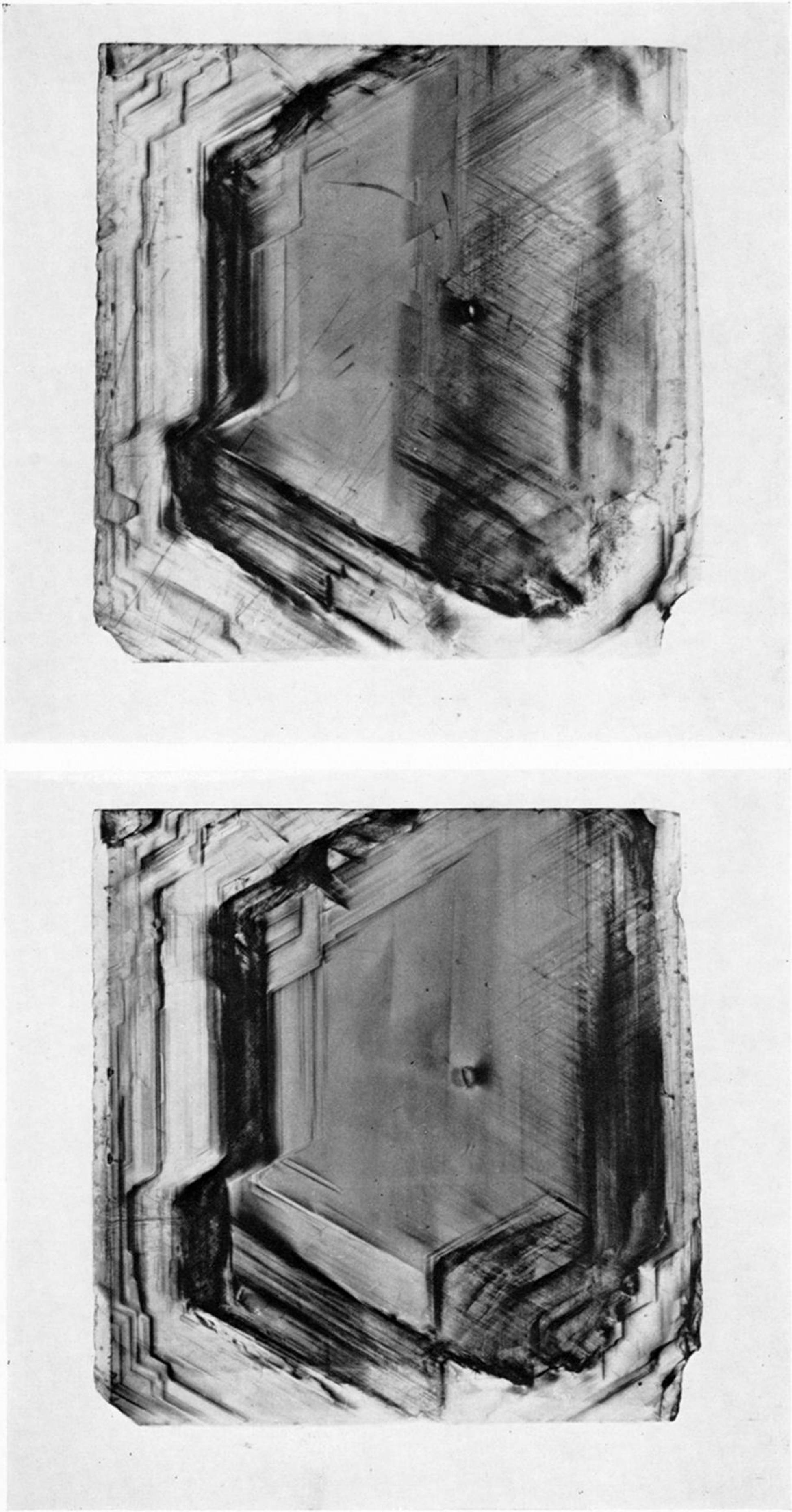

(*a*)

(*b*)

FIGURE 3. Surface reflexion X-ray topographs of specimen GH2, radiation CuKα_1. (*a*) Surface designated 'a', 113 reflexion. (This specimen surface is close to (112) orientation; the direction [1$\bar{1}$0] is nearly parallel to the vertical direction in the plane of the figure but is rotated about 2° out of the specimen surface, towards the observer.) (*b*) Surface designated 'b', $\overline{113}$ reflexion, image printed left-to-right to aid comparison with image of surface 'a'.

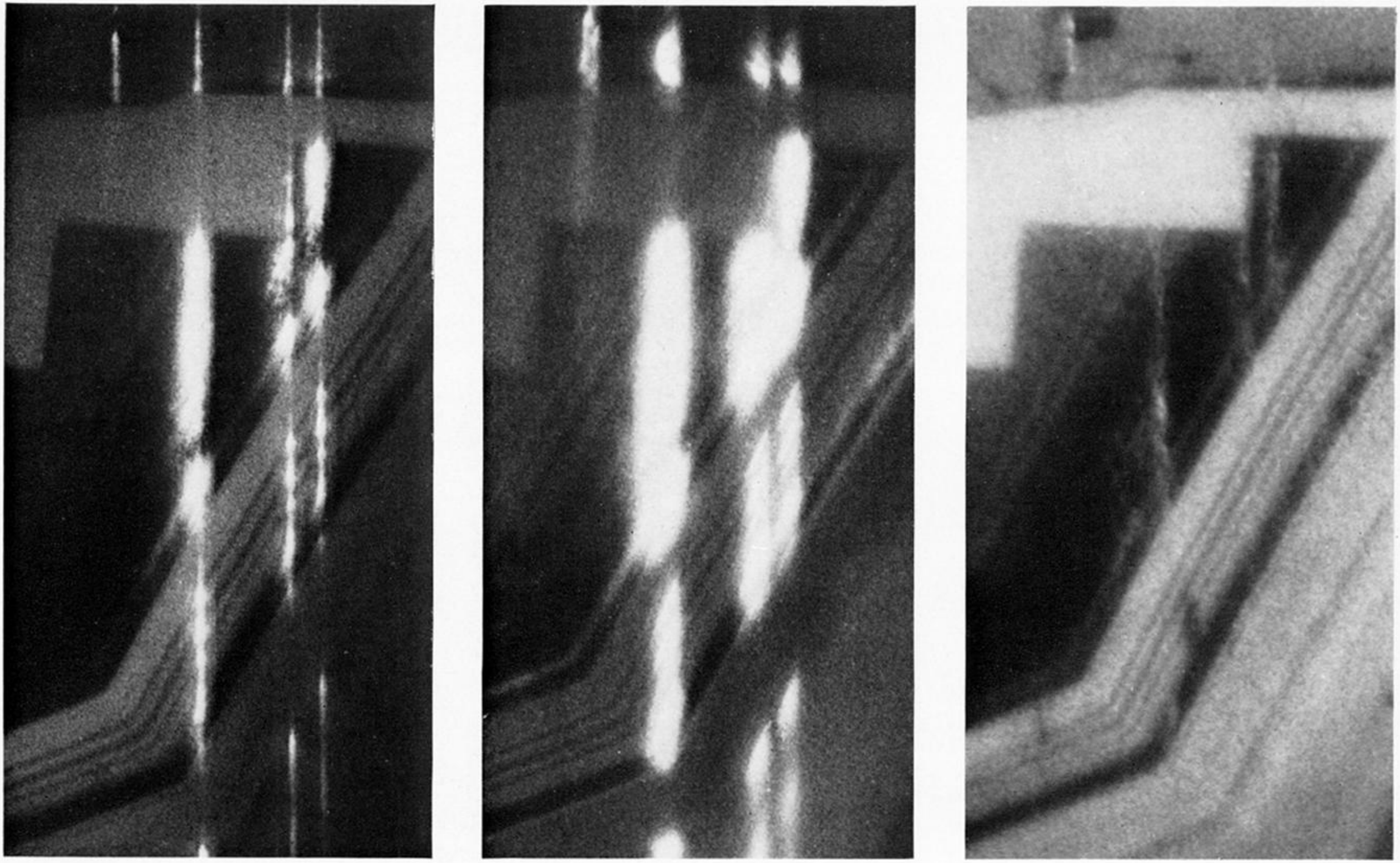

(*a*) (*b*) (*c*)

FIGURE 4. Cathodoluminescence micrographs of a region in the upper left quadrant of specimen S5 (figure 1) where it is cut by slip bands parallel to $(\overline{1}11)$. The micrographs are oriented similarly to figure 1. Field width is 150 μm. (*a*) Electron beam 10 kV, 40 μA mm^{-2}, Kodak–Wratten filter no. 12 transmitting under 1% of wavelengths below 500 nm. The 503 nm-system emission from slip bands appears bright. (*b*) Electron beam 50 kV, 40 μA mm^{-2}, Kodak–Wratten no. 12. Luminescence from slip bands spreads leftwards from their surface outcrops as a consequence of the dip leftwards of $(\overline{1}11)$ below the specimen surface. (*c*) Electron beam 20 kV, 40 μA mm^{-2}, Kodak–Wratten narrow-band, blue-passing filter no. 47B. Image brightness roughly indicates strength of band A cathodoluminescence.

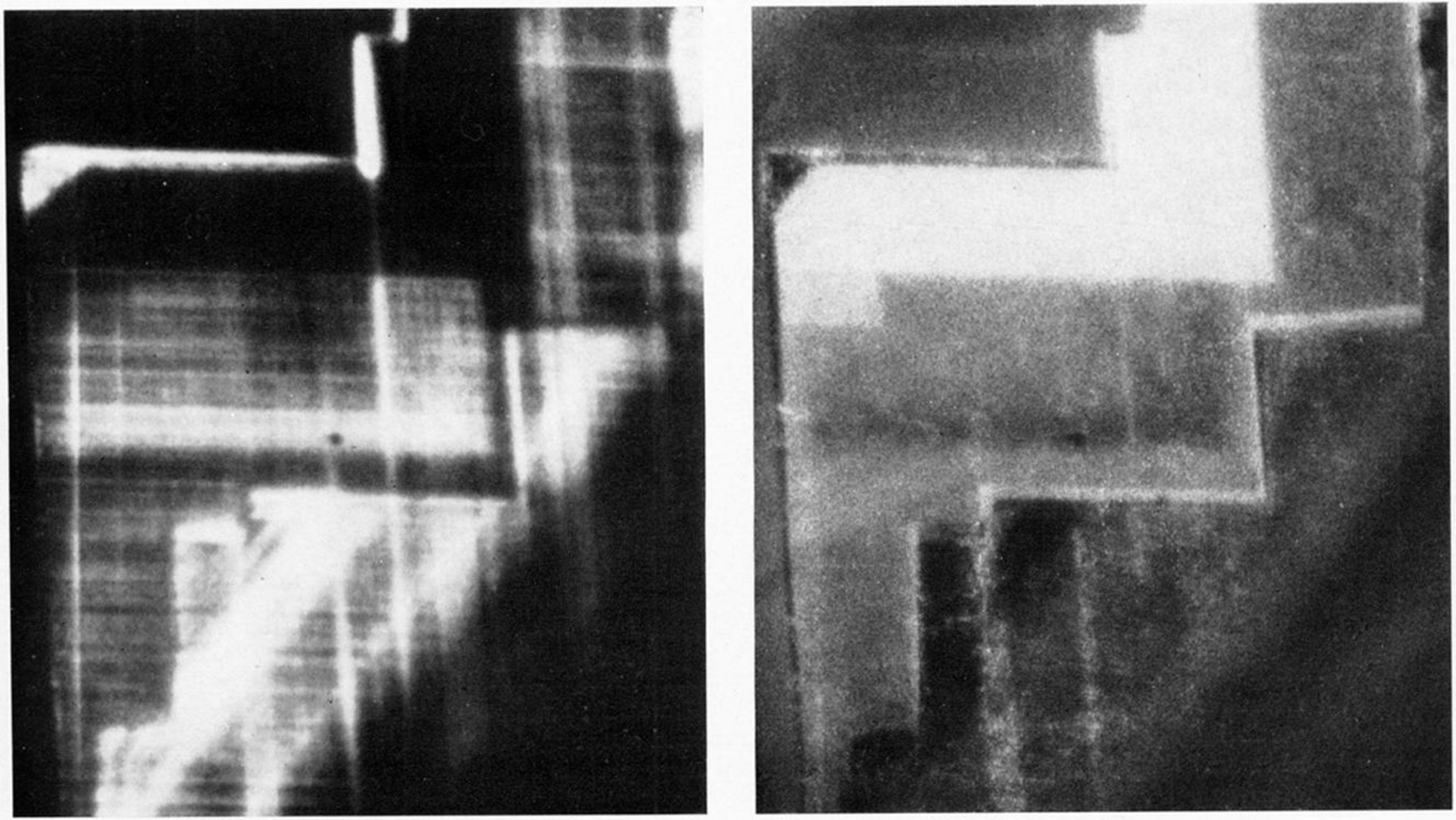

(*a*) (*b*)

FIGURE 5. A region of specimen S1 containing both cuboid and faceted growth layers. The centre of the crystal lies about 2 mm away, below and to the right of the field. Specimen surface roughly parallel to (001). Orientation of figure corresponds to that of figures 1 and 4. Field width is 325 μm. Electron beam 15 kV, 11 μA mm^{-2}. (*a*) Kodak–Wratten filter no. 12. (*b*) Kodak–Wratten filter no. 47B.

(a)

(b)

(c)

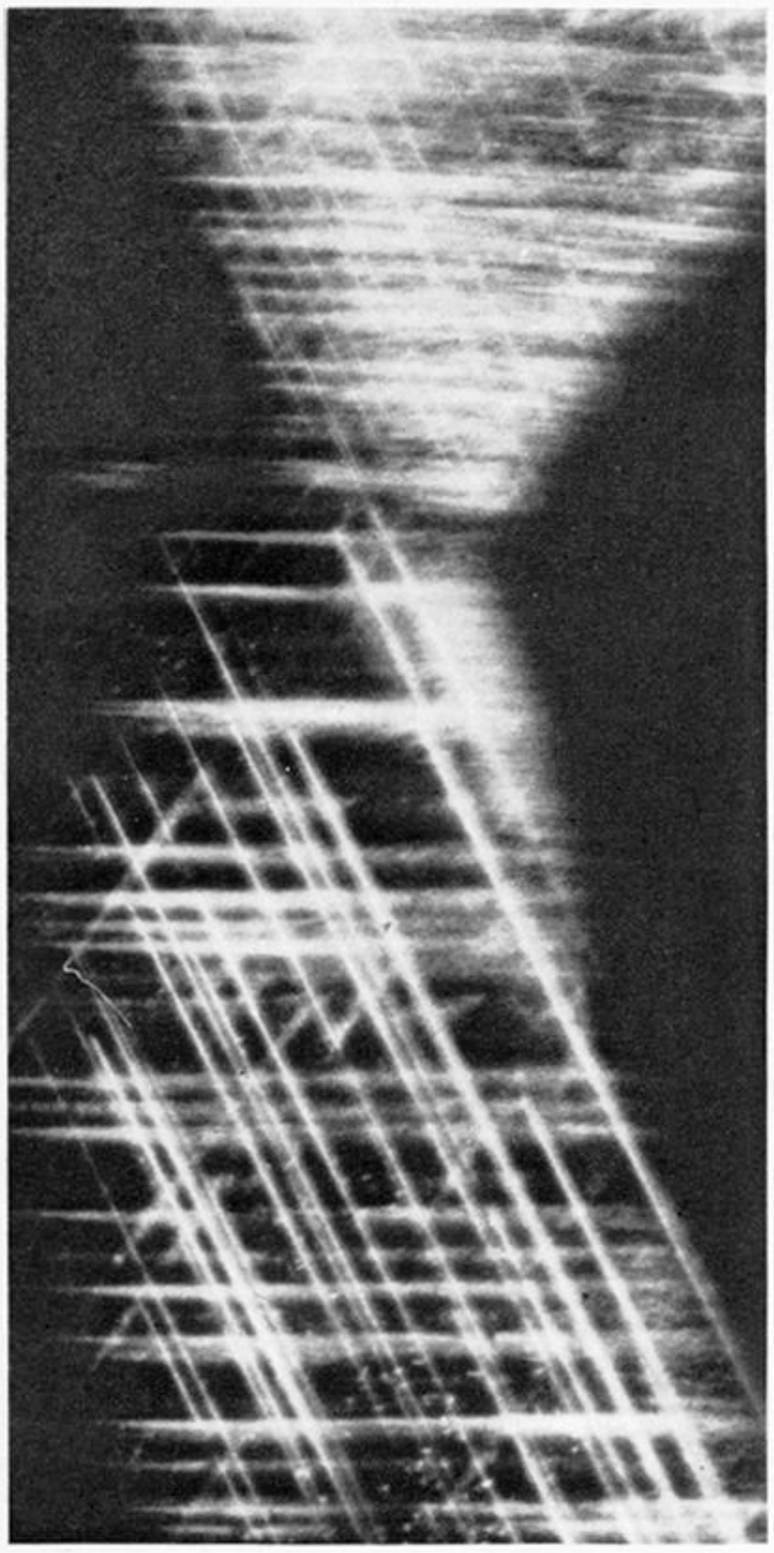

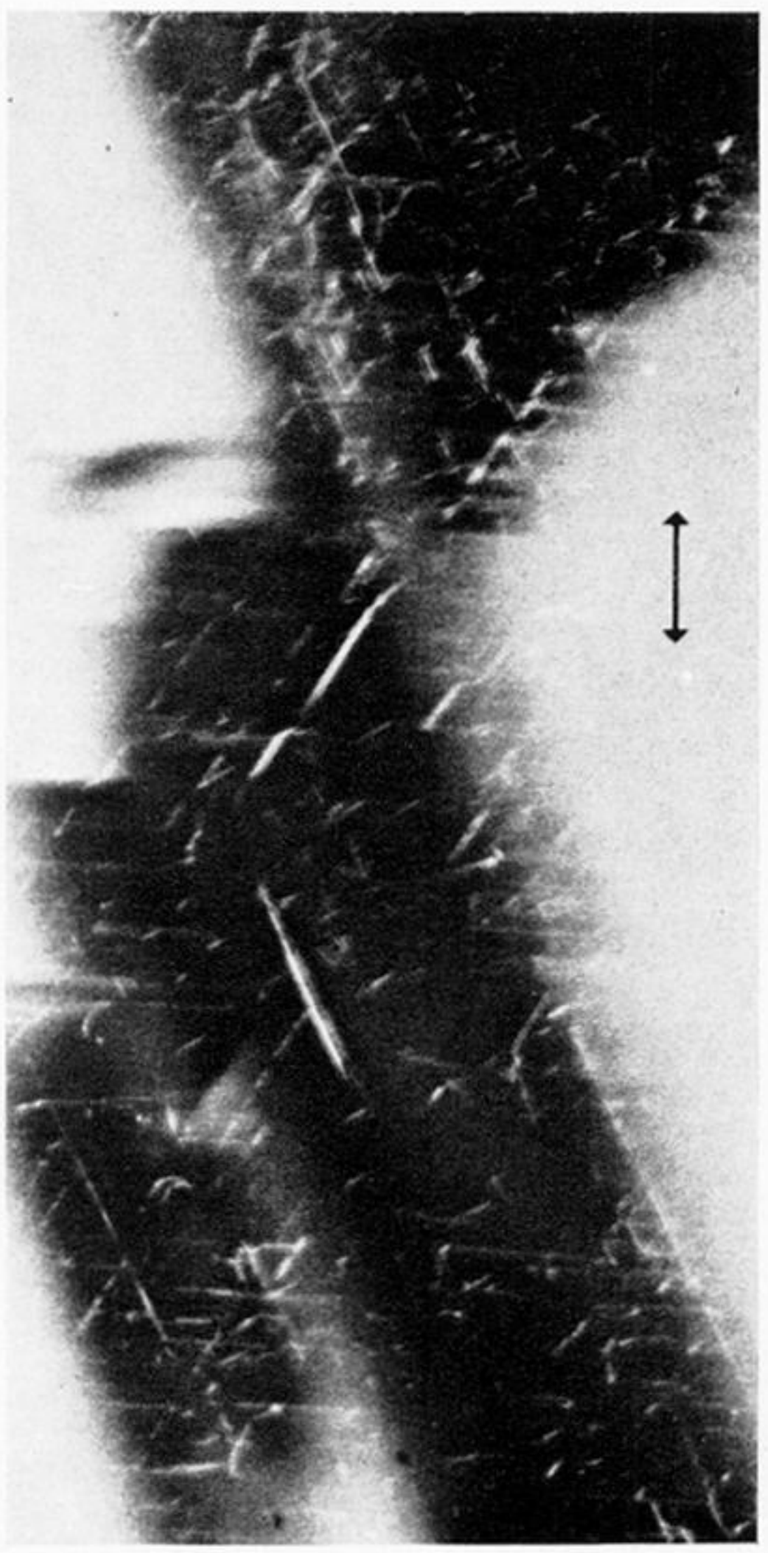

FIGURE 6

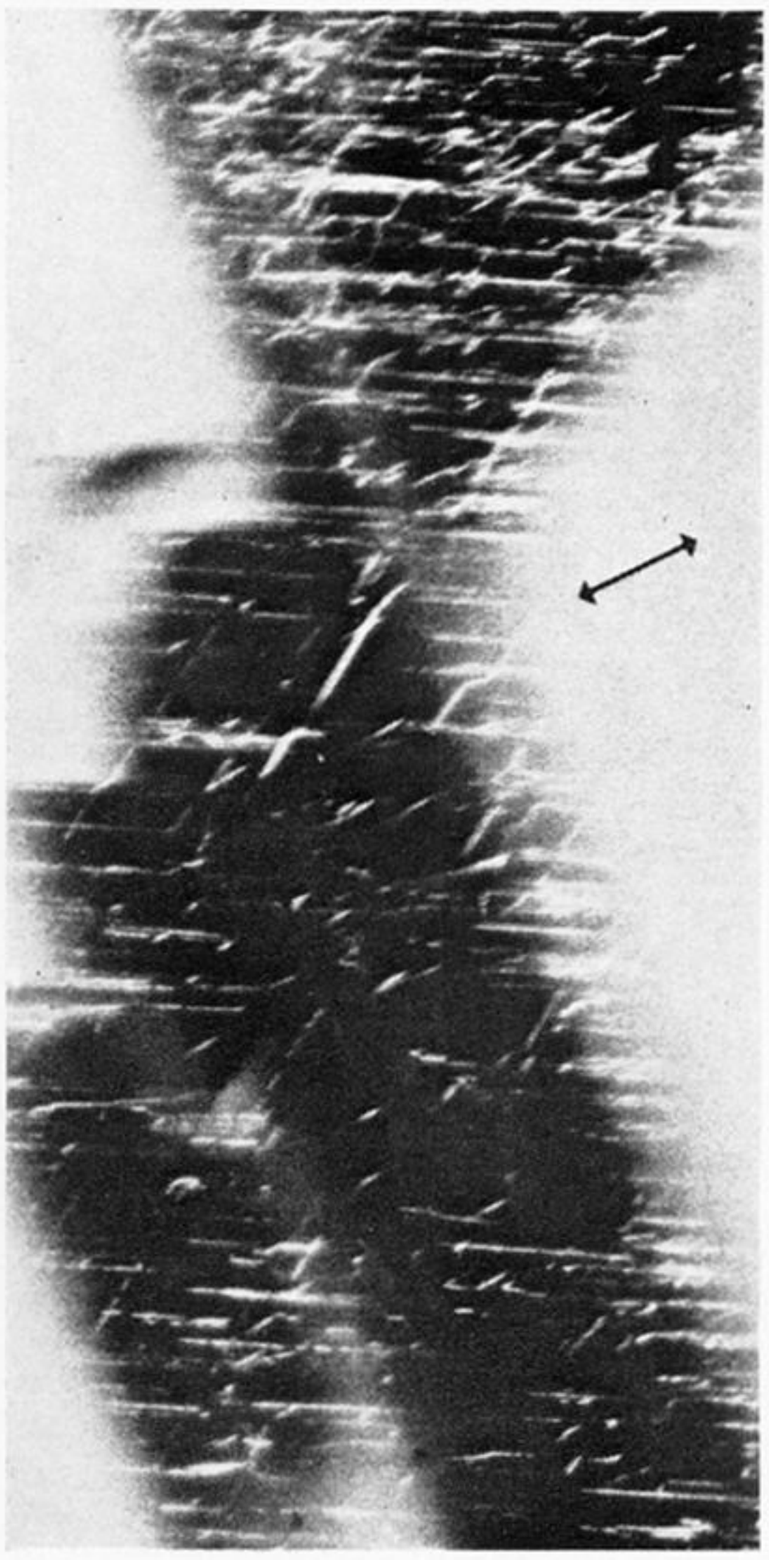

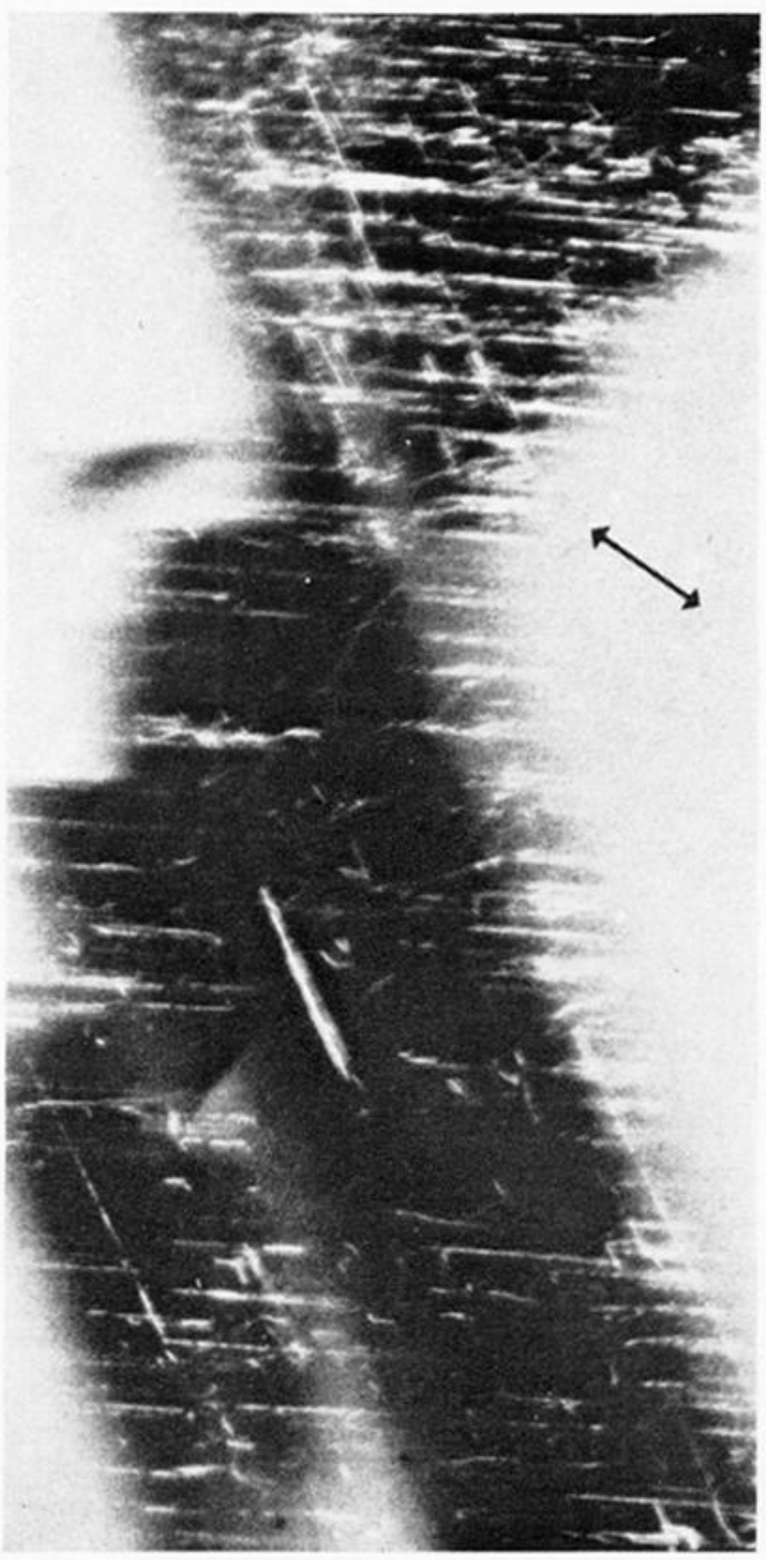

(d)

FIGURE 6

(e)

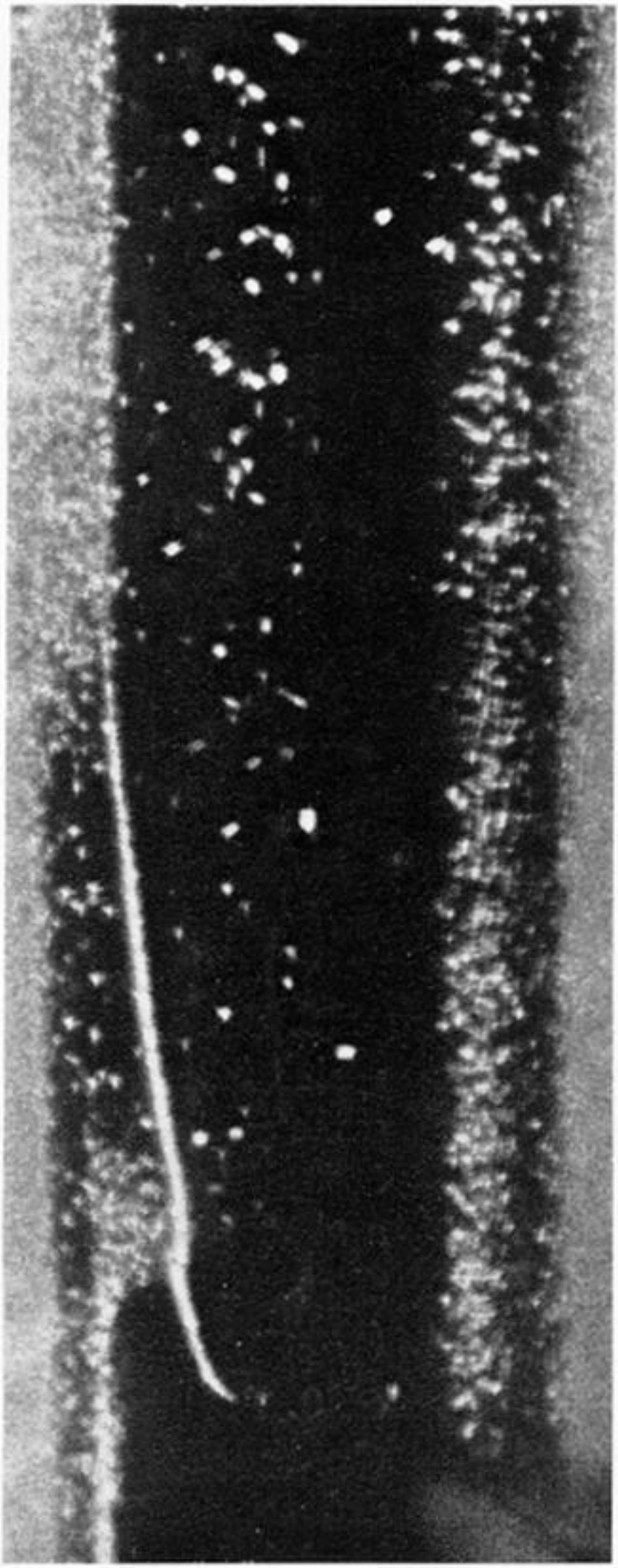

FIGURE 7

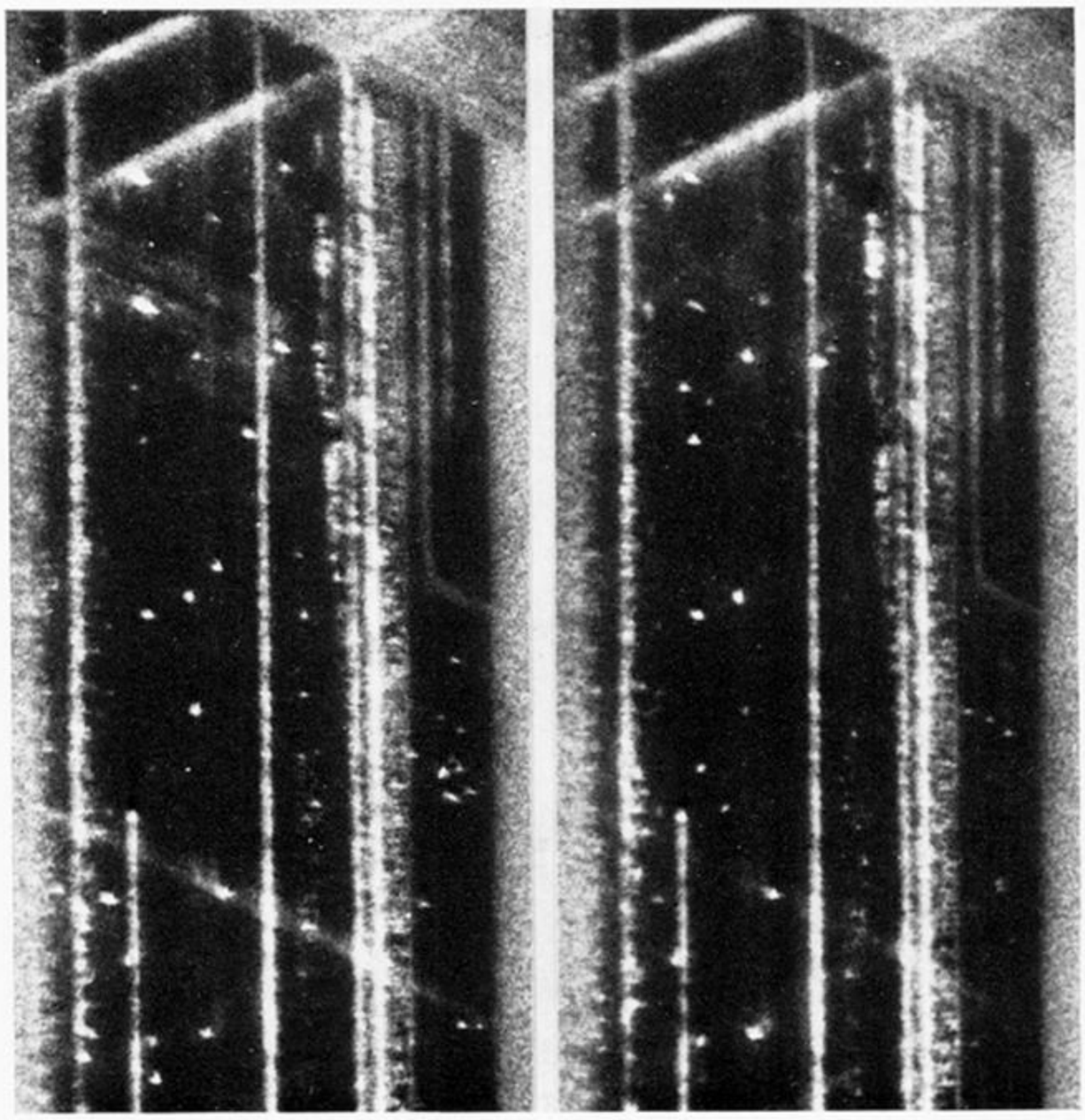

(*a*) (*b*)

FIGURE 8

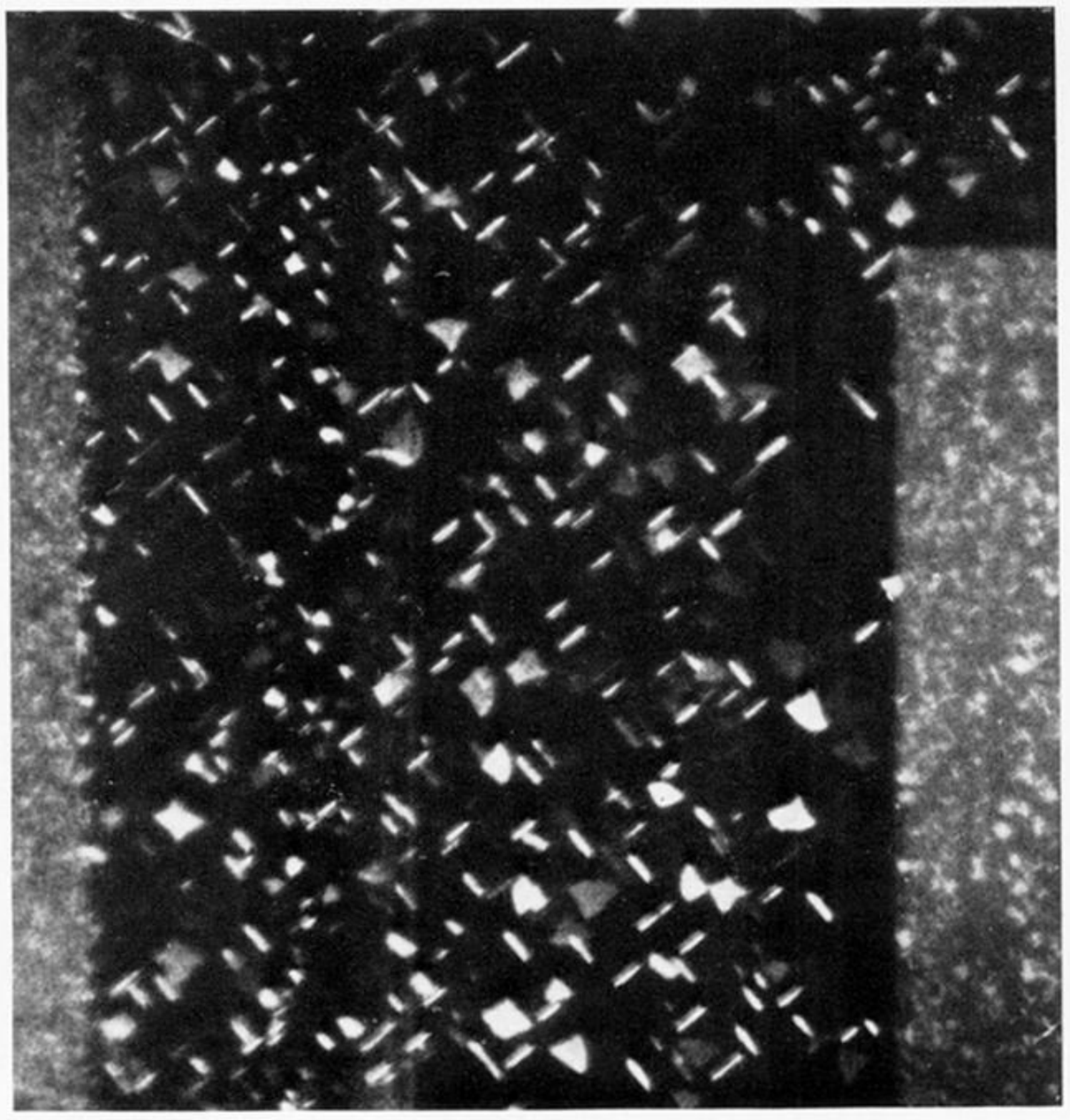

(*a*)

FIGURE 9

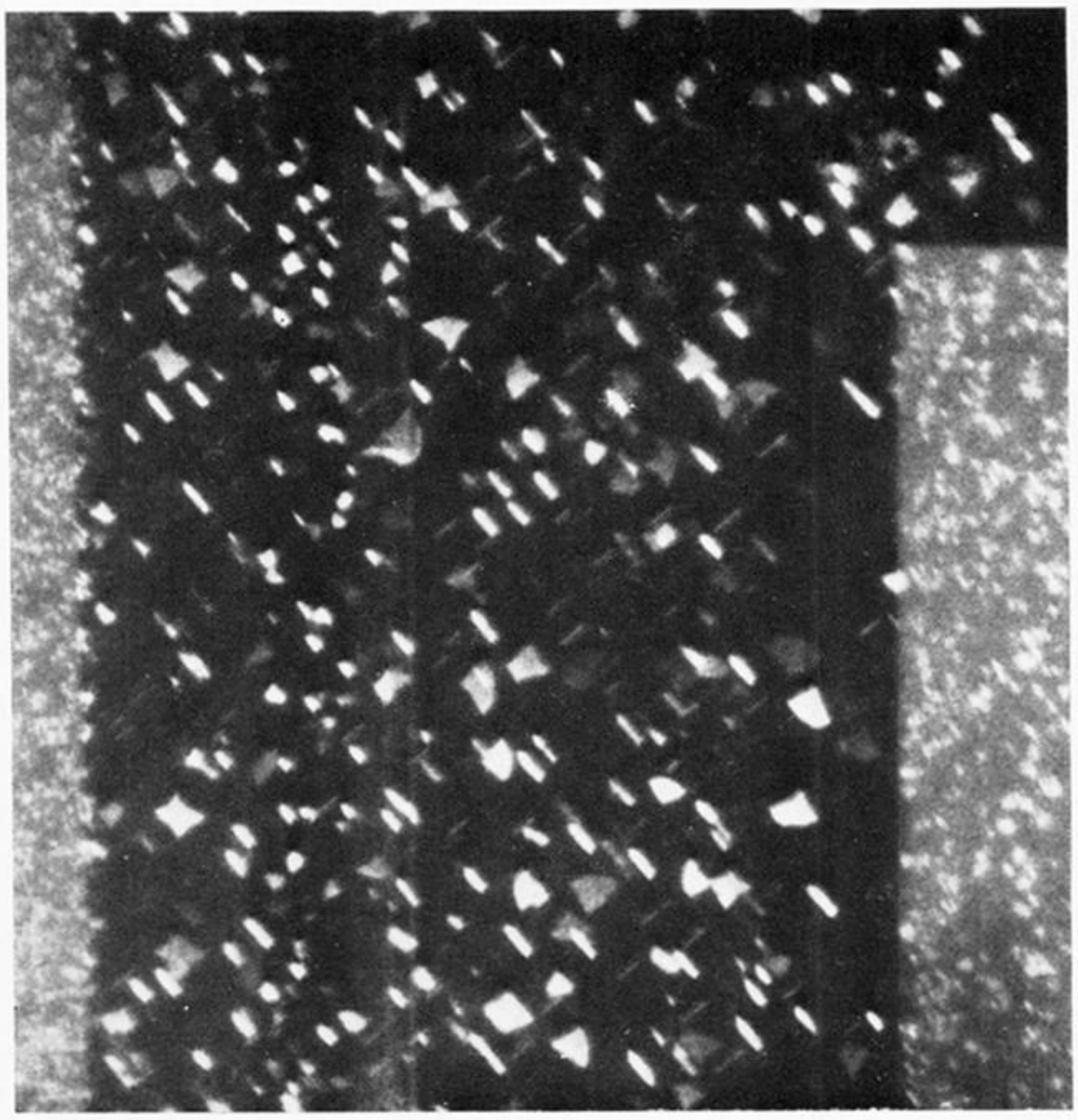

(*b*)

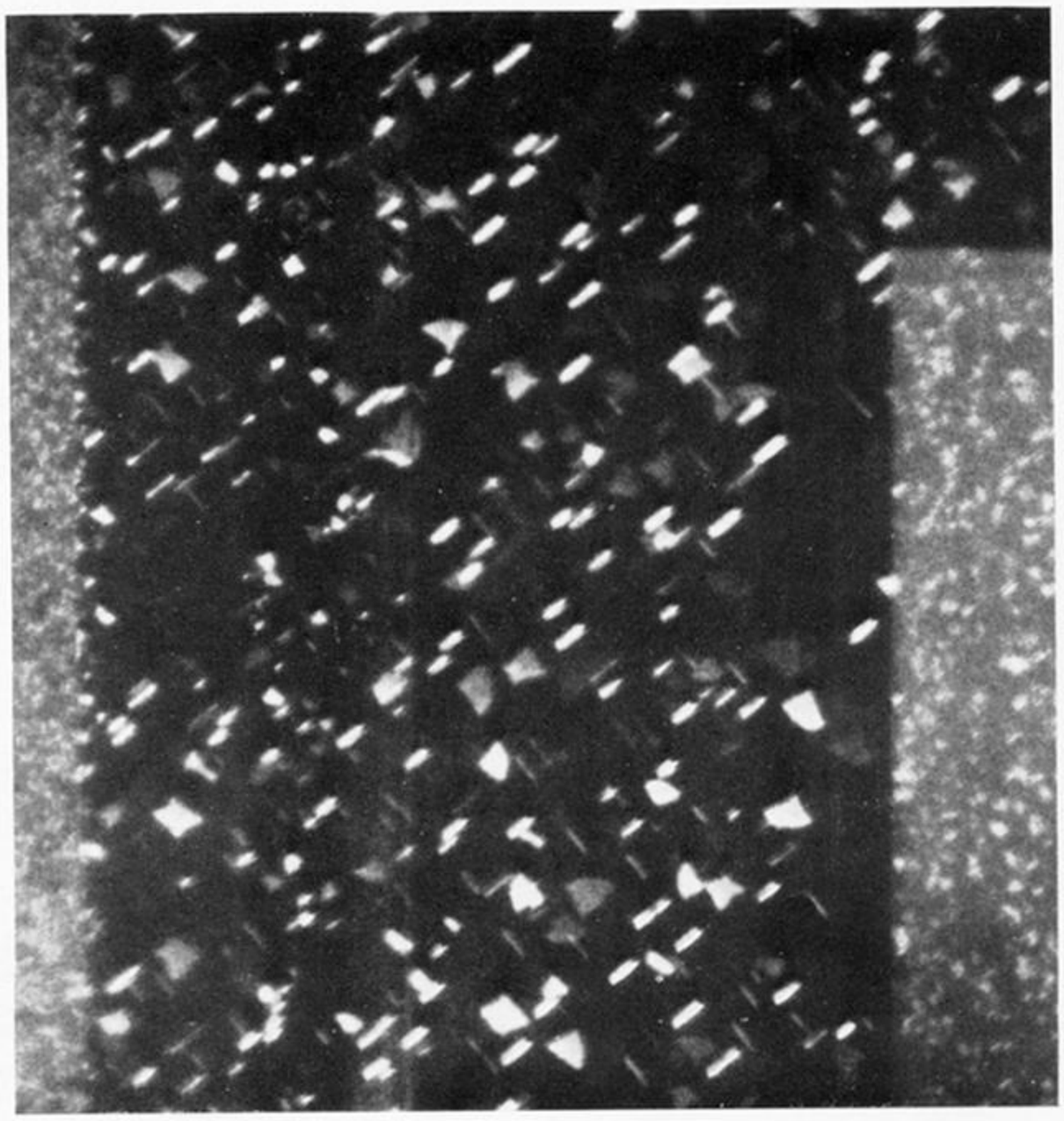

(*c*)

FIGURE 9

FIGURE 8. Polarization of emission from isolated precipitates in a layer of feeble band A cathodoluminescence which is located near the top right corner of face 'b' of specimen GH2, figure 2*b*. Orientation of figure 8 is same as that of figure 2*b*. Traces of $(11\bar{1})$ are vertical, slip traces parallel to $(\bar{1}11)$ slope down to left at about 30° with the horizontal axis, slip traces parallel to $(1\bar{1}1)$ slope down rightwards at about 30° to the horizontal and this is also approximately the direction $[10\bar{1}]$. Electron beam 35 kV, 10.5 μA mm^{-2}. Kodak–Wratten filter no. 12. (*a*) Analyser set to transmit ***E*** vector parallel to $[10\bar{1}]$. (*b*) Analyser perpendicular to setting in (*a*).

FIGURE 9. Polarization of emission from platelets parallel to {100}. Specimen CI9, surface orientation near (001), the direction [110] points horizontally to the right. Field width is 300 μm. Zones of stronger band A cathodoluminescence appear near both left- and right-hand margins. Electron beam 35 kV, 2 μA mm^{-2}. Kodak–Wratten filter no. 12. (*a*) Without Polaroid analyser. (*b*) Analyser rotated to transmit electric vector parallel to [100], i.e. along field diagonal from upper left to lower right. (*c*) Analyser set to transmit electric vector parallel to [010], i.e. along diagonal from upper right to lower left.

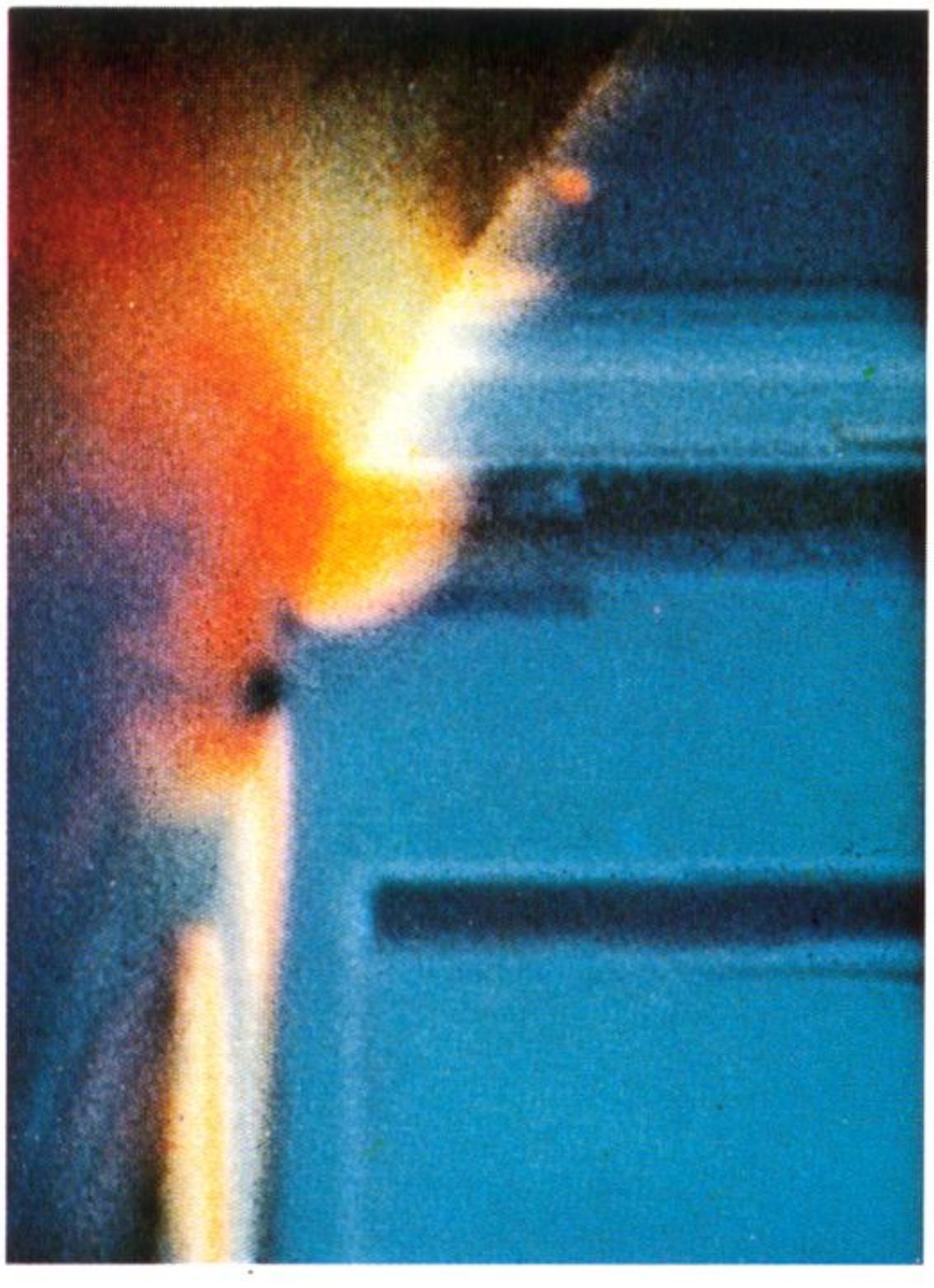

(*a*)

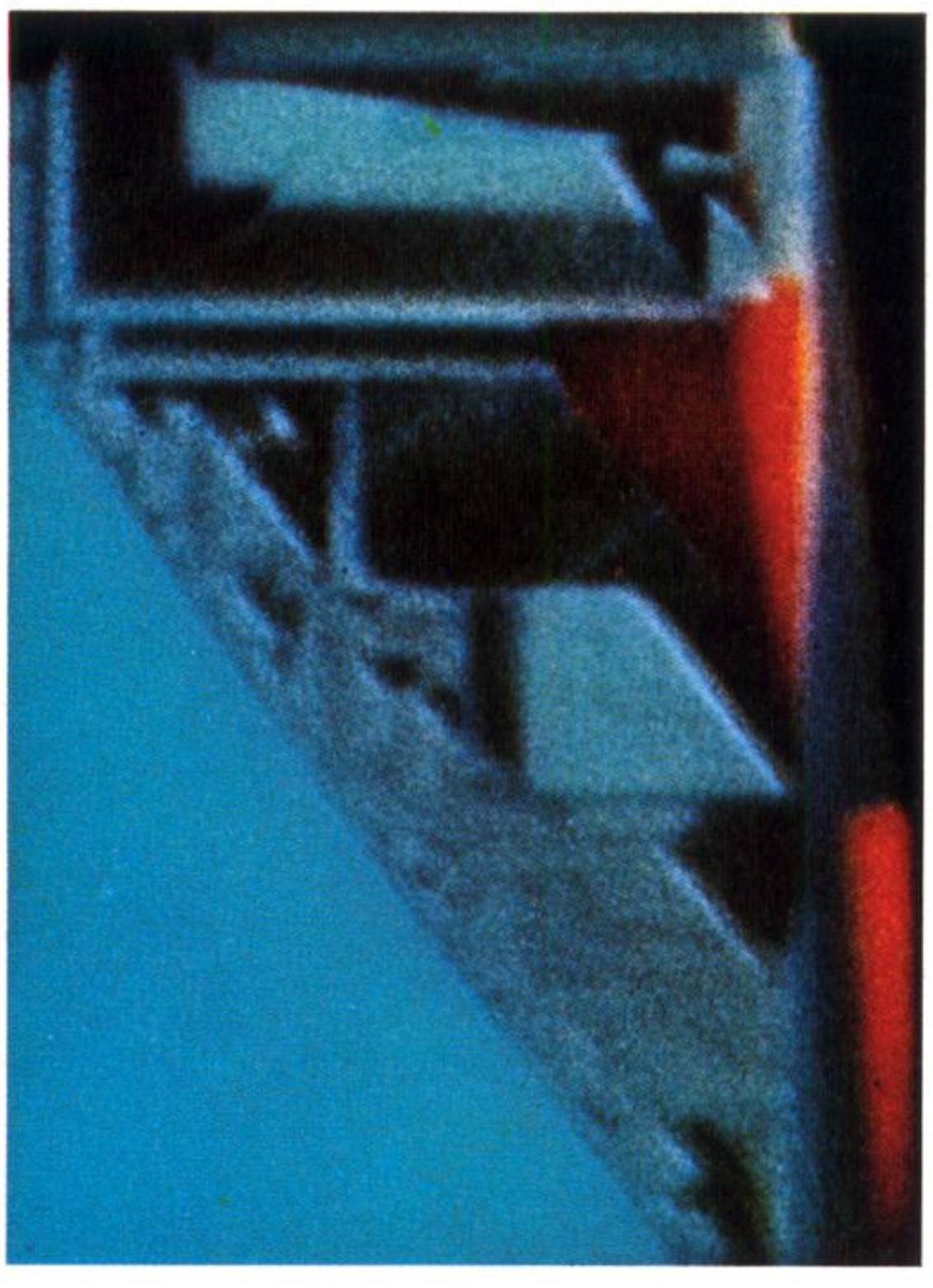

(*b*)

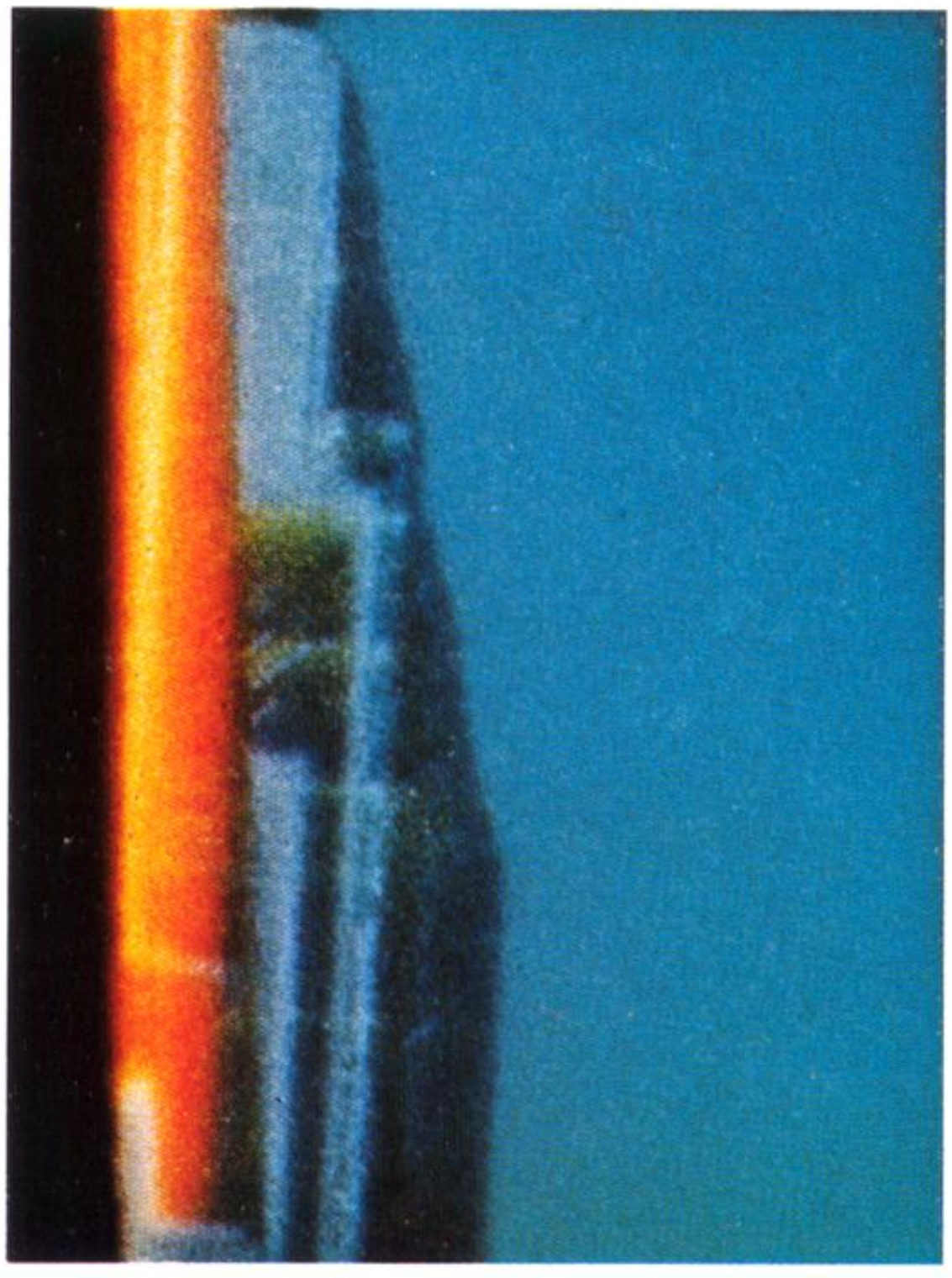

(*c*)

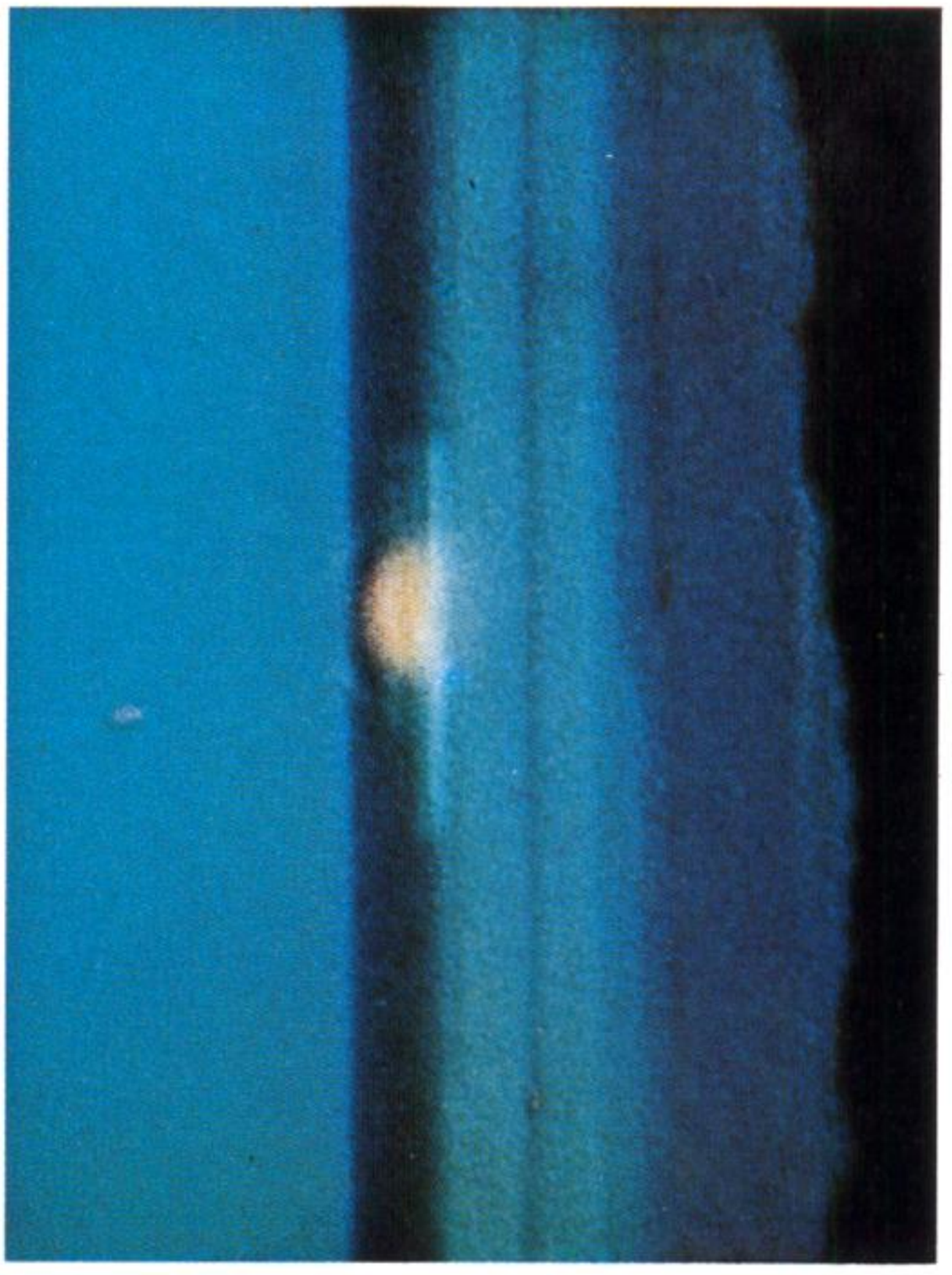

(*d*)

FIGURE 10. For description see opposite.

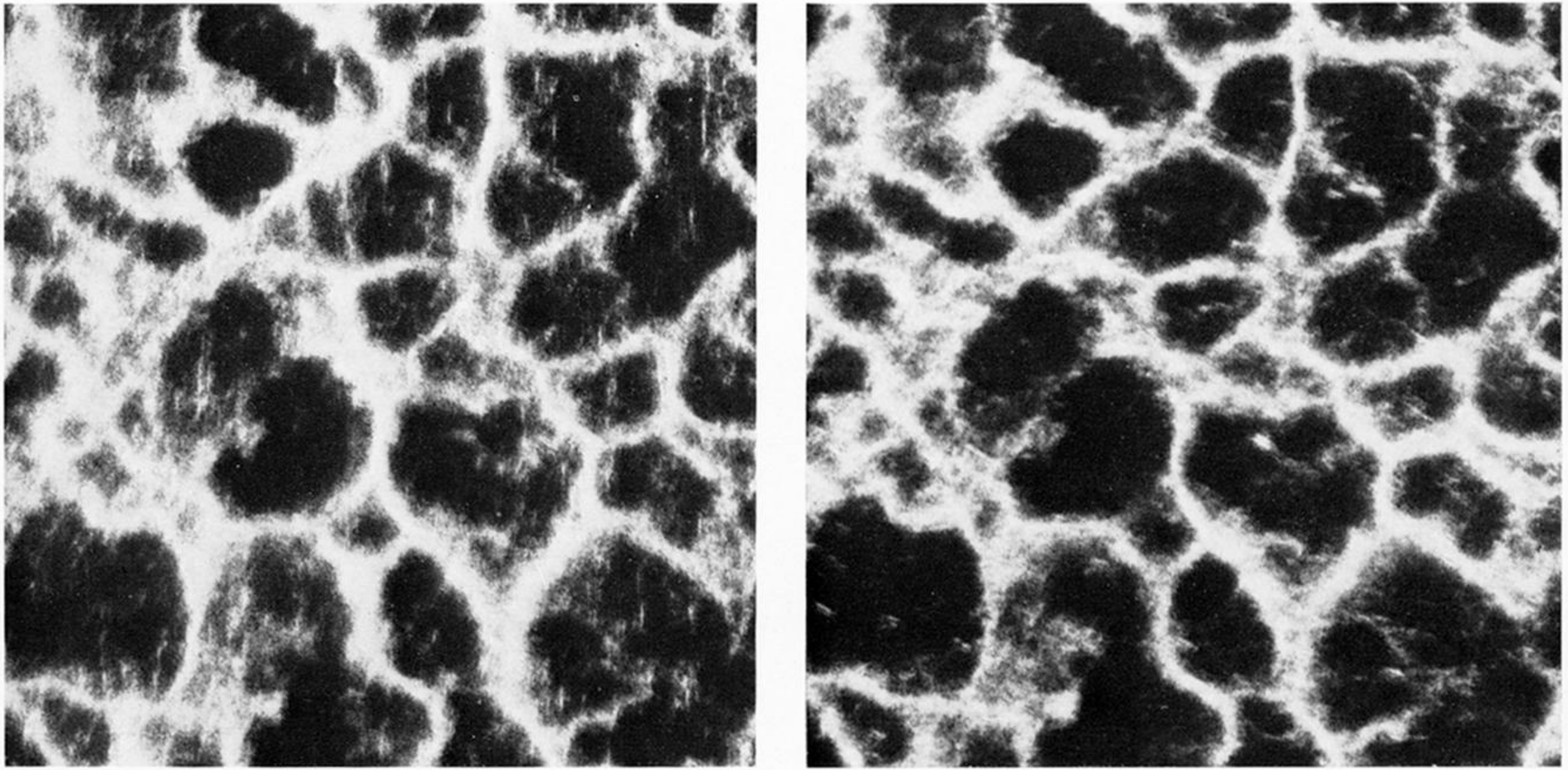

(*a*) (*b*)

FIGURE 11

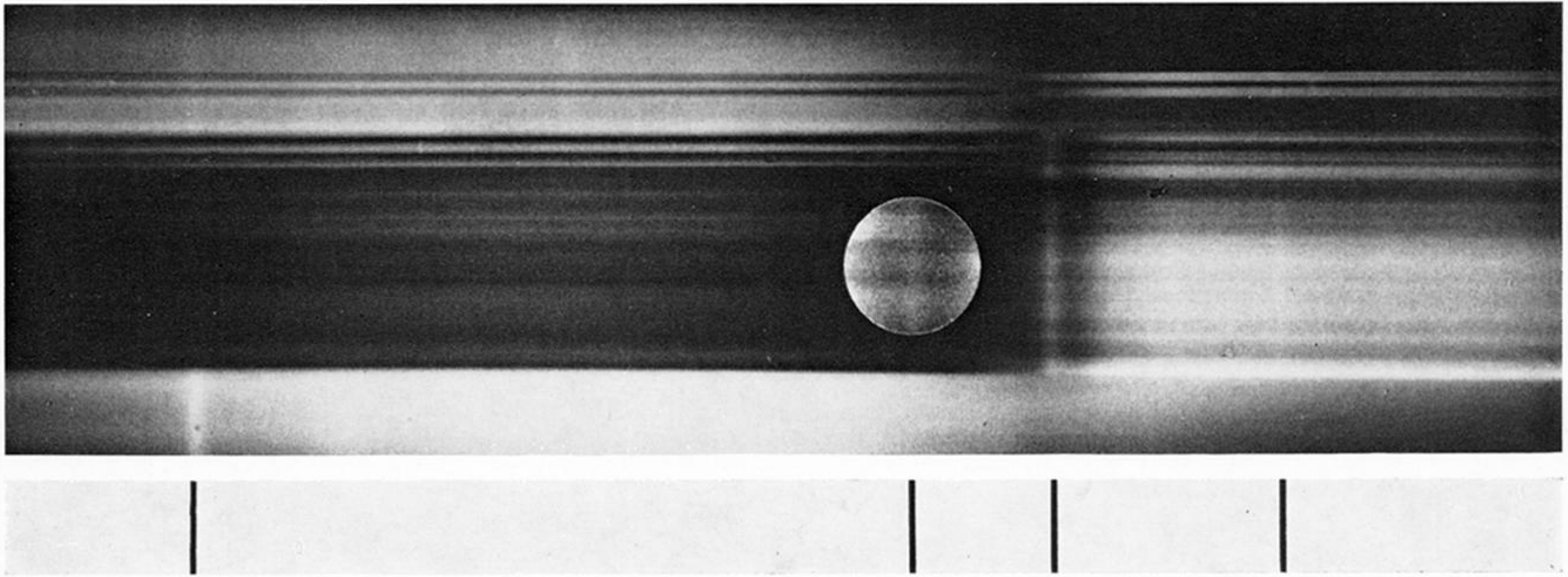

FIGURE 12

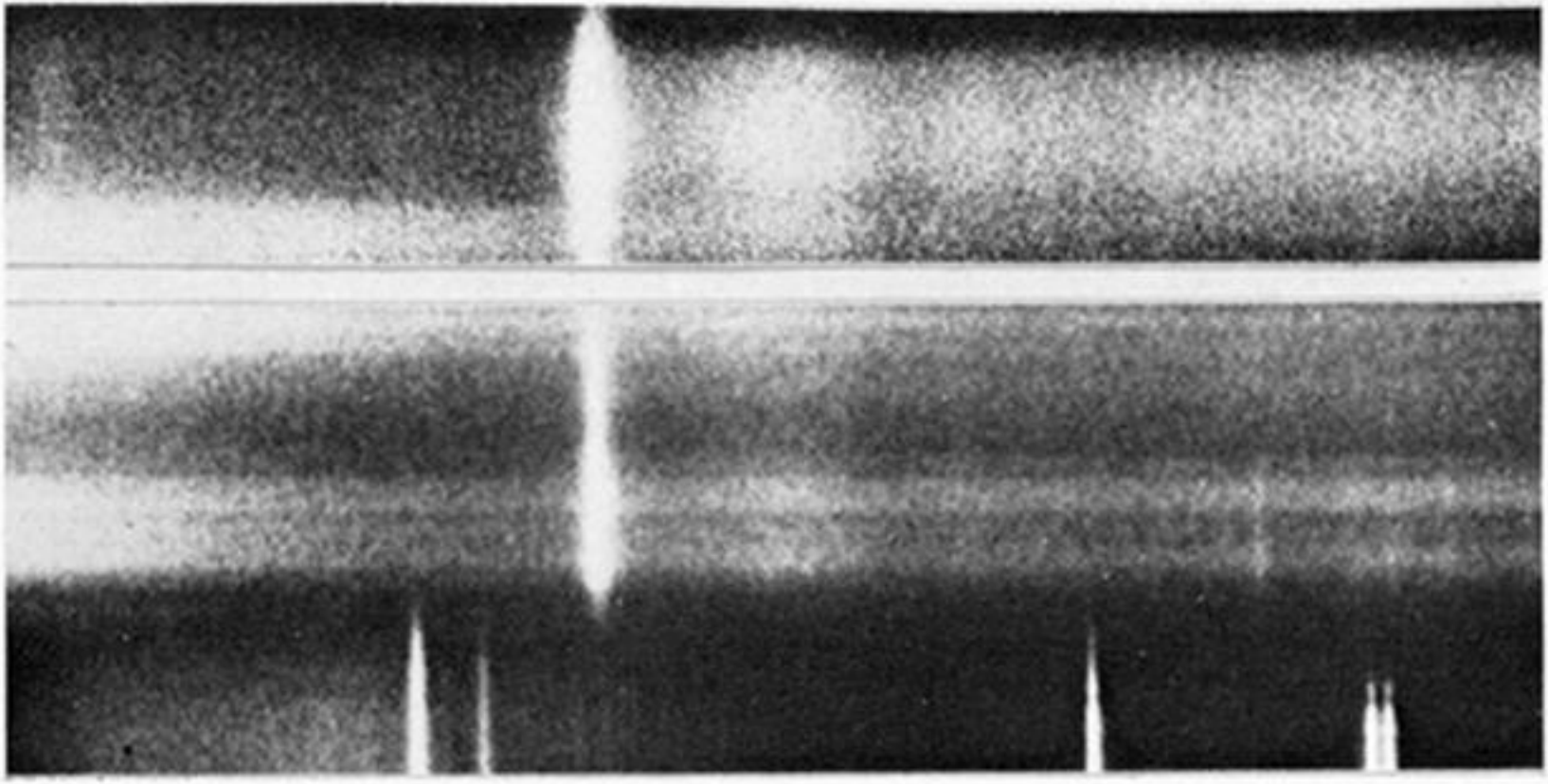

FIGURE 13

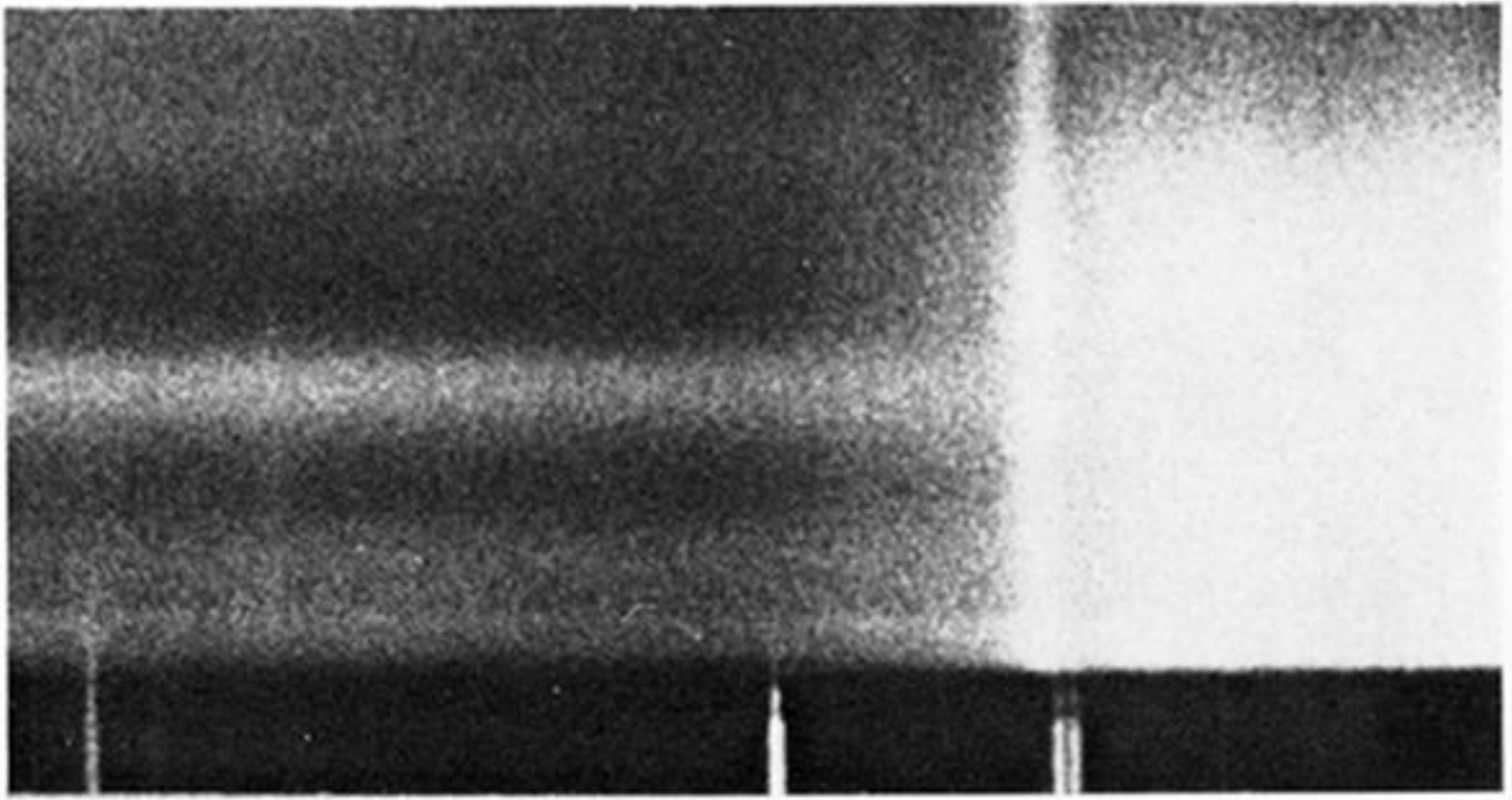

FIGURE 14